Mixed glass former effect in borate and thioborate sodium-ion conducting glass systems

by

Brittany Curtis

A dissertation submitted to the graduate faculty

in partial fulfillment of the requirements for the degree of

DOCTOR OF PHILOSOPHY

Major: Materials Science and Engineering

Program of Study Committee:
Steve Martin, Major Professor
Nicola Bowler
Gordon Miller
Aaron Rossini
Xiaoli Tan

The student author, whose presentation of the scholarship herein was approved by the program of study committee, is solely responsible for the content of this dissertation. The Graduate College will ensure this dissertation is globally accessible and will not permit alterations after a degree is conferred.

Iowa State University

Ames, Iowa

2018

DEDICATION

To my parents Dwight Curtis and Judy Baker along with my sister Stephanie. To all the families that encouraged, inspired, and supported me in my endeavors: Donna Stitt, The Wikanders, The Mendons, and The Ahlvers/Wilkinsons.

TABLE OF CONTENTS

Page

NOMENCLATURE

ASSB	All Solid State Battery
BO	Bridging Oxygen
BS	Bridging Sulfur
IR	Infrared Spectroscopy
LE	Liquid Electrolyte
LIB	Lithium-Ion Battery
MGF	Mixed Glass Former
MGFE	Mixed Glass Former Effect
NBO	Non-Bridging Oxygen
NBS	Non-Bridging Sulfur
NMR	Nuclear Magnetic Resonance
SRO	Short Range Order
SSE	Solid-State Electrolyte

ABSTRACT

As alternative energy sources continue to increase their production, there becomes a higher demand for cost-effective, safe, and energy efficient grid storage. Solid-state batteries are becoming of increased attention due to the demands for grid storage of alternative energy production, especially on days when these sources are under producing. As these solid-state batteries are being developed, many aspects of these batteries are being researched to optimize safety, cost-effectiveness and energy density. Current lithium-ion batteries have been scrutinized due to their safety concerns utilizing a flammable, liquid electrolyte. These concerns may be limited by replacing these organic, liquid electrolytes with an inorganic solid-state electrolyte. Of particular interest are glassy electrolytes. Glassy solid-state electrolytes prove to be an advantageous competitor due to the relatively low manufacturing costs and increased safety. In addition, properties of these electrolytes (i.e ionic conductivity, density, glass transition temperature, etc.) can be modified due to the mixed glass former effect (MGFE) which occurs when varying the ratio of glass formers from one binary system to the other through a ternary system. Physical and electrochemical properties vary in a non-linear, non-additive trend as the composition, and subsequently the structure, is changed. The structure and physical properties of three glass systems, $0.2Na_2O + 0.8[xBO_{3/2} + (1-x)GeO_2]$, $0.6Na_2S + 0.4[xBS_{3/2} + (1-x)GeS_2]$, and $0.6Na_2S + 0.4[xBS_{3/2} + (1-x)SiS_2]$, have been examined in an attempt to understand the MGFE. By examining an oxide and a sulfide system, it will be seen how substituting one anion for another affects the structure and the physical properties of these glassy solid-state electrolytes. The glass structure was examined through Raman, infrared and NMR spectroscopies. Glass transition

temperature was obtained through differential scanning calorimetry. Ionic conductivities were obtained using impedance spectroscopy. Densities were obtained using the Archimedes method.

CHAPTER 1. INTRODUCTION

1.1 Dissertation Organization

This dissertation is organized into 7 chapters. Chapter 1 discusses the background information into the Mixed Glass Former Effect, experimental procedures, and proposed research.

The second chapter discusses the short-range order (SRO) of the sodium borogermanate glasses, $0.2Na_2O + 0.8[xBO_{3/2} + (1-x)GeO_2]$. The structure of these glasses are explored using Raman, infrared (IR) and ^{11}B magic angle spinning solid nuclear magnetic resonance (MASS-NMR). The sodium borate binary, 0.2Na2O + 0.8BO3/2, corresponds to the $Na_3B_3O_6$ isolated six-membered ring. The sodium germanate binary corresponds to the enneagermanate structure consisting of a mixture of GeO_4 and GeO_6 units which are all bridging units. Upon mixing of these two systems in varying ratios, keeping the modifier content constant, the units react to form B^3, B^4, with a small contribution of B^2, Ge^3, Ge^4, and Ge^6.

The third chapter will examine the analogous glass system to the sodium borogermanates, the sodium thioborogermanates. It will include the glass formability of $0.2Na_2S + 0.8[xBS_{3/2} + (1-x)GeS_2]$, $0.5Na_2S + 0.5[xBS_{3/2} + (1-x)GeS_2]$, $0.64Na_2S + 0.36[xBS_{3/2} + (1-x)GeS_2]$. The focus will be on the $0.64Na_2S + 0.36[xBS_{3/2} + (1-x)GeS_2]$ due to its stronger glass formability.

The fourth chapter will explore the structure of a sodium thioborosilicate system. A structural model for this system is developed from the infrared (IR), Raman, ^{11}B Magic Angle Spinning Solid Nuclear Magnetic Resonance (MASS-NMR), and ^{29}Si MASS-NMR spectroscopies and will be discussed in further detail.

Chapter five will examine the MGFE with respect to the ionic conductivity. Further investigation into the structural effects on the ionic conductivity are discussed. The Christensen Martin Anderson Stuart Model is employed to model this system and is seen to be in good agreement with experimental activation energies.

The sixth chapter will detail the glass transition temperatures and densities of the sodium thioborosilicate system. The mixed glass former effect will be examined in both of these properties along with the molar volumes calculated from the densities. An explanation for the trend is given.

The seventh and final chapter will summarize this dissertation with general conclusions and focus on possible future work expanding upon the MGFE. This chapter also includes an acknowledgements section for this dissertation work.

1.2 Dissertation Introduction

In 2015, a global pact known as the Paris Agreement was reached amongst 195 countries including the United States. It plans to limit global warming below 2^{o}C in the coming years call for the decrease use of fossil fuels, which are unsustainable, and move to more green energy sources.[1] Milestones have already been reached in using green energy such as wind energy which now accounts for 28% of the electricity generated in Iowa in 2014.[2] In addition, research is being conducted to improve the ability to store the energy generated to further increase the impact of green energies. A key aspect of energy storage lies in improving battery technology to meet the demand of energy storage. In developing new energy storage systems, specifically batteries, all-solid state batteries are proven to be an advantageous and an obtainable possibility.

1.2.1 Solid State Batteries

Currently, the highest energy density battery is the lithium ion battery, while lowest cost is still the traditional lead-acid battery. Lithium ion batteries are especially used in many portable devices such as computers, mobile phones, and electric cars. The high gravimetric energy density of these batteries is, in part, due to the light weight of lithium. However, lithium ion batteries utilize a graphitic anode which lowers the energy density of the battery due to the lithium stored per carbon atom of Li_1C_6. As a result, the theorectical capacity of a lithium ion battery is utilizing a graphitic anode about 370 Ah/kg of graphite.[3] In a battery that uses a graphitic anode, lithium ions are intercalated in between the layers of the graphite. These graphitic layers add volume to the anode and thereby decrease the energy density of the anode material. In practice, the ideal anode for a lithium ion battery would be lithium metal. However, battery operation and safety concerns arise when lithium ion batteries utilize a lithium metal as the anode material. Dendritic lithium formation at the anode presents safety concerns if lithium dendrite reaches the cathode and short circuits the battery. If the battery does short then rapid heating may occur and ignite the flammable, liquid electrolyte that lithium ion batteries use.[4]

All-solid state batteries are a viable alternative to lithium ion batteries which would allow the use of lithium metal as the anode material. All-solid state batteries utilizing a solid electrolyte could suppress the formation of lithium dendrites thereby eliminate the safety concerns.[5] Futhermore, by using a solid state electrolyte, the energy density could drastically increase having a theoretical capacity of 3860 Ah/kg which is 25 times higher than the typical lithium ion battery.[5]

While lithium batteries are particularly useful for mobile devices, the cost of manufacturing such batteries can be quite expensive since lithium is limited in supply with an average mass fraction of about 20 ppm in the Earth's crust.[6] Due to the rarity of lithium, the price of lithium is rather expensive. On the other hand, sodium is rather abundant in the Earth's crust and provides an inexpensive alternative to lithium.[7] However, sodium is comparatively heavier which is disadvantageous for portable devices such as cell phones and electric cars. But the weight of sodium batteries would not be an issue for stationary energy storage systems such as wind turbines. These types of batteries would prove very beneficial in storing wind energy, possibly increasing the amount of wind energy that can be used.

1.2.2 Benefits of Glassy Electrolytes

While different solid-state materials are being examined, of particular interest are glassy solid-state electrolytes. Glasses do not exhibit long range order or periodic arrangement of atoms, creating an amorphous solid.[8] The amorphous, open structure, which would be conducive for ionic conductivity over a crystalline material. However, to achieve high ionic conductivity there must be a high concentration of mobile ions, or sodium ions in this instance. Unfortunately, using too much modifier, a component that does not network with the structure but modifies its properties,[8] would diminish the glass formability of the samples. Therefore, a good balance of modifier and glass former, a component that serves as the primary sources of the structure,[8] is necessary to optimize the glass formability and ionic conductivity. The ions also need to be bound weakly to the network to encourage conduction. These weakly bound ions would decrease the chemical durability of the glass itself. To achieve high ionic conductivities, some compromises of the glass formation, chemical durability, and the ionic conductivity must be made.

1.2.3 Mixed Glass Former Effect

The current organic liquid electrolytes present some compromising characteristics since they are very good ionic conductors but present safety concerns due to fires and battery performance issues due to electrolyte decomposition. Typical liquid electrolytes have ionic conductivities of ~10^{-3} $(\Omega^{*}cm)^{-1}$.[9-11] Glassy solid state materials are of particular interest due to their ability to improve energy density while limiting safety issues. Oxide-based glassy electrolytes have been widely studied like the sodium germanates.[12-14] For binary sodium ionic conducting glasses, typical room temperature ionic conductivities are around 10^{-9} to 10^{-12} $(\Omega^{*}cm)^{-1}$.[12,13,15,16] However, an interesting phenomenon occurs when mixing the glass formers while maintaining a constant modifier content called the mixed glass former effect, or MGFE.[12,17-19] This phenomenon proves to be a solution that may optimize the glass formation, chemical durability, and the ionic conductivity for their use as glassy electrolytes.

The mixed glass former effect occurs when the physical properties of the glass have a non-linear dependence on composition upon mixing the glass formers. To get a better understanding, fig. 1 illustrates the mixed glass former effect in the sodium borophosphate system.[12] When x=0.0, the ionic conductivity for the sodium phosphate binary is around $3x10^{-11}$ $(\Omega cm)^{-1}$ while the conductivity for the sodium borate binary at x=1.0 is around $5x10^{-10}$ $(\Omega cm)^{-1}$.[12] Upon mixing the glass formers, the borate and phosphate, into a ternary glass, it can be seen that the conductivity increases until reaching a maximum at x=0.5 and then decreases. This non-linear trend in the ionic conductivity exhibits a positive mixed glass former effect, or a positive deviation from linearity with a maximum in ionic conductivity. On the other hand, the activation energy

for ionic conduction exhibits a negative mixed glass former effect, or a negative deviation from linearity with a minimum in the activation energy.

From this study of the mixed glass former effect, it can be seen that upon mixing the glass formers the physical properties of the glass vary in a nonlinear trend. This suggests that glassy electrolytes may be engineered in a way to optimized its physical properties, not only the ionic conductivity but the density, glass transition temperature, etc., based on the glass structure after mixing. It was also shown that the structure of the glass reacted in such a way to form different units upon mixing where a P^2 and B^3 unit react to create a B^4 and P^3.[20] By creating more B^4 units which delocalizes the charge on boron to the oxygens, the sodium boron interaction is weakened allowing the sodium ion to more freedom to diffuse through the glass.

1.2.4 Sulfide-based Glassy Solid State Electrolytes

Oxide-based glasses are very chemically durable making them easier to handle. However, the oxide glasses are known to exhibit low ionic conductivities undesirable for use as solid state electrolytes. For example, fig. 3 compares the ionic conductivity of an oxide-based glassy electrolyte to that of the sulfide-based analog. It can be seen that the ionic conductivity increases by 10^{-2} to 10^{-3} $(\Omega cm)^{-1}$ when substituting sulfur for oxygen.

Figure 4 demonstrates the theory behind increase in ionic conductivity in sulfide-based glassy solid state electrolytes.[20] There are two energy barriers the must be overcome in order for ion conduction to occur contributing to the overall activation in eq.1:

$$\Delta E_{act=} \Delta E_c + \Delta E_s \quad (1)$$

The first is the coloumbic charge attraction, ΔE_c, which takes into account the size of the cation and the anion. If both the cation and the anion are small, then there will be a large attraction creating a large coulombic energy barrier. If for instance the anion is larger, like replacing oxygen with sulfur, then this attraction potential decreases, consequently lowering the coulombic energy barriers.[20]

The other energy barrier is the volumetric strain energy, ΔE_s, which is contributed to the volume of the mobile cation. For the mobile cation to overcome the volumetric strain energy barrier, the size of the cation must be relatively small or the "doorway" radius must enlarge to accommodate the mobile cation. Equation 2 describes the strain energy as proposed by McElfresh *et al.* which describes the enlargement of a cavity through which a mobile cation is migrating:

$$E_S = \pi G \frac{\lambda}{2}(r - r_d)^2 \quad (2)$$

where G is the shear modulus, r is the radius of the mobile cation, and r_d is the doorway radius.[21] The small cation size counteracts the ability to overcome the coulombic energy barrier. However, the higher polarizability of sulfur, when compared to oxygen, allows for a larger doorway radius, decreasing the volumetric strain energy. Altogether the larger anion size of sulfur and its high polarizability would suggest that the ionic conductivity in the sulfide-based glasses should be higher than that of the oxide-based glasses.

1.2 Goals of Research

The goal of this research is to comparatively study the mixed glass former effect in both an oxide and sulfide glass system, specifically looking at a sodium borogermanate system and a sodium thioborogermanate system. Borate and germanate are good glass

formers so are the sulfide counterparts, boron sulfide and germanium sulfide. Extensive research has been done on the sodium borate, sodium germanate, sodium thioborate and sodium thiogermanate in order to understand the binaries of these systems.[13,22-27] The literature of the binary compositions suggests that these systems have potential as prospective sodium-ion glassy solid state electrolytes. However, since the sodium thioborogermanates were found to be poor glass formers under the desired conditions (as will be further discussed), focus was turned to the sodium thioborosilicates.

This project aims to gain comprehensive insight of the structural units as it changes with composition in both the oxide and sulfide systems while more focus is put on the sulfide systems due to their increased ionic conductivity. Furthermore, the physical properties (i.e. density, Tg, ionic conductivity, etc.) of the system will be examined to understand how the mixed glass former effect is exhibited in these systems either positive with a maximum of the property, or negative with a minimum of the property. Researching an oxide and a sulfide ternary system will further the understanding of the differences in physical properties through a structural standpoint. By examining the mixed glass former effect in these systems, it will be possible to engineer glassy solid-state electrolytes based on their structure for their intended properties.

1.4 References

1 *OUTCOMES OF THE U.N. CLIMATE CHANGE CONFERENCE IN PARIS*, <http://www.c2es.org/international/negotiations/cop21-paris/summary> (2015).

2 *News/Updates/Press Releases*, <http://www.iowawindenergy.org/whywind.php> (2015).

3 Yoshio, M. *et al.* Carbon-Coated Si as a Lithium-Ion Battery Anode Material. *Journal of The Electrochemical Society* **149**, A1598-A1603, doi:10.1149/1.1518988 (2002).

4 Bhattacharyya, R. *et al.* In situ NMR observation of the formation of metallic lithium microstructures in lithium batteries. *Nat Mater* **9**, 504-510, doi:http://www.nature.com/nmat/journal/v9/n6/suppinfo/nmat2764_S1.html (2010).

5 Daiwon, C., Wei, W. & Zhenguo, Y. in *Lithium-Ion Batteries Green Chemistry and Chemical Engineering* 1-50 (CRC Press, 2011).

6 Carmichael, R. S. *Practical Handbook of Physical Properties of Rocks and Minerals*. (CRC Press Inc., 1989).

7 Yabuuchi, N. *et al.* P2-type Nax[Fe1/2Mn1/2]O2 made from earth-abundant elements for rechargeable Na batteries. *Nat Mater* **11**, 512-517, doi:http://www.nature.com/nmat/journal/v11/n6/abs/nmat3309.html#supplementary-information (2012).

8 Shelby, J. E. *Introduction to Glass Science and Technology*. second edn, (The Royal Society of Chemistry, 2005).

9 Shin, J.-H., Henderson, W. A. & Passerini, S. Ionic liquids to the rescue? Overcoming the ionic conductivity limitations of polymer electrolytes. *Electrochemistry Communications* **5**, 1016-1020, doi:http://dx.doi.org/10.1016/j.elecom.2003.09.017 (2003).

10 Xu, K. Electrolytes and Interphases in Li-Ion Batteries and Beyond. *Chemical Reviews* **114**, 11503-11618, doi:10.1021/cr500003w (2014).

11 Song, J. Y., Wang, Y. Y. & Wan, C. C. Review of gel-type polymer electrolytes for lithium-ion batteries. *Journal of Power Sources* **77**, 183-197, doi:http://dx.doi.org/10.1016/S0378-7753(98)00193-1 (1999).

12 Christensen, R., Olson, G. & Martin, S. W. Ionic Conductivity of Mixed Glass Former 0.35Na2O + 0.65[xB2O3 + (1 – x)P2O5] Glasses. *The Journal of Physical Chemistry B* **117**, 16577-16586, doi:10.1021/jp409497z (2013).

13 Khan, M. N. & Khawaja, E. E. The Electrical and Optical Properties of Glasses of the Li2O-GeO2 and Na2O -GeO2 systems. *Physica Status Solidi* **74**, 273-277 (1982).

14 Martin, S. W. & Angell, C. A. Dc and ac conductivity in wide composition range Li2O・P2O5 glasses. *Journal of Non-Crystalline Solids* **83**, 185-207, doi:http://dx.doi.org/10.1016/0022-3093(86)90067-0 (1986).

15 Abid, M., Et-tabirou, M. & Taibi, M. Structure and DC conductivity of lead sodium ultraphosphate glasses. *Materials Science and Engineering: B* **97**, 20-24, doi:http://dx.doi.org/10.1016/S0921-5107(02)00390-2 (2003).

16 Han, Y. H., Kreidl, N. J. & Day, D. E. Alkali diffusion and electrical conductivity in sodium borate glasses. *Journal of Non-Crystalline Solids* **30**, 241-252, doi:http://dx.doi.org/10.1016/0022-3093(79)90163-7 (1979).

17 Larink, D., Eckert, H., Reichert, M. & Martin, S. W. Mixed Network Former Effect in Ion-Conducting Alkali Borophosphate Glasses: Structure/Property Correlations in the System [M2O]1/3[(B2O3)x(P2O5)1–x]2/3 (M = Li, K, Cs). *The Journal of Physical Chemistry C* **116**, 26162-26176, doi:10.1021/jp307085t (2012).

18 Bischoff, C. *The Mixed Glass Former Effect in* $0.5Na_2S+0.5[xGeS_2+(1-x)PS_{5/2}]$ *Glasses* Doctor of Philosophy thesis, Iowa State University, (2013).

19 Deshpande, V. K., Pradel, A. & Ribes, M. The mixed glass former effect in the Li2S : SiS2 : GeS2 system. *Materials Research Bulletin* **23**, 379-384, doi:http://dx.doi.org/10.1016/0025-5408(88)90012-8 (1988).

20 Martin, S. in *Handbook of Solid State Batteries Materials and Energy* (ed Leonard C. Feldman) Ch. 14, 433-501 (World Scientific, 2016).

21 McElfresh, D. K. & Howitt, D. G. Activation Enthalpy for Diffusion in Glass. *Journal of the American Ceramic Society* **69**, C-237-C-238 (1986).

22 Bloyer, D. R., Cho, J. & Martin, S. W. Infrared Spectroscopy of Wide Composition Range xNa2S + (1 –x)B2S3 Glasses. *Journal of the American Ceramic Society* **76**, 2753-2759 (1993).

23 Kamitsos, E. I., Karakassides, M. A. & Chryssikos, G. D. Vibrational spectra of magnesium-sodium-borate glasses. 2. Raman and mid-infrared investigation of the network structure. *The Journal of Physical Chemistry* **91**, 1073-1079, doi:10.1021/j100289a014 (1987).

24 Di Martino, D., Santos, L. F., Marques, A. C. & Almeida, R. M. Vibrational spectra and structure of alkali germanate glasses. *Journal of Non-Crystalline Solids* **293–295**, 394-401, doi:http://dx.doi.org/10.1016/S0022-3093(01)00690-1 (2001).

25 Verweij, H. & Buster, J. H. J. M. The structure of lithium, sodium and potassium germanate glasses, studied by Raman scattering. *Journal of Non-Crystalline Solids* **34**, 81-99, doi:http://dx.doi.org/10.1016/0022-3093(79)90008-5 (1979).

26 Royle, M., Cho, J. & Martin, S. W. Raman spectroscopy studies of xNa2S+(1−x)B2S3 glasses and polycrystals. *Journal of Non-Crystalline Solids* **279**, 97-109, doi:http://dx.doi.org/10.1016/S0022-3093(00)00344-6 (2001).

27 Barrau, B., Ribes, M., Maurin, M., Kone, A. & Souquet, J.-L. Glass formation, structure and ionic conduction in the Na2S・GeS2 system. *Journal of Non-Crystalline Solids* **37**, 1-14, doi:http://dx.doi.org/10.1016/0022-3093(80)90473-1 (1980).

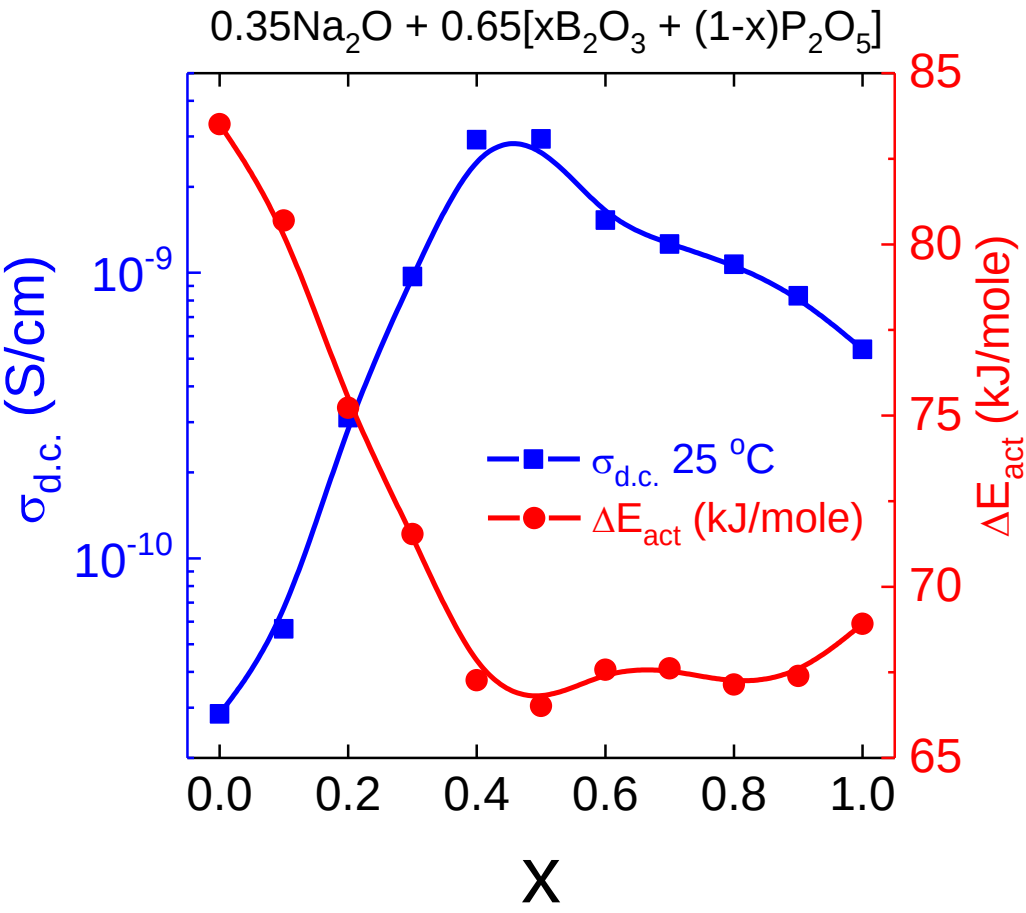

Figure 1.1. The mixed glass former effect in a sodium borophosphate system, specifically the ionic conductivity and the activation energy for conduction.[12]

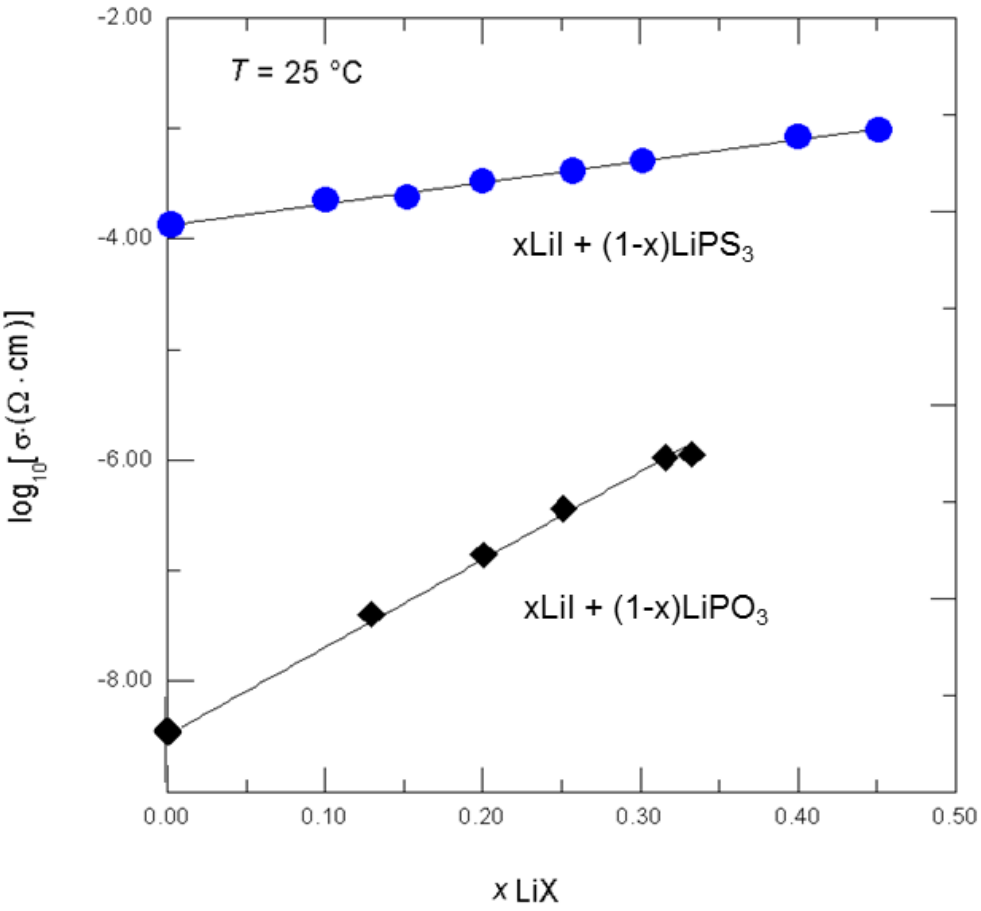

Figure 1.3. Composition plot comparing oxide-based to sulfide-based glassy electrolyte.[20]

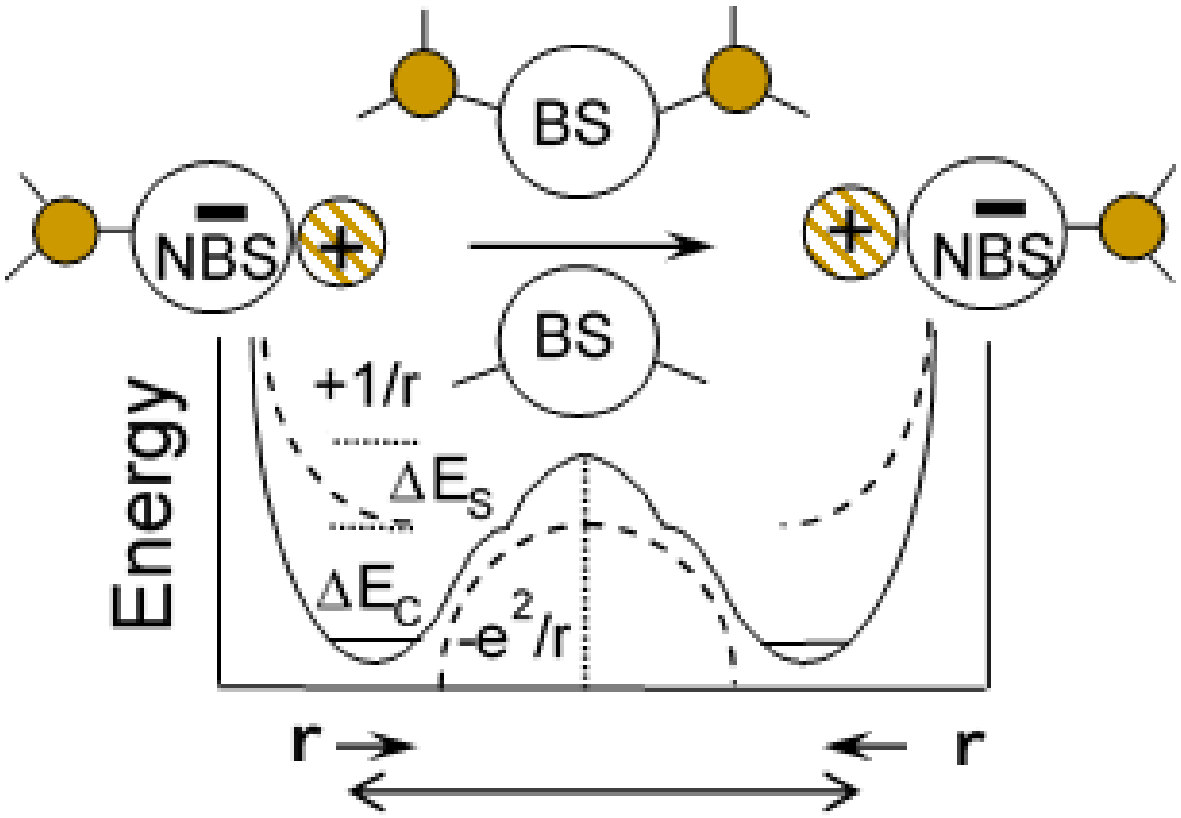

Figure 1.4. Schematic of ionic diffusion in sulfide-based glass.[20]

CHAPTER 2. COMPOSITION DEPENDENCE OF THE SHORT RANGE ORDER STRUCTURES IN $0.2Na_2O + 0.8[xBO_{3/2} + (1-x)GeO_2]$ MIXED GLASS FORMERS

Modified from a paper submitted to the Journal of Non-Crystalline Solids

Brittany Curtis[1], David Hynek[2], Sydney Kaizer[2], Steve Feller[2], and Steve Martin[1*]

[1]Department of Materials Science & Engineering
Iowa State University of Science and Technology
Ames, IA

[2]Department of Physics
Coe College
Cedar Rapids, IA

2.1 Abstract

The atomic level structures of ternary $0.2Na_2O + 0.8[xBO_{3/2} + (1-x)GeO_2]$ glasses have been carefully examined for the first time using a combination of Raman, infrared (IR) and ^{11}B magic angle spinning nuclear magnetic resonance (MAS-NMR) spectroscopies. It was found that, like in other mixed glass former (MGF) systems, there is an unequal sharing of the sodium oxide between the two glass formers, B and Ge, across this series $0 < x < 1$. It is found that for all $x > 0$, the Na_2O preferentially reacts with boron to create a larger number of tetrahedral boron, $BO_{4/2}^{-1} \equiv B^4$, units than would be found for a binary sodium borate glass of the same mole fraction, 0.20, of Na_2O. In addition to this higher than expected fraction of B^4 units as determined by the ^{11}B MAS-NMR measurements, the Raman spectra further suggest the presence of high concentrations of octahedrally coordinated $GeO_{6/2}^{-2}$, Ge^6, units in the GeO_2 rich end of this compositional series, $x \leq 0.2$. Across this series, it is found that there are at most five

* Corresponding author, swmartin@iastate.edu

short range order (SRO) structural units present in these glasses, $BO_{3/2}$ (B^3), B^4, $GeO_{6/2}^{-2}$ (Ge^6), $GeO_{3/2}O^{-1}$ (Ge^3), and $GeO_{4/2}$ (Ge^4), where the superscript gives the number of bridging oxygens (BOs) bonded to the central atom. The composition, x, dependence of all of these SRO structural units were determined by combining the results all of these spectral techniques and requiring that the total sum of all the negatively charged SRO units balance the positive (+0.4) charges from the Na^+ ions and that the total amount of B balance to 0.8x, the total amount of Ge balance to 0.8*(1-x), and the total amount of oxygen balance to1.8-0.4x as required by the stoichiometry of this compositional series.

2.2 Introduction

Safer, lower cost, and more energy dense portable and stationary electrical energy storage systems are increasing in demand with the rapid increase in the number of and pervasive use of portable electronic devices, the rapid increase in the number of electric vehicles, and the rapid increase in the viability of renewable, but temporal, energy systems such as wind and solar.[1] While liquid electrolyte-based Li-ion systems have significantly advanced the performance of batteries in all of these applications, critical problems of safety, cost, and energy density are now pushing the search for newer and improved systems. One particularly attractive approach is all solid-state batteries (ASSBs) that can utilize the high energy density of pure metal anodes, such as Li and Na. However, to achieve the energy density advantages of pure metal anodes, these ASSBs require chemically and electrochemically stable and high Li^+ or Na^+ ion conductivity solid electrolytes. High conductivity single or polycrystalline solid electrolytes are well known, but so far are finding little use in ASSBs due to their high fabrication costs.[2, 3] In this respect, glassy solid electrolytes (GSEs) are attractive alternatives due to their low processing costs, continuous compositional variation which can be used to continuously

vary and improve their properties, especially their ionic conductivities, and their lack of impedance-generating grain boundaries.[4, 5]

Sodium batteries (SBs) provide an appealing substitute for lithium batteris (LBs) in stationary applications, where gravimetric energy density is less important than volumetric energy density, by decreasing the cost of secondary ASSBs.[6-8] Sodium is approximately 1,200 times more abundant than lithium in the Earth's crust.[9, 10] However, sodium is much heavier than lithium which would be disadvantageous for portable devices. Therefore, the use of sodium ASSBs would be intended for stationary devices such as wind turbines and other large-scale energy storage systems.

As the performance of lithium-ion batteries (LIBs) are being pushed to their theoretical limits, they are now presenting safety concerns since, among other problems, dendritic lithium formation can occur causing thermal runaway.[11-14] This leads to the possibility of igniting the flammable, liquid electrolyte (LE) found in lithium ion batteries.[12, 15, 16] The use of a solid-state electrolyte (SSE) could prove advantageous by suppressing dendritic formation further preventing the battery from short-circuiting which can have severe safety implications. So far, SSEs such as glasses, ceramics, and glass-ceramics are among the most promising possibilities.[17, 18] GSEs are advantageous due, in part, to their amorphous long-range structure, which lacks grain boundaries that have been shown to promote growth of dendrites along the boundaries causing short-circuiting.[19, 20]

While most studies of GSEs have examined the alkali oxide or alkali sulfide dependence of the conductivity in a single glass former (SGF) system, such as Na_2O + B_2O_3, new studies in our research group have expanded the compositional search for

higher conductivity and higher performance.[21] In this work, we have recently begun to study so-called mixed glass former (MGF) glasses that consist of two or more glass formers, such as B_2O_3 and GeO_2 considered.[22-24] In these studies, we and others have discovered the phenomenon known as the mixed glass former effect (MGFE) which is a non-linear and non-additive trend in the physical properties arising from the mixing of glass formers in varying ratios.[22, 25, 26] In our research on these MGF systems, we have discovered both positive and negative MGFE systems.[23, 25] In the former systems, the ionic conductivity exhibits a positive maximum in the ionic conductivity between the conductivities of the two end member binary glasses. In the latter systems, they exhibit a negative minimum in the ionic conductivity between the conductivities of the two end member binary glasses.

We have had a particular interest in examining boron-based MGF systems because one of the very first systems we studied, $Na_2O + B_2O_3 + P_2O_5$ (NBPO), exhibited one of the strongest ever reported positive MGFEs in the Na^+ ion conductivity.[23, 27-29] Accompanying this positive MGFE in the conductivity were also positive MGFEs in the glass transition temperature (Tg), the density, and the mechanical modulus, and a negative MGFE in the thermal expansion coefficient. In this way, the co-mixing of sodium boron and sodium phosphate glass structures improved nearly every physical property of the glass. The positive MGFE in the Na^+ ion conductivity in the NBPO system was attributed to the formation of charge delocalizing tetrahedral boron, $BO_{4/2}^{-1} \equiv B^4$ units that were found to decrease the coulombic binding energy between the mobile Na^+ ions and negatively charged compensating short range order (SRO) structural units making up the network structure of the glass. The formation of these B^4 units was also

found to be responsible for the positive MGFE in the Tg and the mechanical modulii of the glasses, as well as the negative MGFE in the thermal expansion coefficient.[23, 27, 29]

For these reasons, we have begun other studies of other boron-based oxide and sulfide MGF systems to determine whether similar positive MGFEs in the ionic conductivity (and other physical properties) are observed. Our study of the most familiar of the boron based MGF systems, the sodium borosilicate (NBSO) glass system, has shown that it in fact has a weak *negative* MGFE in the Na^+ ion conductivity, even while it behaves structurally similar to the NBPO glass system.[28] In the NBSO system, there is a similar disproportional sharing of the Na_2O towards the boron units in the glass leading to a larger than expected fraction of B^4 units. This over-abundance of B^4 units causes similar positive MGFEs in the Tg and all of the mechanical modulii. It appears in this system, however, that the charge delocalization effect caused by the formation of large fractions on B^4 units is not sufficient, as it apparently is in the NPBO system, to overcome the positive MGFEs in the density which reduces the overall free-volume available for Na^+ ion conduction and in the mechanical modulii which increase the energy necessary to dilate the glass structure to accommodate mobile ion conduction.

Therefore, we have begun an iso-compositional study of the corresponding Na_2O + B_2O_3 + GeO_2 (NBGO) system to further explore and characterize the unique role that B^4 units appear to play in governing the physical and electrochemical properties of MGF glass systems containing boron. In this report, we have examined, in more detail, the SRO structures of these glasses to quantify the exact composition dependence of the B^4 units in these glasses and to characterize the compositional dependence of all SRO structural units. Preliminary reports on these glasses have already been published.[30, 31]

Future contributions in this series will report on the B^4 and other SRO structural unit dependence of the physical properties, especially the Na^+ ion conductivity. As we have done in our other studies of MGF glasses, we have purposefully prepared and characterized this system such that there is a one to one replacement of the glass formers, B and Ge. For these reasons, our study is along the compositional line $0.2Na_2O + 0.8[xBO_{3/2} + (1-x)GeO_2]$.

Some studies of the lithium analog of this system exist, but little is understood about their MGF behavior.[32-34] Although some physical properties have been studied, no characterization of these glasses have been done to understand the composition dependence of their SRO structures. Even though these glasses are expected to be poor ionic conductors, knowing their structure-property relationships will help better understand more complex systems that may proceed from this work.

2.3 Background

2.3.1 Notation of Structural Units

As briefly described above, a simple notation will be used to summarize the SRO units present in these NBGO glasses in a concise manner. Figure (1) shows the expected units with their corresponding notation. For example, Ge^3 and B^4 describe germanium and boron centers with three and four BOs, respectively. Note that B exists in both three and four fold coordination, and Ge exists in both four and six fold coordination. For the latter coordinations of B and Ge, all of the bonded oxygens are BOs.

2.3.2 Charge Compensation

Given the low Na_2O concentration in these glasses of $y_{Na2O} = 0.20$, the numbers of the various SRO units that are observed in this series of glasses are quite limited. For B, they include only the charged B^4 (1-) and the neutral B^3 units for all glasses with $0 < x <$

1. For the pure sodium borate glasses at y = 0.2, we have previously shown that a very small fraction of charged B^2 units must be present to account for the less than stoichiometric amount (0.5) B^4 units formed (~0.45).[35] For the binary $0.2Na_2O + 0.8GeO_2$ glasses, the Ge SRO units are equally limited and it is found that only the neutral Ge^4, the singly charged Ge^3, and a very small amount of doubly charged Ge^6 SRO units are required to meet charge neutrality requirements and still be consistent with the IR, Raman, and ^{11}B MAS NMR spectra. Finally, it is important to point out that for this particular glass system, the NMR spectra are limited to ^{11}B MAS NMR since capabilities of ^{73}Ge NMR are quite limited. The NMR active nucleus for germanium,^{73}Ge, is low in abundance ~7%, has a large spin (9/2), and a low gyromagnetic ratio and for these reasons very few solid-state ^{73}Ge NMR data exist.[36, 37] Due to the lack of ^{73}Ge NMR data, the identity and composition dependence of the Ge SRO units were determined by combining the results of the IR and Raman spectra of these glasses with the required charge compensation as determined from the balance of charge not residing on the B SRO units as quantitatively determined by the ^{11}B MAS-NMR spectra.

In the composition range where no Ge^6 units are present, x > 0.2, all of the charge on the Ge SRO units resides on the Ge^3 units. Hence, the fraction of Ge^3 SRO units can be calculated by knowing the number of sodium ions in the glass composition and the fraction of B^4 units calculated from the quantitative ^{11}B NMR spectra. For x > 0.2:

$$[Na^+] = [B^4] + [Ge^3] \qquad \text{Eq. (1)}$$

However, when the Ge concentration is sufficiently large, x < 0.2, the IR and Raman spectra (see below) show the presence of small amounts of Ge^6 units. In this composition

region, the Ge^6 SRO units must be must be included in the charge compensation equation:

$$[Na^+] = [B^4] + [Ge^3] + 2[Ge^6] \quad \text{Eq. (2)}$$

This work will utilize charge balance, Eqs. (1) and (2) to make initial predictions of the SRO especially regarding germanium units.

2.3.3 Brief Review of the SRO Structures the Binary Systems

Sodium germanate (NG) and sodium borate (NB) binary glass systems have been thoroughly studied. The NG binary has a large glass forming range where Kiczenski et al. report glass formation out to 75 mol % Na_2O.[38] In the low Na_2O compositional range of 0 to 0.2 Na_2O, the structural evolution of $yNa_2O + (1\text{-}y)GeO_2$ glasses is for the added Na_2O to convert the normal tetrahedral Ge^4 (with 4 BOs/Ge) units to octahedral $GeO_{6/2}^{2-}$ units according to reaction Eq. (3):

$$Na_2O + GeO_2 \rightarrow Na_2GeO_{6/2} \quad \text{Eq. (3)}$$

The fraction of Ge^6, $f(Ge^6)$, units has been shown to follow Eq. (4) up to y ~ 0.2, where $f(Ge^6)$ reaches about 0.25 and thereafter it decreases to ~0 at y ~ 0.3.[39, 40]

$$f(Ge^6) = \left(\frac{y}{1-y}\right) \quad \text{Eq. (4)}$$

The structure of the binary Ge endmember glass of the system studied here, $0.2Na_2O + 0.8GeO_2$, has been shown to consist in part of the tetrasodium enneagermanate, $Na_4Ge_9O_{20}$ ($yNa_2O = 2/9 \sim 0.18$), structure and corresponds to a mixing of Ge^6 and Ge^4 units, which possess only BOs, in the ratio of about 1 to 3.[40-42] Equation (4) predicts a slightly lower ratio of 1 to 4. At higher levels of modifier y > 0.2, (but not studied here), like the sodium silicate (NS) glasses, $Na_2O + SiO_2$, the further addition of Na_2O causes the conversion of Ge^6 and Ge^4 SRO units to Ge^3 SRO units each possessing

one non-bridging oxygen (NBO). The creation of NBOs in the glass structure decreases the average network connectivity and in doing so decreases the viscosity at the liquidus temperature and therefore reduces glass formability (increasing the critical cooling rate to avoid crystallization events).

In the NG, and other binary alkali germanate (AG) glasses, the initial formation of Ge^6 SRO units causes a unique composition dependence in the physical properties of the glasses and has been called the germanium anomaly. A particularly good example of this is seen in the composition (y) dependence of the density.[38, 43, 44] As the modifier content, sodium oxide, is increased from y = 0, there is an initial increase in density until ~ 20 mol % and thereafter the density begins to decrease.[38] Combined computational, IR and Raman spectroscopy studies of these glasses have been done to fully understand the enneagermanate structure and its formation in binary AG glasses.[37, 39-42, 45-50]

The glass forming range of the binary NB glass, $yNa_2O + (1-y)B_2O_3$ system (here we use the traditional formula for B_2O_3 to be consistent with the literature) is significantly larger than that of the binary NG system and lies between 0 to 75 mol %.[51] There is a small non-glass forming region between 45 to 55 mol % that is caused by the formation of the high melting point compound sodium metaborate, $NaBO_2$.[51, 52] This compound is totally depolymerized in that it consists of molecular units of six membered rings, $Na_3B_3O_6$, see Fig. (1). Feller et al. has examined this system in great detail and observed that this gap in glass formation cannot be closed even with the most rapid roller quenching techniques.[53]

As has been examined and reported in detail over many years and a full review is not given here, the addition of one formula unit of Na_2O to B_2O_3 converts two borons

from three-fold coordination to four-fold coordination according to the reaction equation given in Eq. (5).[54-56]

$$Na_2O + B_2O_3 \rightarrow 2\ NaBO_{4/2} \qquad \text{Eq. (5)}$$

This conversion reaction has been shown to quantitatively follow Eq. (6) up to y ~ 0.33 (the composition of the binary glass studied here), where Eq. (6) shows that 50% of the B would be converted to B^4 units. Note that Eq. (4) and Eq. (6) have the same form because one Na_2O formula converts two borons to the B^4 SRO, but there are 2 B in each B_2O_3 formula unit.

$$f(B^4) = \left(\frac{2y}{2(1-y)}\right) = \left(\frac{y}{1-y}\right) \qquad \text{Eq. (6)}$$

This maximum of ~ 0.5 in the fraction of B^4 units is thought to occur because the charged B^4 SRO units would necessarily have to bond to one another at higher fractions of B^4 units and this has been termed the boron avoidance principle.[57, 58] Beyond this maximum, the B^4 fraction decreases to zero at the limit of the glass forming range, y = 0.75 using normal quenching techniques. In this compositional range, $0.33 < y < 0.75$, the added Na_2O creates trigonal boron SRO units with progressively decreasing numbers of BOs, B^2, B^1 and B^0. It is believed that the wide range of glass formation in these NB glasses arises from the buildup of BOs through the creation of B^4 units from 1.5 BO/B at y = 0 to ~1.75 BO/B at the B^4 maximum, y ~ 0.33. Beyond this maximum, while NBOs are created, there is still a non-zero fraction of B^4 units which in turn creates some level of glass network connectivity that is absent in the NG and NS systems at such high levels of Na_2O. All of the boron SRO units in this system are given in Fig. (1).

The NB binary glass corresponding to the system studied here is $0.33Na_2O + 0.67B_2O_3$ and as described above consists primarily of B^3 and B^4 units in approximately

equal fractions. However, upon closely examining this composition, both as shown by us and others, it does not reach the full 50% conversion fraction of B^4 units.[35, 59] As such, it is necessary to include a small fraction of B^2 units, ~ 0.05, to account for the charge balance for the small fraction of Na_2O not incorporated into B^4 units.

Finally, it must be recognized that the approach used here is that we are determining and characterizing only the SRO structural units present in the glasses. The formation of intermediate range order (IRO) super-structural units, as they are called, are well known in NB glasses.[56, 60, 61] We restrict our focus to only those SRO units formed in these glasses, those shown in Fig. (1), because we can directly and quantitatively determine the B SRO units from the ^{11}B MAS-NMR and the Ge SRO units from charge and composition balance criterion. We will examine, characterize, and report on the structure of these glasses on longer length scales in future publications. It is noted again, that in this and other studies of MGF systems we have completed, we have purposefully selected the compositional series along the $0.2Na_2O + 0.8[xBO_{3/2} + (1-x)GeO_2]$ so that there is a one-to-one substitution of Ge by B.[22, 26, 27, 62]

2.4 Experimental

2.4.1 Sample Preparation

Reagent grade sodium carbonate Na_2CO_3 (Sigma Aldrich 99.97%), boric acid H_3BO_3 (Sigma Aldrich 99.5%) and germanium oxide GeO_2 (Sigma Aldrich 99.99%) were thoroughly mixed in stoichiometric amounts in a platinum crucible. The mixture was then melted at 1,000 to 1,200 ^oC, depending on composition, higher temperatures were used for the GeO_2 rich compositions, for 5 minutes and air quenched to room temperature. Weight loss measurements were used to ensure the appropriate amount of

carbon dioxide and water, and no more, were removed from the sample. The composition was remelted at the same temperature for another five minutes and glass samples were quenched in a brass mold held at 50 ^{o}C below the glass transition temperature (Tg), held for one hour to fully anneal the glass, then cooled at 5 ^{o}C/min to room temperature. The samples were slightly hygroscopic and were stored in a nitrogen glovebox in between experiments. It is noted that in our lab using our facilities, we could not melt nor cast the pure $0.2Na_2O + 0.8GeO_2$ x = 0 sample. New attempts are being made on this composition and will be reported on in the future.

2.4.2 Raman Spectroscopy

The Raman spectra were obtained using a Renishaw inVia spectrometer with a 488 nm laser. An internal Si reference was used to calibrate the instrument. The Si reference mode appeared at 520 $cm^{-1} \pm 1$ cm^{-1} for each calibration run. Due to the hygroscopic nature of these samples, the glass disc samples were polished to remove surface impurities prior to measurement. Samples were placed directly on the stage under a 5x objective. Spectra were obtained from 150 to 1700 cm^{-1}, co-adding 5 to 10 accumulations with acquisition times of 10 to 60 seconds to achieve comparable signal-to-noise ratios.

2.4.3 Infrared Spectroscopy

A Bruker IFS 66 v/s infrared (IR) spectrometer was used to obtain the mid-IR spectra from 4000 to 400 cm^{-1} using a KBr beam splitter. CsI pellets were prepared inside a nitrogen glovebox using ~2-3 wt % of crushed glass sample diluted and hand milled into about 200 mg. of CsI. For each spectra, 32 scans were collected at a resolution of 4 cm^{-1}. Samples were loaded into the IR spectrometer through a nitrogen atmosphere mini-glovebox attached to the spectrometer and spectra were collected under vacuum.

2.4.4 Solid State MAS-NMR

The ^{11}B MAS-NMR spectra were collected using a Bruker Avance II 600 MHz solid state NMR at room temperature. The samples were packed into 4 mm zirconia rotors. Samples were spun at 12 kHz to reduce the chemical shift anisotropy (CSA) and to spin out the spinning side bands sufficiently away from the central lines. It was seen that the baseline was broadened from interaction with dilute boron species in the NMR probe itself. Therefore, a spin-echo sequence was used to reduce this interference and provide more accurate spectra. A pulse width of 2.5 μs and a delay time of 3 sec for 512 scans was used for each spectrum. All spectra were indirectly referenced using the IUPAC convention by establishing a relative reference frequency using tetramethylsilane.[63]

Finally, the ^{11}B NMR spectra were analyzed using the DMFit software package using combined Gaussian and Lorentzian line shapes to fit the spectral envelope for the tetrahedral boron SRO units and Quad MAS ½ software package was used to fit the quadrupolar broadened line shapes of the trigonal boron units.[64] Due to the low signal quality of the of ^{73}Ge nuclei (as described above), no germanium NMR spectra were obtained for this experiment.

2.5 Results

2.5.1 Raman Spectra of the Glasses

The Raman spectra for the NBGO glass series are given in Fig. (2). The pure NB glass, at x = 1.0, contains a prominent peak at 765 cm^{-1} arising from a six-membered ring with two B^4 SRO units and two B^3 SRO units known as the diborate, $Na_2O•2B_2O_3$, structure.[60, 61, 65] A very weak peak is observed at ~465 cm^{-1} and corresponds to the

triborate, $Na_2O•3B_2O_3$, structure which is a mixture of one B^3 and two B^4 SRO units.[60, 61] While the intensity of the peak at 465 cm^{-1} is weak at x = 1.0, it grows in intensity as the borate concentration decreases, x → 0. This peak becomes difficult to resolve from the increasing intensity of the peak at 540 cm^{-1}, which is associated with Ge SRO units (see below) at lower x-values. Isolated diborate units, $2Na_2O•2B_2O_3$, that consist of two B^2 SRO units with one NBO each that replace the B^3 groups of the normal diborate group and the two original B^4 SRO units have a vibrational mode at 575 cm^{-1} in the compositional range of x = 0.6 to 1.0. However, these are also difficult to resolve from the adjacent peak of the BO on Ge SRO units. Finally, the peak at 1,430 cm^{-1} is due to stretching of NBOs on B^2 units, $=B\text{-}O^-$, units within large borate units suggesting that an NBO exists on boron SRO units, further supporting the existence of the isolated diborate groups described above.[60] This peak is the most intense when x = 1.0 and decreases in intensity to ~ 0 at x ~ 0.6.

The Raman spectrum of the pure NG glass, at x = 0.0, contains a peak located at 860 cm^{-1} corresponding to the $Ge\text{-}O^-$ mode of Ge^3 SRO unit.[40-42] This mode gradually shifts to ~840 cm^{-1} as borate is added to the glass composition. The peak reaches a maximum intensity at x = 0.6 and decreases to zero intensity at x = 1.0, the pure NB glass. A second intense peak appears at 557 cm^{-1} and is assigned to the ≡Ge-O-Ge≡ BO mode in the pure NG glass and this mode shifts to ~580 cm^{-1} as x increases.[40, 41, 46] This shift in peak positions to higher wavenumbers suggests a change in the Ge environments as the second coordination sphere begins to add B with increasing x. A weak shoulder at 600 cm^{-1} is seen at the x = 0.1 composition. This shoulder has been seen in previous studies by Ivanova et. al. [31] and Verweij[33] at similar modifier contents for NG glasses.

These authors have associated this mode at 600 cm^{-1} with the symmetrical stretch of a small amount of GeO_6 octahedra.[40, 41] Indeed, many studies have found that at low modifier content the structure of NG glasses consists of GeO_4 tetrahedra connected by $GeO_{6/2}$ octahedra, the enneagermanate unit, with all BOs.[40, 41, 47] However, Sharma and Matson have studied sodium aluminogermanate (NAG) glasses and found that there was no evidence in the Raman spectra to support the existence of GeO_6 in this glassy system.[66] A likely reason for this is that Al preferentially reacts with the added Na_2O, as it does in low alkali sodium aluminosilicate (NAS) glasses, to form AlO_4^{-1} units[67-69]. Another peak seen in the germanate rich glasses, $x < 0.5$, appears in the low wavenumber shift region at 330 cm^{-1} and has been assigned to Ge motions involving mode admixture with BO motions.[42, 48, 66, 70] This peak is rather weak in intensity compared to the other peaks in the Raman spectra of the pure germanium glass at $x = 0.0$ where it is most intense and slowly decreases in intensity until at $x = 1.0$ where none exists.

2.5.2 IR Spectra of the Glasses

The IR spectra of the NBGO glasses in this series are shown in Fig. (3). An intense, broad peak occurs between 1,200 to 1,450 cm^{-1} and is assigned to the boron-oxygen stretching mode of the B^3 SRO units.[60] The intensity of this peak is greatest at $x = 1$ and decreases until it vanishes at $x = 0.0$, where no borate is present, indicating that it is a pure borate vibration. A second broad peak centered between 785 to 1,220 cm^{-1} is assigned to the boron-oxygen stretch in a B^4 SRO unit.[54] It is the most intense at $x = 1.0$ and decreases with decreasing borate concentration, $x \rightarrow 0$. At lower borate concentrations, this peak appears as a shoulder to an adjacent peak assigned (see below) to a vibrational mode of a Ge SRO unit. A low intensity peak located at lower

frequencies at ~720 cm^{-1} is attributed to the B-O-B BO bending mode in the network.[55, 71, 72] This peak is only seen in the boron-rich compositional range, x = 0.8 to 1.0. At lower concentrations, an intense peak assigned to a Ge mode (see below) grows in intensity, overtaking this peak.

For the other binary member glass where x = 0, the pure NG glass, the first main spectral feature in the IR spectra is seen as a broad peak centered around 800 cm^{-1} and is assigned to the asymmetric stretching of the GeO_4 tetrahedra.[45, 46] The intensity of this peak decreases with the increase of the borate concentration. The peak seen around 400 to 600 cm^{-1} is assigned to ≡Ge-O-Ge≡ BO mode.[46] This peak is most intense at x = 0.0 and decreases in intensity until x = 0.7 and is not seen thereafter in the IR spectra.

2.5.3 ^{11}B MAS-NMR Spectra

The ^{11}B MAS NMR spectra are shown in Fig. (4). No data were obtained for x = 0 glass, of course, since no boron exists in the pure NG glass. Starting with the boron rich end, x = 1.0, the first spectral feature is a centrally symmetric peak centered at ~1 ppm. This peak is assigned to the B^4 SRO units.[27, 73] The presence of this peak can be seen throughout the series of compositions. A quadrupolar broaden peak can be seen centered ~12 ppm and is assigned to the B^3 units with both BOs and NBOs.[74] This peak is of very weak intensity at lower borate concentrations where most the spectral intensity is associated to the B^4 SRO unit, but it does emerge around x = 0.6 and continues to grow in intensity with increasing borate concentration, x → 1. As described above, the binary NB glass is found to have approximately equal proporitons of B^3 and B^4 SRO units with a minor concentration of B^2 required for charge neutrality when the B^4 fraction does not exactly increase to 0.5 as predicted by Eq. (6) above.

From the ^{11}B MAS-NMR spectra, the chemical shift of the B^4 SRO unit decreases from higher ppm (~1.1 ppm) to lower ppm (~0.22 ppm) with addition of borate. This is explained by the systematic replacement of germanium by boron within the second coordination sphere, ≡B-O-Ge≡ to ≡B-O-B=. When x is just greater then 0, e.g., x = 0.1, most of the atoms in the second coordination sphere of the B^4 SRO unit are Ge atoms, such as B^{4Ge}. With the addition of borate, boron starts to replace the germanium causing the central boron atom to be more shielded shifting the ^{11}B resonance downfield. In between the two binary systems, $0 < x < 1$, there should be a mixture of B and Ge atoms in the second coordination sphere creating a series of species of the form $B^{4(1-x)Ge + 4xB}$, where there are 4(1-x) Ge and 4xB atoms in the second coordination sphere around the B center. The continuous shifting of this peak to downfield frequencies (in contrast to an obvious stepwise shift at intermediate compositions) of the B^4 peak suggests that there is a uniform and continuous replacement of Ge atoms for B atoms in the second coordination sphere and suggests a simple linear compositional depenndence. This behavior appears to be unlike that in the analogous NBSO system $0.2Na_2O + 0.8[xBO_{3/2} + (1-x)SiO_2]$ where a discontinuous change in the chemical shift is seen from ~-3.5 to ~-1.5 at x ~ 0.4 for the B^4 units.[75]

The deconvolution of the ^{11}B MAS-NMR spectra was performed to quantify the fraction of B in the various SRO units, predominantly, B^4, B^3 for the mixed $x \neq 0$ and 1 glasses and a very small fraction of B^2 only for the pure sodium borate glass at x = 1. An example of the deconvolution of a spectrum is given in Fig. (5). Since the bonding environment of B^4 SRO units is symmetric, the asymmetry parameter, η, describing the

magnitude of the quadrupolar broadening of the B resonance peak, is very small[76, 77]. Consequently, the B^4 peaks were fit using a single Gaussian (non-broadened) curve. For the broad peak centered at ~12 ppm assigned to the trigonal B SRO units in the glass, two quadrupolar peaks were used to fit the trigonal boron sites. One is assigned to the asymmetric B^2 SRO unit having one NBO and the other for the symmetric B^3 SRO unit with no NBOs.[74, 78] The fitting parameters of the asymmetric B^2 and B^3 symmetric site were determined to be $C_q = 2.9 \pm 0.2$ MHz and $\eta = 0.16 \pm 0.03$, and $C_q = 2.5 \pm 0.1$ MHz and $\eta = 0.34 \pm 0.03$, respectively.

2.6 Discussion

The composition dependence of all of the B and Ge SRO units in these glasses has been determined by combining the processes of identifying and confirming the various SRO units in the IR and Raman spectra with the process of deconvoluting the ^{11}B MAS NMR spectra to determine the factions of the various B SRO units in the glass. The corresponding fractions of the various Ge SRO units identified through the IR and Raman spectra were quantified using the charge compensation requirements defined above.

From this analysis, the overall dominant SRO structural change in these glasses as x changes from x = 0 to x =1 is the formation of a large fraction of B^4 units through the Lewis acid (B^3 SRO unit) reaction with the Lewis base $Ge^{3\,(1-)}$ NBO SRO unit and the $Ge^{6(-2)}$ NBO unit given below in Eqs. (7) and (8).

$$Ge^3 + B^3 \rightarrow Ge^4 + B^4 \qquad \text{Eq. (7)}$$

$$Ge^6 + B^3 \rightarrow Ge^3 + B^4 \qquad \text{Eq. (8)}$$

We have seen and characterized this same behavior, Eq. (7) only since Si^6 SRO units do not exist in NBS glasses at ambient pressures, in analogous and iso-

compositional $0.2Na_2O + 0.8[xBO_{3/2} + (1-x)SiO_2]$ glasses, where the added NB eliminates NBOs on the Si^3 groups to form B^4 groups and Si^4 as described by Eq. (7).[75]

The fraction of B^4 SRO units in the ternary MGF glasses reaches a fraction, 0.66, higher than the boron-avoidance principle limit of 0.5 in the binary NB glasses[79], see Fig. (6), because the overall fraction of the B glass former is only equal to 1 for the x = 1 composition. Therefore, because the formation reaction of Eq. (7) shows that the B^4 units at low x values will primarily have uncharged Ge^4 units in their second coordination spheres, this decreases the number and probability of the charged B^4 SRO units bonding to other charged B^4 SRO units and therefore pushes the B^4 to B^4 bonding avoidance criterion to higher overall B^4 fractions.

At the borate rich end of the series, $x \rightarrow 1$, we see that B^3 and B^4 SRO units are the primary B SRO units with the existence of a small amount of B^2 units present, as described above, to maintain charge neutrality in the presence of a less than stoichiometric amount (0.5) B^4 units. This is consistent with the Raman and ^{11}B MAS NMR spectra which shows the existence of isolated diborate B^2 groups and an asymmetric quadrupolar broadened peak, respectively. The quantification of B^2 units from ^{11}B NMR (~0.05) is consistent with literature where B^2 fractions are reported to be ~0.05 for this same faction of Na_2O.[59]

As expected, moving to the smaller x, germanate-rich, glasses, the fraction of B^2 units become much less until x ~ 0.5, disappearing entirely. Moving further to the germanate-rich glass, the presence of Ge^3 and Ge^4 SRO units dominate. As described above, there is a small fraction of Ge^6 units for the MGF glasses with $0 < x < 0.2$.

2.6.1 Quantification of the fractions of the SRO units

From the deconvolution of the quantitative ^{11}B MAS-NMR spectra, charge neutrality, and atom fraction requirements (0.8x is the total amount of B, 0.8(1-x) is the total amount of Ge, and 1.8-0.4x is the total amount of O), the fractions of all of the SRO units in these glasses were determined and are shown in Fig. (6). In Fig. (6), the sum of all of the fractions of varous SRO units at any one composition is equal to 1. The number moles of any B SRO unit in the glass is the fraction of that specific SRO unit times 0.8*x. Likewise, the amount of moles of any Ge SRO unit in the glass is the fraction of that specific SRO unit times 0.8*(1-x).

First, it can be seen that Ge^6 units formed in the binary NG glasses, as described above, decrease in a sharp linear fashion until x = 0.3 following Eq. (8), where the fraction reaches zero in correspondence with the disappearance in the Raman mode at 600 cm^{-1} in the Raman spectra of these glasses. The composition dependence of the fraction of Ge^3 units has three different compositional regions. First, at small $x < 0.3$, there is a rapid increase up to a maximum at x = 0.3 as predicted by Eq. (8). For $0.3 < x < 0.6$, the fraction of Ge^3 SRO units decrease less quickly than they do in the third compositional range of behavior, $0.6 < x < 1.0$. In the intermediate range of x, the competition between forming Ge^3 units from Ge^6 units in Eq. (7) and the Ge^3 units being consumed in Eq. (8) is approximately balanced. Finally, the fraction of the Ge^4 units also have three corresponding compositional behaviors in the same compositional ranges. In the first range, $x < 0.3$, the fraction of Ge^4 decreases simply as expected from the composition with a slope of -1. This suggests that all of the compositional changes in this region involving Ge are restricted to equal molar exchanges between the Ge^6 and the Ge^3 units according to Eq. (6). In the intermediate compositional range, $0.3 < x < 0.6$, there is

a slowing in the decrease of the fraction of the Ge^4 units as the fraction of Ge^6 units decrease to zero, and Eq. (7) becomes the dominant compositional change. Finally, in the compositional range $0.6 < x$ the rate of decrease in the fraction of Ge^4 units returns to -1 again reflecting simply that total Ge content in the glasses is decreasing to zero at this rate. This behavior is consistent with reaction Eq. (8) similar to Eq. (7) but where one B^3 SRO group reacts with the doubly negatively charged Ge^6 to form a singly charged Ge^3 and B^4 units.

Once all of the Ge^6 units are consumed, at $x = 0.3$, then the fraction of Ge^3 SRO units would commence to decrease as they are converted to Ge^4 SRO units by B^3 SRO units according to reaction Eq. (6). This would explain the slowing in the rate of decrease of the fraction of Ge^4 SRO units in the compositional region $0.3 < x < 0.6$ as they are formed by the conversion of Ge^3 SRO units to Ge^4 SRO units. Beyond $x = 0.6$, nearly all of the Ge^3 SRO units have been converted to Ge^4 SRO units and as such the fraction of Ge^4 SRO units begins to once again decrease with a slope of -1 indicative of a simple depletion of the total amount of Ge in the glass as 1-x. A dashed line has been added to Fig. (6) of slope of -1 to show the expected maximum rate of Ge depletion in the glass series as $x \rightarrow 1$.

The compositional trends of the B SRO units are interrelated with the compositional changes described above of the Ge SRO units. So, as Ge^6 SRO units are converted to Ge^3 units, so a B^3 unit is converted to a B^4 unit. This reaction, Eq. (8), appears to be preferred over reaction Eq. (7) in the Ge rich compositional region since the fraction of Ge^3 actually increases rather than decreases as expected by reaction Eq. (7). This conversion reaction causes the B^4 units to increase strongly in concentration

compared to the B^3 SRO units. Once all of the Ge^6 units are converted to Ge^3 units, the Ge^3 units are then converted to Ge^4 units according to reaction Eq. (7) generating more B^4 units. Finally, once nearly all of the Ge^3 SRO units are converted to Ge^4 units, the rate of formation of B^4 units must necessarily decrease. Indeed, beyond x = 0.6, the fraction of B^3 must necessarily increase while the B^4 fraction must decrease and the two compositional curves cross over at x ~ 0.5. At x = 1.0, the fractions of the B^4 and B^3 converge to values of 0.45 and 0.50, respectively, observed by others for the binary sodium borate glass.[35, 59] At this x =1 composition, the 0.45 fraction of B^4 requires a fraction of 0.05 of singly charged B^2 units, as seen in Fig. (6), for charge neutrality. In addition, the fraction of the remaining Ge^3 and Ge^4 units must by compositional necessity vanish to zero at x = 1.

There is a significant crossover in the structural conversion in these glasses at x ~ 0.6. At this crossover point, B becomes the dominant glass former and Ge becomes the minority glass former. Assuming the expression $B^{4(1-x)Ge + 4xB}$, see above, applies to the compositions here, the species in the second coordination sphere is random, for glasses with x > 0.5, this expression shows that 2 or more of the second coordination sphere glass formers will be B. Returning to Fig. (7), the B^4 fraction at 0.5 is ~ 0.35 and the fraction of B^3 units is ~ 0.15. Hence, 4*0.35 = 1.4 (less than 50%) of the next nearest glass formers will be boron. Below this fraction, more than 50% of the next nearest glass formers will on average be Ge. This fraction of next nearest neighbor borons will increase up to just under 2 at the pure NB end of the compositional series.

It is significant to note that the relatively large amount of Ge^6 SRO units in the pure binary NG glass cannot be ignored even though they exist only over a narrow

compositional range from x = 0 to 0.2 in the ternary MGF glasses. In the pure NG glass, the fraction (0.2) of the Ge^6 SRO units is twice the fraction (0.1) of Ge^3, but because of their -2 charge, this same fraction of Ge^6 SRO units possess four times the amount of Na^+ ions. The fraction of 0.2 reported here agrees with the studies from Verweij and Du.[39, 40]

Finally, as discussed above, the initial increase in the fraction of the Ge^3 SRO units must come from the conversion of Ge^6 SRO units into Ge^3 SRO units. However, as the dashed line added to Fig. (6) shows, the rate of decrease of the fraction of the Ge^6 SRO units is not a linear one to one with the addition of added B, x. However, the fraction of Ge^4 SRO units do exhibit a linear decrease with x indicating that the only chemical reactions in the $0 < x < 0.3$ region is the conversation reaction Eq. (8). The fraction of Ge^4 SRO units must go down linearly with x as there is a conservation of Ge in the reaction Eq. (8). The conversion of Ge^6 SRO units to Ge^3 units therefore does not have unit slope with x because as Fig. (6) shows, the fraction of neutral B^3 SRO units is not zero. There is a non-zero amount of B remaining after reaction Eq. (8) completes. The ratio between the fraction of B^4 and B^3 groups is higher than that in binary sodium borate glasses because as describe above, the boron avoidance principle can be active to higher total fraction of B since there are fewer B centers available in these ternary glasses to be present in the second coordination sphere of these glasses. However, the conversion of B^3 to B^4 units is not complete and the equilibrium constant governing this reaction is therefore large, but not infinite.

Finally, unlike the binary NG glasses that can support a high fraction of Ge^6 units in the presence of charged Ge^3 units, the ternary NBGO glasses appear to not to support a high fraction of charged Ge^6 units in the presence of charged B^4 units.

2.7 Conclusions

NBGE glasses in the $0.2Na_2O + 0.8[xBO_{3/2} + (1-x)GeO_2]$ series were characterized by Raman, Infrared, and ^{11}B MAS-NMR spectroscopies. It was shown that upon mixing of the NG (sodium enneagermanate) and the NB (sodium diborate) glasses, that an unequal sharing of sodium ions occurs with preference being for the two systems to react to form high fractions of B^4 SRO units. A SRO structure model was proposed based on the spectroscopic evidence which incorporated Ge^6 units seen for glasses with $x \leq 0.2$. The Ge^6 units appear to be stronger Lewis base than the Ge^3 units as the added Lewis acid B^3 preferentially reacts with Ge^6 units. Only after all of the Ge^6 units have been consumed do the added B^3 units then react with the remaining Ge^3 units in a manner similar to that observed in NBS glasses.

2.8 Acknowledgements

The work at ISU was supported in part by NSF grants DMR 0710564 and DMR1304977 and at Coe College by DMR 1407404 The authors would like to thank and acknowledge the help and assistance of Professor Aaron Rossini and Dr. Sarah Cady for their continuing and sustained help with the collection and data analysis of the ^{11}B MAS-NMR spectra.

2.9 References

1. Armand, M.; Tarascon, J. M. Building better batteries. *Nature* **2008,** 451, 652 DOI: 10.1038/451652a.

2. Hodge, I. M.; Ingram, M. D.; West, A. R. Impedance and modulus spectroscopy of polycrystalline solid electrolytes. *Journal of Electroanalytical Chemistry and Interfacial Electrochemistry* **1976,** 74 (2), 125-143.

3. Inaguma, Y.; Liquan, C.; Itoh, M.; Nakamura, T.; Uchida, T.; Ikuta, H.; Wakihara, M. High ionic conductivity in lithium lanthanum titanate. *Solid State Communications* **1993,** 86 (10), 689-693 DOI: https://doi.org/10.1016/0038-1098(93)90841-A.

4. Monroe, C.; Newman, J. Dendrite Growth in Lithium/Polymer Systems: A Propagation Model for Liquid Electrolytes under Galvanostatic Conditions. *Journal of The Electrochemical Society* **2003,** 150 (10), A1377-A1384.

5. Porz, L.; Swamy, T.; Sheldon, B. W.; Rettenwander, D.; Frömling, T.; Thaman, H. L.; Berendts, S.; Uecker, R.; Carter, W. C.; Chiang, Y.-M. Mechanism of Lithium Metal Penetration through Inorganic Solid Electrolytes. *Advanced Energy Materials* **2017,** 7 (20), 1701003-n/a DOI: 10.1002/aenm.201701003.

6. Slater, M. D.; Kim, D.; Lee, E.; Johnson, C. S. Sodium-Ion Batteries. *Advanced Functional Materials* **2013,** 23 (8), 947-958 DOI: 10.1002/adfm.201200691.

7. Park, Y.-U.; Seo, D.-H.; Kwon, H.-S.; Kim, B.; Kim, J.; Kim, H.; Kim, I.; Yoo, H.-I.; Kang, K. A New High-Energy Cathode for a Na-Ion Battery with Ultrahigh Stability. *Journal of the American Chemical Society* **2013,** 135 (37), 13870-13878 DOI: 10.1021/ja406016j.

8. Yabuuchi, N.; Kajiyama, M.; Iwatate, J.; Nishikawa, H.; Hitomi, S.; Okuyama, R.; Usui, R.; Yamada, Y.; Komaba, S. P2-type Nax[Fe1/2Mn1/2]O2 made from earth-abundant elements for rechargeable Na batteries. *Nat Mater* **2012,** 11 (6), 512-517 DOI: http://www.nature.com/nmat/journal/v11/n6/abs/nmat3309.html#supplementary-information.

9. Carmichael, R. S. *Practical Handbook of Physical Properties of Rocks and Minerals*. CRC Press Inc.: Boca Raton, 1989.

10. Ene-Parent, J.; Zikovsky, L. Neutron activation analysis of laundry dryer lint. *Journal of Radioanalytical and Nuclear Chemistry* **2014,** 247 (1), 197-198 DOI: 10.1023/A:1006712408990.

11. Suo, L.; Hu, Y.-S.; Li, H.; Armand, M.; Chen, L. A new class of Solvent-in-Salt electrolyte for high-energy rechargeable metallic lithium batteries. *Nature Communications* **2013,** 4, 1481 DOI: 10.1038/ncomms2513 https://www.nature.com/articles/ncomms2513#supplementary-information.

12. Wang, Q.; Ping, P.; Zhao, X.; Chu, G.; Sun, J.; Chen, C. Thermal runaway caused fire and explosion of lithium ion battery. *Journal of Power Sources* **2012,** 208 (Supplement C), 210-224 DOI: https://doi.org/10.1016/j.jpowsour.2012.02.038.

13. Wen, J.; Yu, Y.; Chen, C. A Review on Lithium-Ion Batteries Safety Issues: Existing Problems and Possible Solutions. *Materials Express* **2012,** 2 (3), 197-212 DOI: 10.1166/mex.2012.1075.

14. Lisbona, D.; Snee, T. A review of hazards associated with primary lithium and lithium-ion batteries. *Process Safety and Environmental Protection* **2011,** 89 (6), 434-442 DOI: https://doi.org/10.1016/j.psep.2011.06.022.

15. Tobishima, S.-i.; Takei, K.; Sakurai, Y.; Yamaki, J.-i. Lithium ion cell safety. *Journal of Power Sources* **2000,** 90 (2), 188-195 DOI: https://doi.org/10.1016/S0378-7753(00)00409-2.

16. Scrosati, B.; Hassoun, J.; Sun, Y.-K. Lithium-ion batteries. A look into the future. *Energy & Environmental Science* **2011,** 4 (9), 3287-3295 DOI: 10.1039/C1EE01388B.

17. Kharton, V. V.; Marques, F. M. B.; Atkinson, A. Transport properties of solid oxide electrolyte ceramics: a brief review. *Solid State Ionics* **2004,** 174 (1), 135-149 DOI: https://doi.org/10.1016/j.ssi.2004.06.015.

18. Hayashi, A.; Ohtomo, T.; Mizuno, F.; Tadanaga, K.; Tatsumisago, M. All-solid-state Li/S batteries with highly conductive glass–ceramic electrolytes. *Electrochemistry Communications* **2003,** 5 (8), 701-705 DOI: https://doi.org/10.1016/S1388-2481(03)00167-X.

19. Kalnaus, S.; Tenhaeff, W. E.; Sakamoto, J.; Sabau, A. S.; Daniel, C.; Dudney, N. J. Analysis of composite electrolytes with sintered reinforcement structure for energy storage applications. *Journal of Power Sources* **2013,** 241 (Supplement C), 178-185 DOI: https://doi.org/10.1016/j.jpowsour.2013.04.096.

20. Rosso, M.; Brissot, C.; Teyssot, A.; Dollé, M.; Sannier, L.; Tarascon, J.-M.; Bouchet, R.; Lascaud, S. Dendrite short-circuit and fuse effect on Li/polymer/Li cells. *Electrochimica Acta* **2006,** 51 (25), 5334-5340 DOI: https://doi.org/10.1016/j.electacta.2006.02.004.

21. Watson, D. E.; Martin, S. W. Short range order characterization of the Na2S+SiS2 glass system using Raman, infrared and 29Si magic angle spinning nuclear magnetic

resonance spectroscopies. *Journal of Non-Crystalline Solids* **2017,** 471 (Supplement C), 39-50 DOI: https://doi.org/10.1016/j.jnoncrysol.2017.04.032.

22. Bischoff, C. The Mixed Glass Former Effect in $0.5Na_2S+0.5[xGeS_2+(1-x)PS_{5/2}]$ Glasses. Iowa State University, Ames, Iowa, 2013.

23. Christensen, R.; Olson, G.; Martin, S. W. Ionic Conductivity of Mixed Glass Former 0.35Na2O + 0.65[xB2O3 + (1 – x)P2O5] Glasses. *The Journal of Physical Chemistry B* **2013,** 117 (51), 16577-16586 DOI: 10.1021/jp409497z.

24. Deshpande, V. K.; Pradel, A.; Ribes, M. The mixed glass former effect in the Li2S : SiS2 : GeS2 system. *Materials Research Bulletin* **1988,** 23 (3), 379-384 DOI: http://dx.doi.org/10.1016/0025-5408(88)90012-8.

25. Martin, S. W.; Bischoff, C.; Schuller, K. Composition Dependence of the Na+ Ion Conductivity in 0.5Na2S + 0.5[xGeS2 + (1 – x)PS5/2] Mixed Glass Former Glasses: A Structural Interpretation of a Negative Mixed Glass Former Effect. *The Journal of Physical Chemistry B* **2015,** 119 (51), 15738-15751 DOI: 10.1021/acs.jpcb.5b07383.

26. Pradel, A.; Rau, C.; Bittencourt, D.; Armand, P.; Philippot, E.; Ribes, M. Mixed Glass Former Effect in the System 0.3Li2S−0.7[(1−x)SiS2−xGeS2]: A Structural Explanation. *Chemistry of Materials* **1998,** 10 (8), 2162-2166 DOI: 10.1021/cm980701j.

27. Christensen, R.; Olson, G.; Martin, S. W. Structural Studies of Mixed Glass Former 0.35Na2O + 0.65[xB2O3 + (1 – x)P2O5] Glasses by Raman and 11B and 31P Magic Angle Spinning Nuclear Magnetic Resonance Spectroscopies. *The Journal of Physical Chemistry B* **2013,** 117 (7), 2169-2179 DOI: 10.1021/jp308494a.

28. Storek, M.; Adjei-Acheamfour, M.; Christensen, R.; Martin, S. W.; Böhmer, R. Positive and Negative Mixed Glass Former Effects in Sodium Borosilicate and Borophosphate Glasses Studied by 23Na NMR. *The Journal of Physical Chemistry B* **2016,** 120 (19), 4482-4495 DOI: 10.1021/acs.jpcb.6b00482.

29. Christensen, R.; Byer, J.; Olson, G.; Martin, S. W. The glass transition temperature of mixed glass former 0.35Na2O+0.65[xB2O3+(1−x)P2O5] glasses. *Journal of Non-Crystalline Solids* **2012,** 358 (4), 826-831 DOI: http://dx.doi.org/10.1016/j.jnoncrysol.2011.12.068.

30. Wang, W.; Christensen, R.; Curtis, B.; Martin, S. W.; Kieffer, J. A new model linking elastic properties and ionic conductivity of mixed network former glasses. *Phys. Chem. Chem. Phys.* **2017**, Ahead of Print DOI: 10.1039/c7cp04534d.

31. Wang, W.; Christensen, R.; Curtis, B.; Hynek, D.; Keizer, S.; Wang, J.; Feller, S.; Martin, S. W.; Kieffer, J. Elastic properties and short-range structural order in mixed network former glasses. *Phys. Chem. Chem. Phys.* **2017,** 19 (24), 15942-15952 DOI: 10.1039/c6cp08939a.

32. El; Egili, K.; Doweidar, H. Density and dc conductivity of Li2O–Bi2O3–B2O3 and Li2O–GeO2–B2O3 glasses. *Physics and Chemistry of Glasses* **1998,** 39 (6), 332-337.

33. Mansour, E. Raman spectra and density of Li2O–B2O3–GeO2 glasses with high Li2O content. *Physica B: Condensed Matter* **2010,** 405 (1), 281-286 DOI: http://dx.doi.org/10.1016/j.physb.2009.08.074.

34. Błaszczak, K.; Jelonek, W.; Adamczyk, A. Infrared studies of glasses in the Li2O–B2O3–GeO2(SiO2) systems. *Journal of Molecular Structure* **1999,** 511-512 (Supplement C), 163-166 DOI: https://doi.org/10.1016/S0022-2860(99)00155-6.

35. Bray, P.; O'keefe, J. Nuclear magnetic resonance investigations of the structure of alkali borate glasses. *J Phys. Chem. Glasses* **1963,** 4 (2), 37-46.

36. Michaelis, V. K.; Kroeker, S. 73Ge Solid-State NMR of Germanium Oxide Materials: Experimental and Theoretical Studies. *The Journal of Physical Chemistry C* **2010,** 114 (49), 21736-21744 DOI: 10.1021/jp1071082.

37. Michaelis, V. K.; Aguiar, P. M.; Terskikh, V. V.; Kroeker, S. Germanium-73 NMR of amorphous and crystalline GeO2. *Chemical Communications* **2009,** (31), 4660-4662 DOI: 10.1039/B906642J.

38. Kiczenski, T. J.; Ma, C.; Hammarsten, E.; Wilkerson, D.; Affatigato, M.; Feller, S. A study of selected physical properties of alkali germanate glasses over wide ranges of composition. *Journal of Non-Crystalline Solids* **2000,** 272 (1), 57-66 DOI: http://dx.doi.org/10.1016/S0022-3093(00)00158-7.

39. Du, L.-S.; Stebbins, J. F. Oxygen Sites and Network Coordination in Sodium Germanate Glasses and Crystals: High-Resolution Oxygen-17 and Sodium-23 NMR. *The Journal of Physical Chemistry B* **2006,** 110 (25), 12427-12437 DOI: 10.1021/jp0615510.

40. Verweij, H.; Buster, J. H. J. M. The structure of lithium, sodium and potassium germanate glasses, studied by Raman scattering. *Journal of Non-Crystalline Solids* **1979,** 34 (1), 81-99 DOI: http://dx.doi.org/10.1016/0022-3093(79)90008-5.

41. Ivanova, T. N.; Bykov, V. N. Raman spectroscopy of glasses and melts of the Na2O-GeO2 system. *Russian Metallurgy (Metally)* **2010,** 2010 (8), 678-680 DOI: 10.1134/S0036029510080033.

42. Henderson, G. S.; Fleet, M. E. The structure of glasses along the Na_2O-GeO_2 join *Journal of Non-Crystalline Solids* **1991,** 134, 259-269.

43. Henderson, G. S.; Wang, H. M. Germanium coordination and the germanate anomaly. *European Journal of Mineralogy* **2002,** 14 (4), 733-744 DOI: 10.1127/0935-1221/2002/0014-0733.

44. Karthikeyan, A.; Almeida, R. M. Structural anomaly in sodium germanate glasses by molecular dynamics simulation. *Journal of Non-Crystalline Solids* **2001,** 281 (1), 152-161 DOI: https://doi.org/10.1016/S0022-3093(00)00435-X.

45. Murthy, M. K.; Kirby, E. M. Infra-red spectra of alkali-germanate glasses. *Physics and Chemistry of Glasses* **1964,** 5 (5), 144-146.

46. Efimov, A. M. Infrared spectra, band frequencies and structure of sodium germanate glasses. *Physics and Chemistry of Glasses* **1999,** 40 (4), 199-206.

47. Di Martino, D.; Santos, L. F.; Marques, A. C.; Almeida, R. M. Vibrational spectra and structure of alkali germanate glasses. *Journal of Non-Crystalline Solids* **2001,** 293–295, 394-401 DOI: http://dx.doi.org/10.1016/S0022-3093(01)00690-1.

48. Henderson, G. S.; Soltay, L. G.; Wang, H. M. Q speciation in alkali germanate glasses. *Journal of Non-Crystalline Solids* **2010,** 356 (44–49), 2480-2485 DOI: http://doi.org/10.1016/j.jnoncrysol.2010.03.023.

49. Hussin, R.; Holland, D.; Dupree, R. Does six-coordinate germanium exist in Na2O–GeO2 glasses? Oxygen-17 nuclear magnetic resonance measurements. *Journal of Non-Crystalline Solids* **1998,** 232–234, 440-445 DOI: http://dx.doi.org/10.1016/S0022-3093(98)00394-9.

50. Nanba, T.; Kieffer, J.; Miura, Y. Molecular dynamic simulation on the structure of sodium germanate glasses. *Journal of Non-Crystalline Solids* **2000,** 277 (2), 188-206 DOI: https://doi.org/10.1016/S0022-3093(00)00313-6.

51. Martin, S. W.; Angell, C. A. Glass Formation and Transition Temperatures in Sodium and Lithium Borate and Aluminoborate Melts up to 72 mol.% Alkali. *Journal of Non-Crystalline Solids* **1984**.

52. Yiannopoulos, Y. D.; Chryssikos, G. D.; Kamitsos, E. I. Structure and properties of alkaline earth borate glasses. *Physics and Chemistry of Glasses* **2001,** 42 (3), 164-172.

53. Kasper, J. E.; Feller, S. A.; Sumcad, G. L.; Boyd, D. C. New Sodium Borate Glasses. *Journal of the American Ceramic Society* **1984,** 67 (4), 71-72.

54. Kamitsos, E. I.; Chryssikos, G. D. Borate glass structure by Raman and infrared spectroscopies. *Journal of Molecular Structure* **1991,** 247, 1-16 DOI: http://dx.doi.org/10.1016/0022-2860(91)87058-P.

55. Kamitsos, E. I.; Patsis, A. P.; Chryssikos, G. D. Infrared reflectance investigation of alkali diborate glasses. *Journal of Non-Crystalline Solids* **1993,** 152 (2), 246-257 DOI: http://dx.doi.org/10.1016/0022-3093(93)90258-Y.

56. Jellison, G. E.; Bray, P. J. A structural interpretation of B10 and B11 NMR spectra in sodium borate glasses. *Journal of Non-Crystalline Solids* **1978,** 29 (2), 187-206 DOI: https://doi.org/10.1016/0022-3093(78)90113-8.

57. Loewenstein, W. The Distribution of Aluminum in the Tetrahedra of Silicates and Aluminates. *Am. Mineral.* **1954,** 92, 92-96.

58. Rao, K. J. In *Structural Chemistry of Glasses*; Elsevier, Ed.; Elsevier: Kidlington, Oxford, UK, 2002; Chapter Oxide Glasses, pp 478-482.

59. Zhong, J.; Bray, P. J. Change in boron coordination in alkali borate glasses, and mixed alkali effects, as elucidated by NMR. *Journal of Non-Crystalline Solids* **1989,** 111 (1), 67-76 DOI: https://doi.org/10.1016/0022-3093(89)90425-0.

60. Kamitsos, E. I.; Karakassides, M. A.; Chryssikos, G. D. Vibrational spectra of magnesium-sodium-borate glasses. 2. Raman and mid-infrared investigation of the network structure. *The Journal of Physical Chemistry* **1987,** 91 (5), 1073-1079 DOI: 10.1021/j100289a014.

61. Kamitsos, E. I.; Chryssikos, G. D. Borate glass structure by Raman and infrared spectroscopies. *Journal of Molecular Structure* **1991,** 247 (Supplement C), 1-16 DOI: https://doi.org/10.1016/0022-2860(91)87058-P.

62. Bischoff, C.; Schuller, K.; Dunlap, N.; Martin, S. W. IR, Raman, and NMR Studies of the Short-Range Structures of 0.5Na2S + 0.5[xGeS2 + (1–x)PS5/2] Mixed Glass-Former Glasses. *The Journal of Physical Chemistry B* **2014,** 118 (7), 1943-1953 DOI: 10.1021/jp4111053.

63. Harris, R. K.; Becker, E. D.; Cabral de Menezes, S. M.; Goddfellow, R.; Granger, P. NMR Nomenclature. Nuclear spin properties and conventions for chemical shifts (IUPAC Recommendations 2001). *Pure and Applied Chemistry* **2001,** 73 (11), 1795-1818.

64. Massiot, D.; Fayon, F.; Capron, M.; King, I.; Le Calvé, S.; Alonso, B.; Durand, J.-O.; Bujoli, B.; Gan, Z.; Hoatson, G. Modelling one- and two-dimensional solid-state NMR spectra. *Magnetic Resonance in Chemistry* **2002,** 40 (1), 70-76 DOI: 10.1002/mrc.984.

65. Konijnendijk, W. L.; Stevels, J. M. The structure of borate glasses studied by Raman scattering. *Journal of Non-Crystalline Solids* **1975,** 18 (3), 307-331 DOI: http://dx.doi.org/10.1016/0022-3093(75)90137-4.

66. Sharma, S.; W Matson, D. *Raman spectra and structure of sodium aluminogermanate glasses*. 1984; Vol. 69, p 81–96.

67. Ishii, Y.; Salanne, M.; Charpentier, T.; Shiraki, K.; Kasahara, K.; Ohtori, N. A DFT-Based Aspherical Ion Model for Sodium Aluminosilicate Glasses and Melts. *J. Phys. Chem. C* **2016,** 120 (42), 24370-24381 DOI: 10.1021/acs.jpcc.6b08052.

68. Xiang, Y.; Du, J.; Smedskjaer, M. M.; Mauro, J. C. Structure and properties of sodium aluminosilicate glasses from molecular dynamics simulations. *J. Chem. Phys.* **2013,** 139 (4), 044507/1-044507/17 DOI: 10.1063/1.4816378.

69. Lee, S. K.; Stebbins, J. F. The Structure of Aluminosilicate Glasses: High-Resolution 17O and 27Al MAS and 3QMAS NMR Study. *J. Phys. Chem. B* **2000,** 104 (17), 4091-4100 DOI: 10.1021/jp994273w.

70. Galeener, F. L.; Geissberger, A. E.; Ogar, G. W.; Loehman, R. E. Vibrational dynamics in isotopically substituted vitreous GeO2. *Physical Review B* **1983,** 28 (8), 4768-4773.

71. Borrelli, N. F.; McSwain, B. D.; Su, G.-j. The infra-red spectra of vitreous boron oxide and sodium borate glasses. *Physics and Chemistry of Glasses* **1963,** 4 (1), 11-21.

72. Liu, C.; Angell, C. A. Mid- and far-infrared absorption of alkali borate glasses and the limit of superionic conductivity. *The Journal of Chemical Physics* **1990,** 93 (10), 7378-7386.

73. Du, L.-S.; Stebbins, J. F. Nature of Silicon−Boron Mixing in Sodium Borosilicate Glasses: A High-Resolution 11B and 17O NMR Study. *The Journal of Physical Chemistry B* **2003,** 107 (37), 10063-10076 DOI: 10.1021/jp034048l.

74. Stebbins, J. F.; Zhao, P.; Kroeker, S. Non-bridging oxygens in borate glasses: characterization by 11B and 17O MAS and 3QMAS NMR. *Solid State Nuclear Magnetic Resonance* **2000,** 16 (1), 9-19 DOI: https://doi.org/10.1016/S0926-2040(00)00050-3.

75. Christensen, R.; Olson, G.; Martin, S. W.; Kieffer, J., Na+ Ion conduction in and the Structures and Properties of 0.33Na2O+0.66[xB2O3+(1-x)2SiO2] Mixed Glass Former Glasses. In.

76. Bray, P. J.; Feller, S. A.; Jellison, G. E., Jr.; Yun, Y. H. Boron-10 NMR studies of the structure of borate glasses. *J.Non-Cryst.Solids* **1980,** 38-39 (1), 93-98.

77. Bray, P. J.; Dell, W. J. NMR studies of the structure of glass. *Journal de Physique* **1982,** 43 (12), 131-142.

78. Irwin, A. D.; Holmgren, J. S.; Jonas, J. Solid state 29Si and 11B NMR studies of sol-gel derived borosilicates. *Journal of Non-Crystalline Solids* **1988,** 101 (2), 249-254 DOI: https://doi.org/10.1016/0022-3093(88)90160-3.

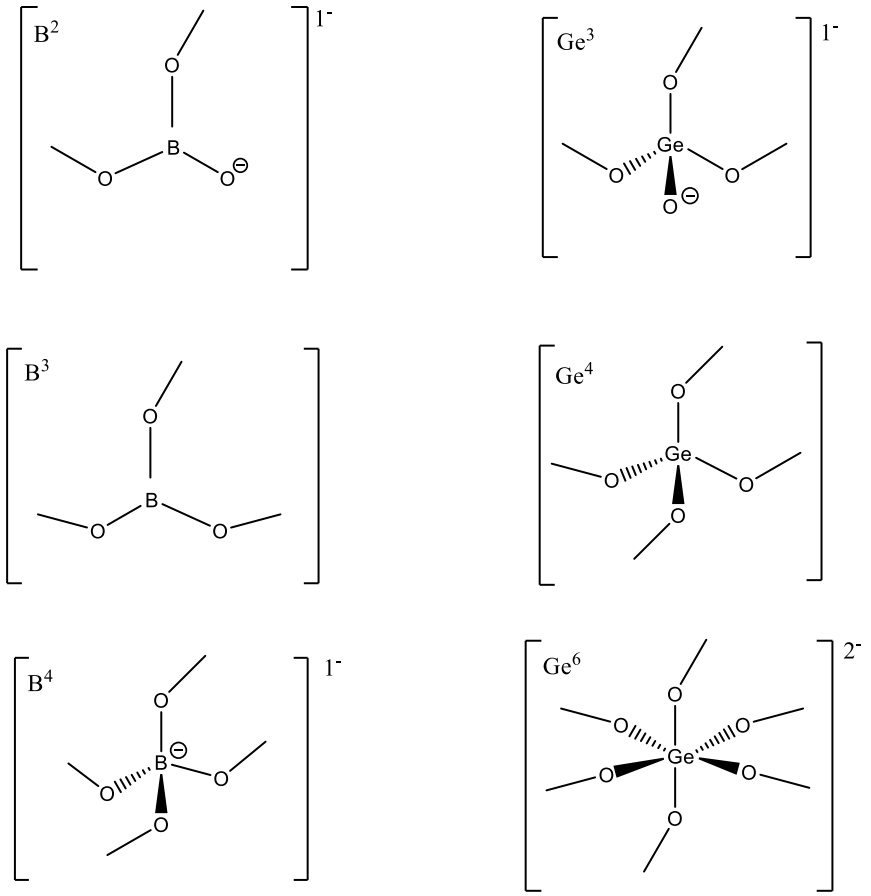

Figure 2.1. Structural units and corresponding notation for units found in NBGO series $0.2Na_2O + 0.8[xBO_{3/2} + (1\text{-}x)GeO_2]$.

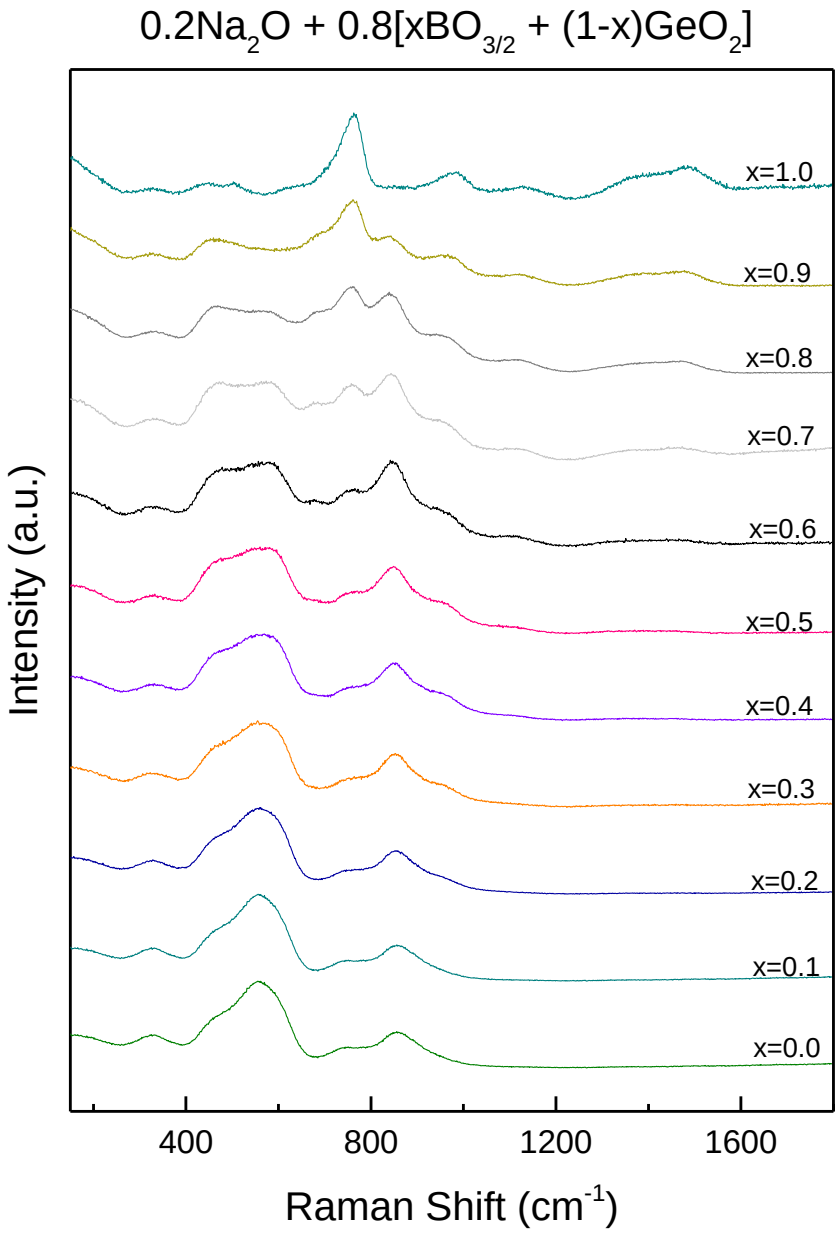

Figure 2.2. Raman spectra of the $0.2Na_2O + 0.8[xBO_{3/2} + (1\text{-}x)GeO_2]$ glasses.

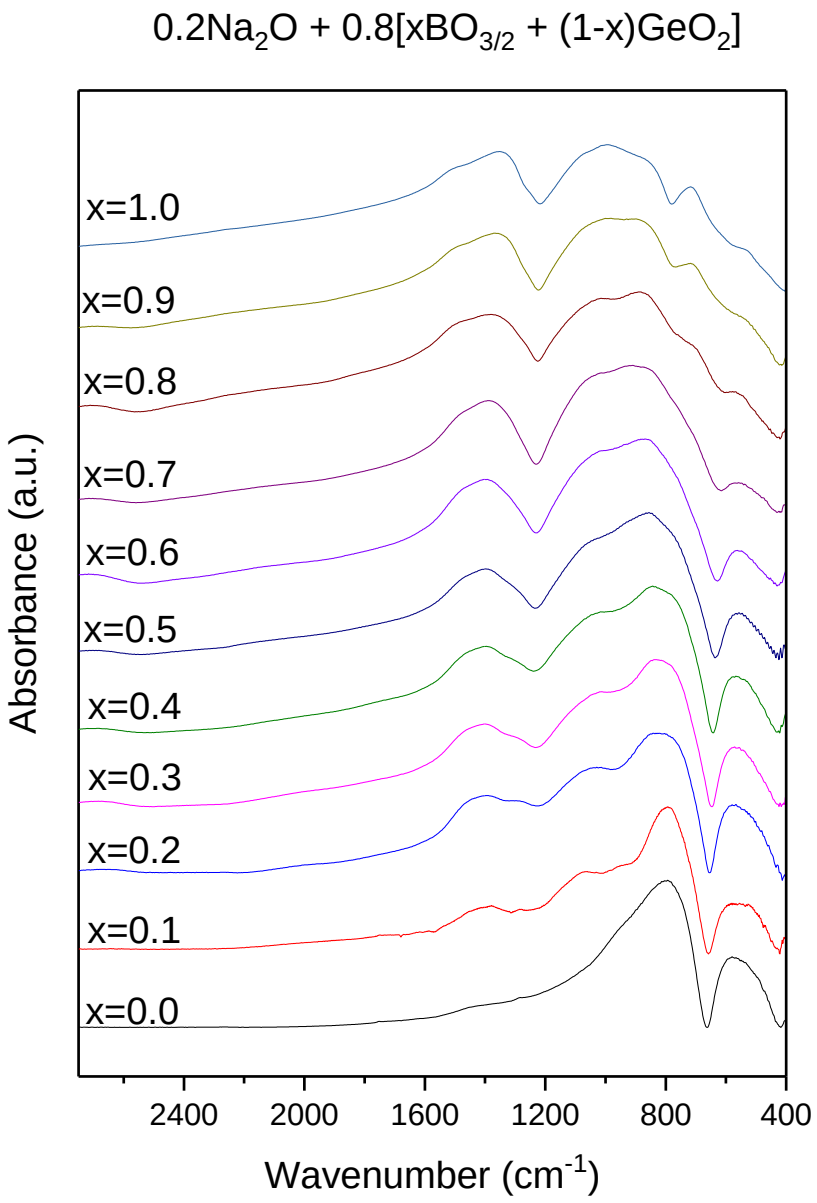

Figure 2.3. Infrared spectroscopy of $0.2Na_2O + 0.8[xBO_{3/2} + (1-x)GeO_2]$ glasses.

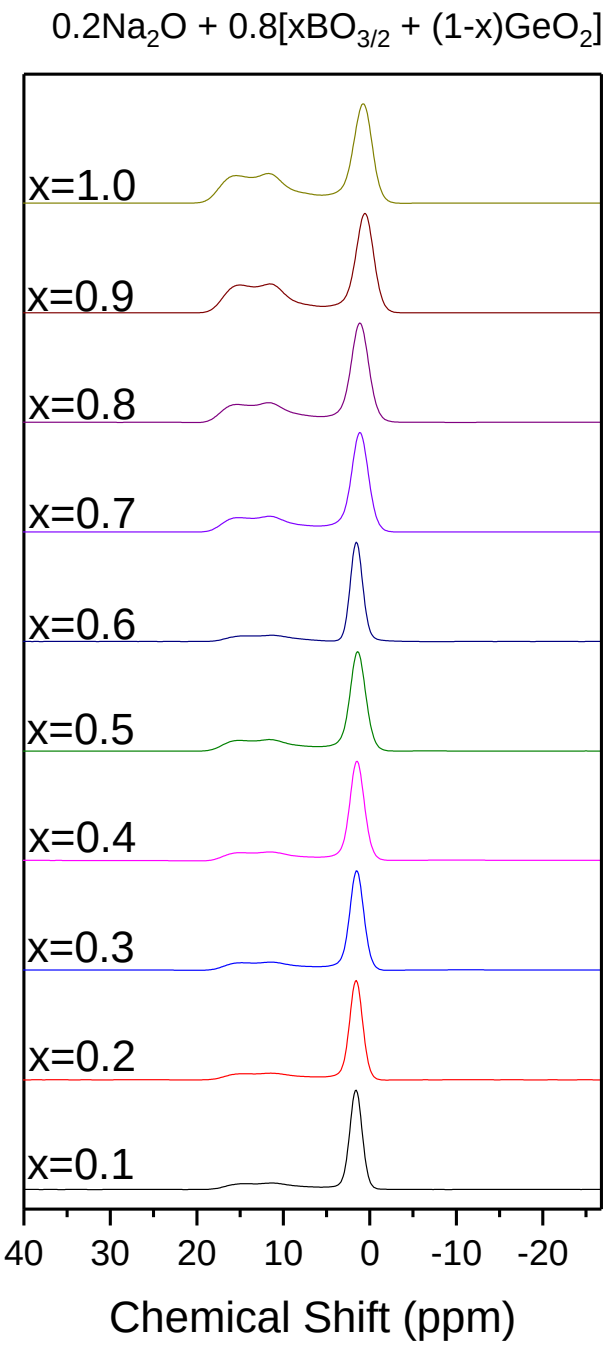

Figure 2.4. The ^{11}B MAS-NMR spectra of the $0.2Na_2O + 0.8[xBO_{3/2} + (1-x)GeO_2]$ glasses.

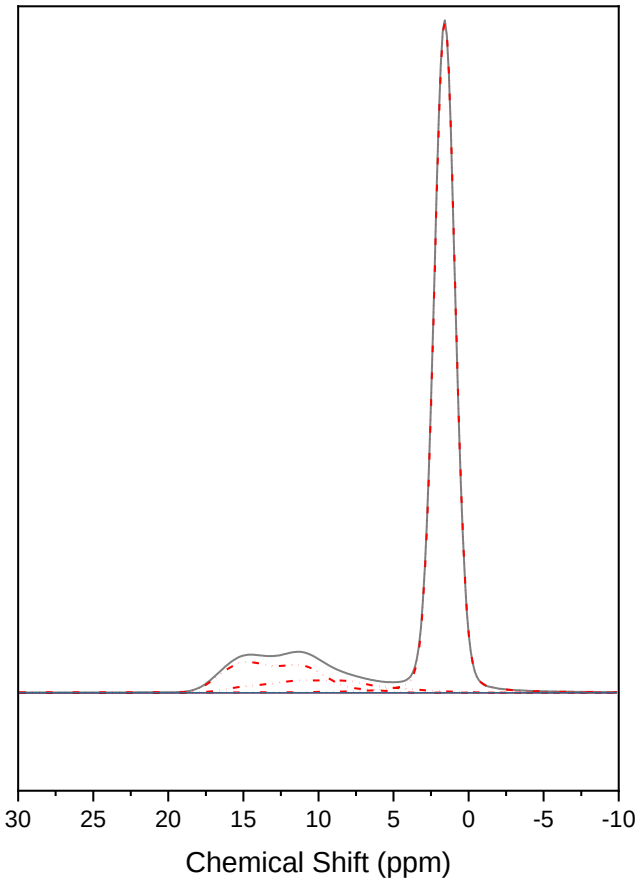

Figure 2.5. Example of deconvolution of ^{11}B MAS NMR spectra for the $0.2Na_2O + 0.8[xBO_{3/2} + (1-x)GeO_2]$ x = 0.9 glass.

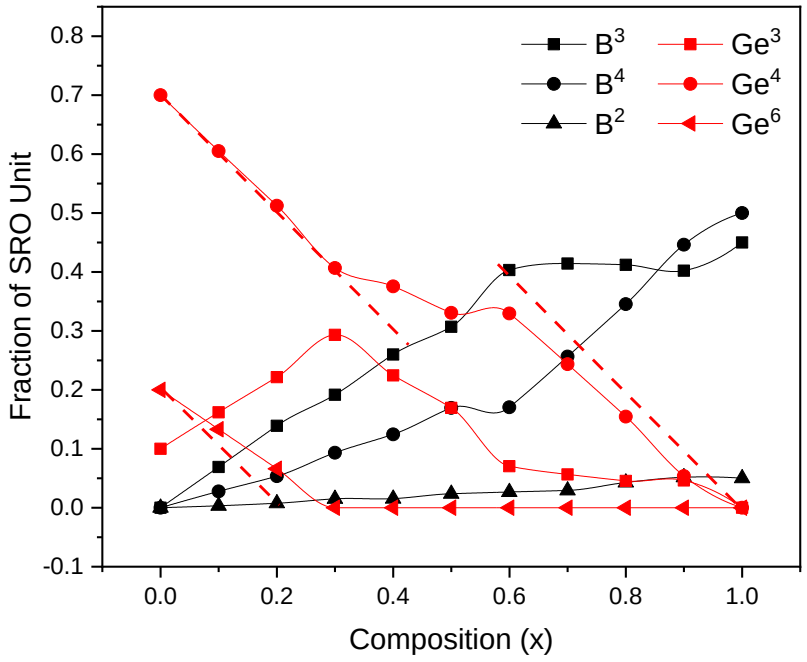

Figure 2.6. The fraction of SRO throughout the $0.2Na_2O + 0.8[xBO_{3/2} + (1\text{-}x)GeO_2]$ compositional series.

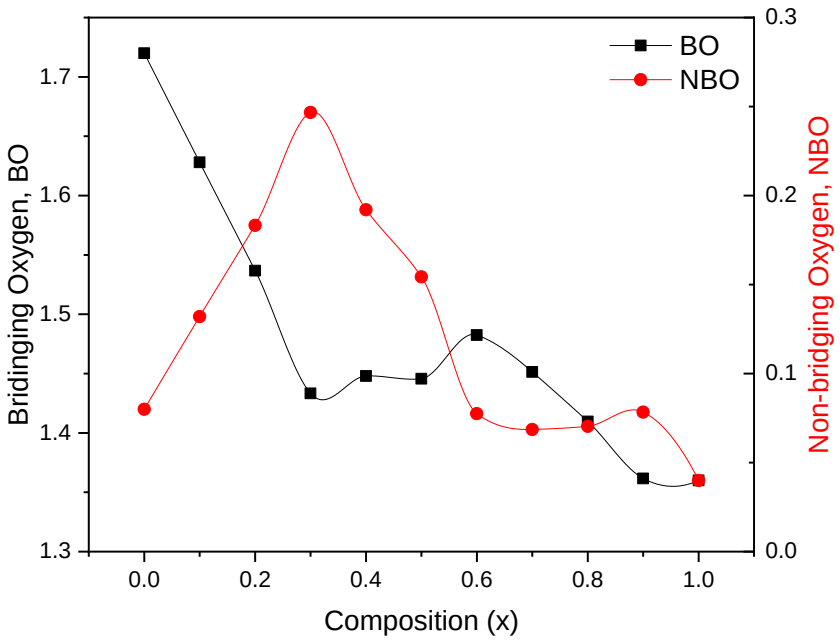

Figure 2.7. The number of BOs and NBOs per mole of glass.

CHAPTER 3. GLASS FORMABILITY AND WORKING RANGE OF SODIUM THIOBOROGERMANATE GLASS SYSTEMS

A paper to be submitted to the Journal of Non-Crystalline Solids

Brittany Curtis and Steve Martin*

Department of Materials Science & Engineering
Iowa State University of Science and Technology
Ames, IA

Brittany Curtis and Dr. Steve W. Martin

3.1 Abstract

Sulfide-based glasses are being explored as possibly solid-state electrolytes. Their increased ionic conductivity over oxide-based glasses make them more appealing. The potential suppression of dendritic formation due to amorphous structure of these materials make them promising competitors to those that facilitate dendritic growth causing thermal runaway. Contrastingly, the sulfide glasses are not as strong of glass formers as their oxide counterparts making it difficult to synthesize a fully, uniform glass sample where in some cases a glass-ceramic may form. This study examines three sodium thioborogermanate systems, $0.2Na_2S + 0.8[xBS_{3/2} + (1\text{-}x)GeS_2]$, $0.5Na_2S + 0.5[xBS_{3/2} + (1\text{-}x)GeS_2]$, and $0.6Na_2S + 0.4[xBS_{3/2} + (1\text{-}x)GeS_2]$ to discover which system will create a uniform glass that can be annealed into a glass disk for use as a solid-state electrolyte in an all solid state battery. It was found that the lower modified series, $0.2Na_2S + 0.8[xBS_{3/2} + (1\text{-}x)GeS_2]$ and $0.5Na_2S + 0.5[xBS_{3/2} + (1\text{-}x)GeS_2]$, created phase separated glasses which cannot be used to study the mixed glass former effect. The highly modified series, $0.6Na_2S + 0.4[xBS_{3/2} + (1\text{-}x)GeS_2]$, created glass samples through

* Corresponding author, swmartin@iastate.edu

plate quenching methods. However, the working range of these glasses were insufficient for easily annealing glass disks needed for ionic conductivity measurements.

3.2 Introduction

Ionically conductive glasses are becoming of particular interest in the field of battery research. Their use as all solid-state electrolytes provide a promising alternative to liquid, organic electrolytes, which present safety concerns due to thermal runaway.[1-3] By replacing the liquid electrolyte with a solid, may prevent dendritic formation, which causes short-circuiting.[4, 5] Glasses are even more attractive than their polycrystalline counter parts, which contain grain boundaries that can facilitate dendritic growth leading to thermal runaway.

Many glass systems have been explored as solid electrolytes although the most promising is the sulfide-based glasses over oxide-based. Sulfide-based glasses have increased ionic conductivities by six orders of magnitude over their oxide analogs making them even more competitive as solid-state electrolytes. Binary sulfide systems have been well explored for both lithium and sodium systems.[6-10] While lithium is most widely used, it is much more expensive due to the limited availability. Sodium is much more abundant in the earth's crust allowing for cheaper manufacturing costs.[11, 12] The only downfall for sodium is that it is considerably heavier than lithium making it an unlikely candidate as a battery in portable devices. These sodium batteries would be ideal for stationary grid storage devices such as wind turbines.

Improving upon the initial ionic conductivities of binary systems, the mixed glass former effect is a phenomenon that may help increase the ionic conductivities even further.[13-15] The mixed glass former effect occurs when two glass formers are mixed in variable ratios, keeping the modifier constant, and observing a non-linear, non-additive

trend in the corresponding physical properties (i.e. ionic conductivity, glass transition temperature, density, etc.). Such systems as the sodium borophosphates studied by Christensen et al. observed a positive mixed glass former effect with respect to the ionic conductivity.[13] Ultimately, on mixing sodium borate and sodium phosphate, the optimized ionic conductivity reach three magnitudes higher. The focus of this study aims to explore the mixed glass former effect of the sodium thioborogermanates, a sulfides system, and determine the glass formability and glass working ranges.

3.3 Background

Glasses are typically synthesized by supercooling a liquid consequently surpassing the crystallization creating an amporphous material and giving rise to a glass transition T_g.[16] The glass transition is a thermodynamic process which can be detected through differential scanning calorimetry as an endothermic process. The glass transition is an initial indication to determine if a material is glassy. However, other materials such as polymers exhibit a glass transition temperature requiring more characterization techniques to be implored to fully define the material. For the purposes of this study, the glass transition temperature along with the crystallization temperature is determined. The difference of these values is of particular interest when producing annealed, stress-free glass disks to be utilized as solid-state electrolytes. This difference in these values determines the working range, and essentially gives an idea of how easily the glass will form. If the working range is small, the melt will need to be cooled rapidly to achieve a glass. However, if the working range is large then slower quenching rates will be sufficient.

The working range is essential for creating stress-free glassy disks that can be used as electrolytes. In order to make stress-free glasses, these samples need to produce

uniform glassy disks through a slower quenching process that plate quenching to room temperature. Typically, when annealing, the glasses are quench to 30 to 50 degrees below their Tg and held at this temperature for while then allowed to slowly cool to room temperature.

3.3.1 Sodium Thioborate Binary $yNa_2S + (1-y)B_2S_3$

The glass forming range of the sodium thioborates has been reported by Bloyer et al. to be in two ranges. The lower modified region ranges from $0 \leq y \leq 0.33$ while the higher modified range is $0.55 \leq y \leq 0.80$.[9, 17] The glass transition temperatures for these glasses can be seen in table 3.1. As the modifier increases, the glass transition is decreases due the "loose" network of the glass.

3.3.2 Sodium Thiogermanate Binary $yNa_2S + (1-y)GeS_2$

Ribes *et al.* report a glass forming range from $0 \leq y \leq 0.60$ while Bischoff reported a slightly larger glass forming range of $0 \leq y \leq 0.67$.[6, 18] The glass transition temperatures can be seen in table 3.2. A similar trend is seen in the glass transition temperature as the sodium thioborates where the T_g decreases with increasing modifier content, Na_2S.

3.4 Experimental

3.4.1 Synthesis of Raw Materials: Sodium Sulfide, Boron Sulfide, and Germanium (IV) Sulfide

Boron sulfide was synthesized through the methods used by Bloyer et al.[19] Stoichiometric amounts of boron (NOAH Technologies, crystalline, 99.5%) and sulfur (Acros Organic, 99.999%) were massed inside a nitrogen glovebox. The powders were then loaded into a carbon coated ampule and sealed with a rubber tube and clamped. The ampule was then sealed using a torch outside of the glovebox and the ampule loaded into

a furnace. The sample was slowly heated to 850 C and held for 4 hours and then allowed to free fall to room temperature producing a vitreous boron sulfide boule which is then milled into a powder.

Germanium sulfide is synthesized in a similar manner using germanium (Acros Organic, 99.999%) and sulfur powders. The powders are massed in stoichiometric amounts and loaded into a bare silica ampule that is then sealed with a rubber tube and clamp. The ampule is sealed with a torch outside of the glovebox and the ampule is loaded into a furnace and allowed to slowly reach 900 C and held at this temperature for 7 hours. Once the hold is complete the reacted sample is cooled to room temperature.

Sodium sulfide nonahydrate (Acros Organics, 98%) is packed into a sealable chamber. The chamber is placed into a furnace, as well as connected to a vacuum system with a cold trap. The sample chamber is heated to 250 C and the sodium sulfide nonahydrate is dehydrated over the course of 45 hours.

3.4.2 Synthesis of Glasses

Each sodium thioborogermante system was prepared through similar methods. Glasses were prepared with stoichiometric amounts of sodium sulfide, boron sulfide and/or germanium sulfide in an inert, nitrogen glovebox. The unreacted powders were placed in a vitreous carbon crucible and melted for 5 minutes at temperatures ranging from 550 and 840 C depending on composition. The higher modified glasses melted at lower tempertures. A weight loss was obtained after the first melt to ensure no more than 2 wt % was lost. The sample is then melted for a second time and plate quenched between two brass plates at room temperature.

3.4.3 Determining Glass Transition Temperature

The onset of the glass transition temperature was determined by differential scanning calorimetry using the Pyris software. Samples were hermetically sealed in aluminum pans inside the nitrogen glovebox. Each glass forming sample was initially scanned from 50 to 350 C or until a crystallization event occurred. Care was taken to prevent alloying of the sample with the hermetically sealed aluminum pan to further prevent damage to the DSC platinum pans. Once the glass transition and crystallization temperatures were determined, a second pan was remade with a fresh sample and cycled through the glass transition temperature multiple times. The working range of these glasses were obtained by calculating the different between the crystallization and glass transition temperatures. In cases where the crystallization was not observed, the upper limit of the scan was taken as the minimum working range.

3.5 Results

3.5.1 $0.2Na_2S + 0.8[xBS_{3/2} + (1-x)GeS_2]$

Glasses were obtained for the series $0.2Na_2S + 0.8[xBS_{3/2} + (1-x)GeS_2]$ through plate quenching methods at room temperature. The glass transition temperatures are can be seen in Fig. (3.1). Phase separation occurred in two glasses, x=0.3 and 0.5, indicated by the two glass transition temperatures. The working ranges of these glasses varied from around 35 to 120 degrees C and can be seen in table 3.3. The phases separated glasses, x=0.3 and x=0.5, do not have a clear working range and was not reported.

3.5.2 $0.5Na_2S + 0.5[xBS_{3/2} + (1-x)GeS_2]$

However, for the glass series $0.5Na_2S + 0.5[xBS_{3/2} + (1-x)GeS_2]$, the boron rich samples, $x \geq 0.5$, glasses were obtained and their glass transition temperatures can been seen in Fig. (3.2). Evidence for phase separated glasses is evident from the two glass

transition temperatures obtained for multiple samples. Due to a large amount of these glasses being phase separated the working range is not reported.

3.5.3 $0.6Na_2S + 0.4[xBS_{3/2} + (1-x)GeS_2]$

The highest modified glass series, $0.6Na_2S + 0.4[xBS_{3/2} + (1-x)GeS_2]$, produced uniform glasses across the entire series. Only one T_g was observed in the DSC scan. The working ranges are reported in table 3.2. It is important to point out for the majority of the glasses, $x \geq 0.8$, a crystallization process was not seen before the upper limit of the scan was reached. The values with a greater than sign indicate that the crystallization was not observed and therefore the value reported is the difference between the upper limit to the scan and T_g.

3.6 Discussion and Conclusion

As with the two series, $0.2Na_2S + 0.8[xBS_{3/2} + (1-x)GeS_2]$ and $0.5Na_2S + 0.5[xBS_{3/2} + (1-x)GeS_2]$, glasses were made through plate quenching techniques. However, upon annealing, the working ranges of these glasses made it impossible to make uniform glass samples and instead made glassy-ceramics. It was also seen that some of the glasses synthesized were phase separated. Phase separation makes studying the MGFE in these glasses virtually impossible and making these series incomplete for a complete MGFE analysis.

The boron-rich glasses, $x \geq 0.4$, of the $0.5Na_2S + 0.5[xBS_{3/2} + (1-x)GeS_2]$ series created phase separated glasses indicated by the existence of two T_gs. The working range of these glasses is difficult since the instrument was only ran to 300 C to prevent damage to the DSC instrument. However, the presence of phase separation makes studying the MGFE of this series impossible.

However, the $0.6Na_2S + 0.4[xBS_{3/2} + (1-x)GeS_2]$ series did not produce any phase separated glasses through plate quenching methods. Upon annealing, most of the glasses formed uniformed glass disks. Unfortunately, x=0.2 and 0.3 are difficult to make due to the limited working range where it can be seen that the glass transition temperature is immediately adjacent to the crystallization temperature. This series provides an almost complete glass forming range, allowing for better insight into the MGFE for this sulfide system.

3.7 References

1. Lisbona, D.; Snee, T. A review of hazards associated with primary lithium and lithium-ion batteries. *Process Safety and Environmental Protection* **2011,** 89 (6), 434-442 DOI: https://doi.org/10.1016/j.psep.2011.06.022.

2. Wen, J.; Yu, Y.; Chen, C. A Review on Lithium-Ion Batteries Safety Issues: Existing Problems and Possible Solutions. *Materials Express* **2012,** 2 (3), 197-212 DOI: 10.1166/mex.2012.1075.

3. Wang, Q.; Ping, P.; Zhao, X.; Chu, G.; Sun, J.; Chen, C. Thermal runaway caused fire and explosion of lithium ion battery. *Journal of Power Sources* **2012,** 208 (Supplement C), 210-224 DOI: https://doi.org/10.1016/j.jpowsour.2012.02.038.

4. Monroe, C.; Newman, J. Dendrite Growth in Lithium/Polymer Systems: A Propagation Model for Liquid Electrolytes under Galvanostatic Conditions. *Journal of The Electrochemical Society* **2003,** 150 (10), A1377-A1384.

5. Rosso, M.; Brissot, C.; Teyssot, A.; Dollé, M.; Sannier, L.; Tarascon, J.-M.; Bouchet, R.; Lascaud, S. Dendrite short-circuit and fuse effect on Li/polymer/Li cells. *Electrochimica Acta* **2006,** 51 (25), 5334-5340 DOI: https://doi.org/10.1016/j.electacta.2006.02.004.

6. Ribes, M.; Barrau, B.; Souquet, J. L. Sulfide glasses: Glass forming region, structure and ionic conduction of glasses in Na2S・XS2 (X・Si; Ge), Na2S・P2S5 and Li2S・GeS2 systems. *Journal of Non-Crystalline Solids* **1980,** 38-39, 271-276 DOI: https://doi.org/10.1016/0022-3093(80)90430-5.

7. Kennedy, J. H.; Zhang, Z.; Eckert, H. Ionically conductive sulfide-based lithium glasses. *Journal of Non-Crystalline Solids* **1990,** 123 (1), 328-338 DOI: https://doi.org/10.1016/0022-3093(90)90804-U.

8. Kim, Y.; Hwang, H.; Lawler, K.; Martin, S. W.; Cho, J. Electrochemical behavior of Ge and GeX2 (X = O, S) glasses: Improved reversibility of the reaction of Li with Ge in a sulfide medium. *Electrochimica Acta* **2008,** 53 (15), 5058-5064 DOI: https://doi.org/10.1016/j.electacta.2007.12.015.

9. Bloyer, D. R.; Cho, J.; Martin, S. W. Infrared Spectroscopy of Wide Composition Range xNa2S + (1 –x)B2S3 Glasses. *Journal of the American Ceramic Society* **1993,** 76 (11), 2753-2759.

10. Royle, M.; Cho, J.; Martin, S. W. Raman spectroscopy studies of xNa2S+(1−x)B2S3 glasses and polycrystals. *Journal of Non-Crystalline Solids* **2001,** 279 (2–3), 97-109 DOI: http://dx.doi.org/10.1016/S0022-3093(00)00344-6.

11. Carmichael, R. S. *Practical Handbook of Physical Properties of Rocks and Minerals*. CRC Press Inc.: Boca Raton, 1989.

12. Ene-Parent, J.; Zikovsky, L. Neutron activation analysis of laundry dryer lint. *Journal of Radioanalytical and Nuclear Chemistry* **2014,** 247 (1), 197-198 DOI: 10.1023/A:1006712408990.

13. Christensen, R.; Olson, G.; Martin, S. W. Ionic Conductivity of Mixed Glass Former 0.35Na2O + 0.65[xB2O3 + (1 – x)P2O5] Glasses. *The Journal of Physical Chemistry B* **2013,** 117 (51), 16577-16586 DOI: 10.1021/jp409497z.

14. Martin, S. W.; Bischoff, C.; Schuller, K. Composition Dependence of the Na+ Ion Conductivity in 0.5Na2S + 0.5[xGeS2 + (1 – x)PS5/2] Mixed Glass Former Glasses: A Structural Interpretation of a Negative Mixed Glass Former Effect. *The Journal of Physical Chemistry B* **2015,** 119 (51), 15738-15751 DOI: 10.1021/acs.jpcb.5b07383.

15. Deshpande, V. K.; Pradel, A.; Ribes, M. The mixed glass former effect in the Li2S : SiS2 : GeS2 system. *Materials Research Bulletin* **1988,** 23 (3), 379-384 DOI: http://dx.doi.org/10.1016/0025-5408(88)90012-8.

16. Rao, K. J. In *Structural Chemistry of Glass*; 1st ed.; Elsevier: Boston, MA, 2002; Chapter 1, p 23.

17. Cho, J. Preparation and Characterization of B2S3-Based Chalcogenide Glasses. Iowa State University, 1995.

18. Bischoff, C. The Mixed Glass Former Effect in $0.5Na_2S+0.5[xGeS_2+(1-x)PS_{5/2}]$ Glasses. Iowa State University, Ames, Iowa, 2013.

19. Martin, S.; Bloyer, D. Preparation of High-Purity Vitreous B_2S_3. *Journal of the American Ceramic Society* **1990,** 73 (11), 3481-3485.

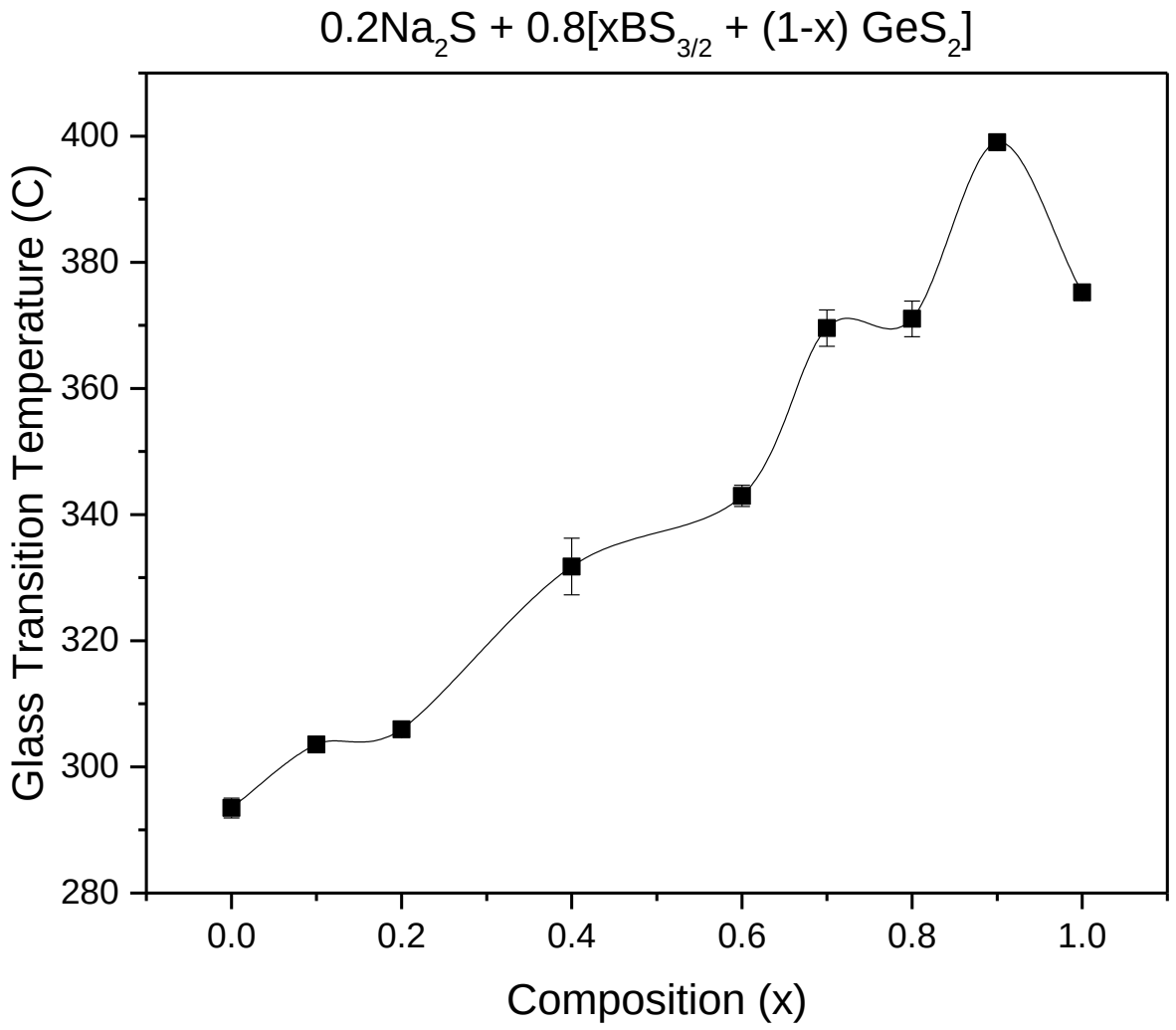

Figure 3.1. Glass transition temperatures of the $0.2Na_2S + 0.8[xBS_{3/2} + (1\text{-}x)GeS_2]$ series.

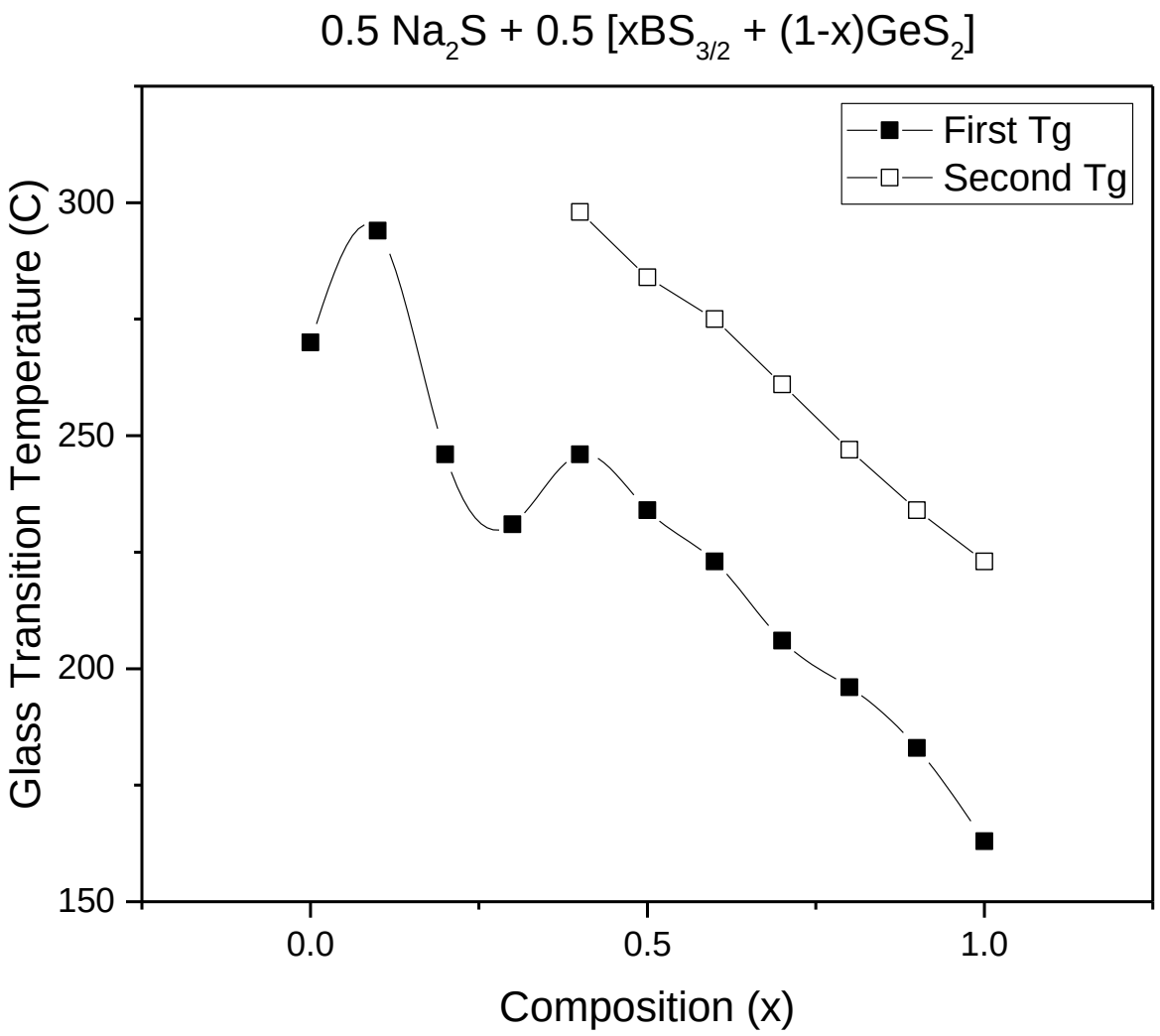

Figure 3.2. Glass transition temperatures of the $0.5Na_2S + 0.5[xBS_{3/2} + (1-x)GeS_2]$ series including the second glass transition temperature of the phase separated glasses.

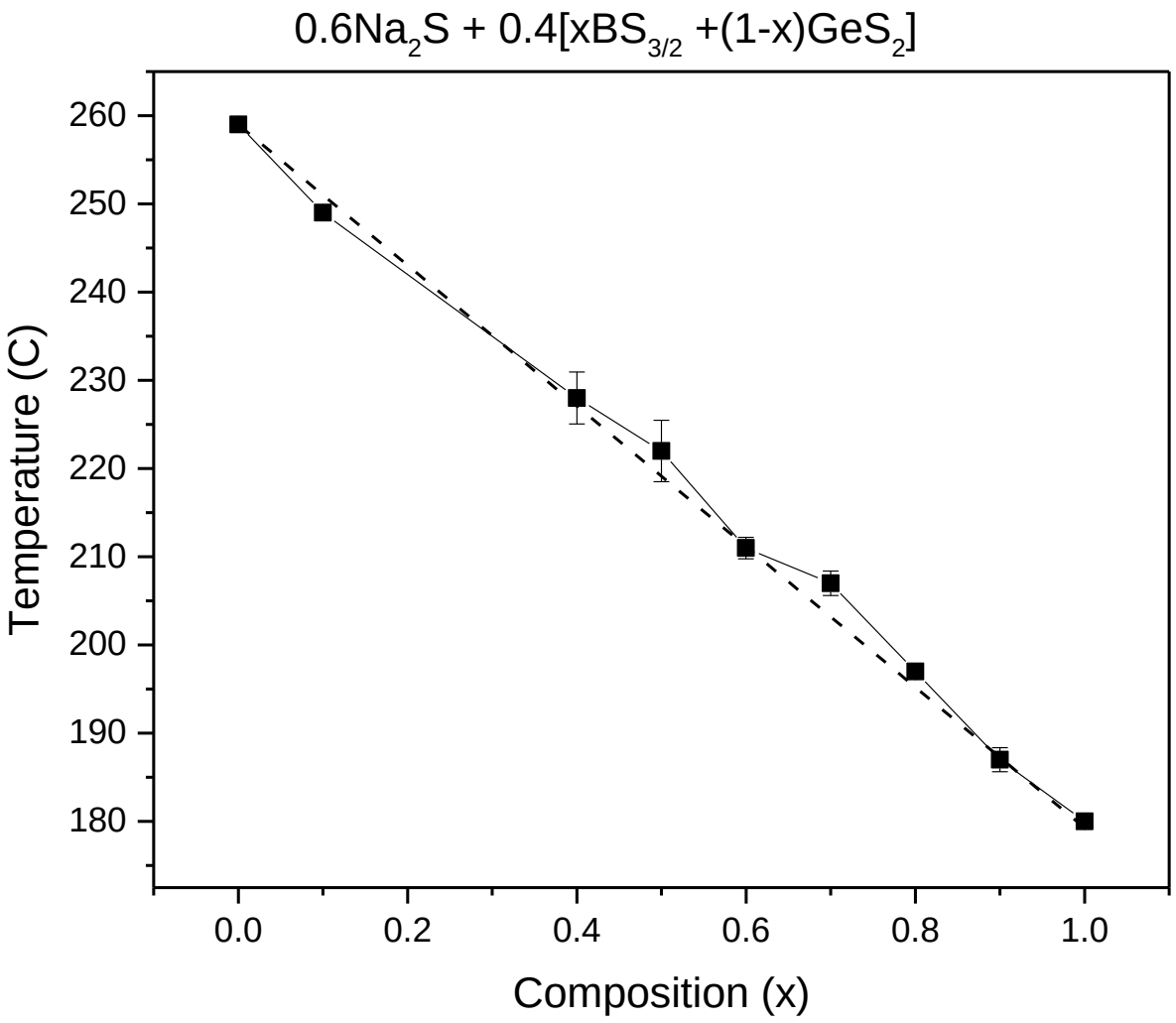

Figure 3.3. The composition plot of the glass transition temperature for the sodium thioborogermanates.

Table 3.1. The glass transition temperatures of the binary system $yNa_2S + (1-y)B_2S_3$.[17]

Mole % of Na2S	Tg (C)
30	300
33	365
55	180
60	173
65	162
70	155
75	157
80	163

Table 3.3. Working range for the glass series, $0.2Na_2S + 0.8[xBS_{3/2} + (1-x)GeS_2]$. Since x=0.3 and 0.5 are phase separated no working range was calculated.

Composition	Tx-Tg
0	120
0.1	97
0.2	120
0.3	
0.4	118
0.5	
0.6	107
0.7	80
0.8	53
0.9	36
1	45

Table 3.4. Working ranges of the glass series $0.6Na_2S + 0.4[xBS_{3/2} + (1-x)GeS_2]$.

Composition	Tx-Tg
0	40
0.1	64
0.2	33
0.3	43
0.4	85
0.5	128
0.6	123
0.7	152
0.8	153
0.9	112
1	70

CHAPTER 4. STRUCTURAL INVESTIGATION OF THE SODIUM THIOBOROSILICATE MIXED GLASS FORMER SYSTEM $0.6Na_2S + 0.4[xBS_{3/2} + (1-x)SiS_2]$

A paper to be submitted the Journal of Non-Crystalline Solids

Brittany Curtis, Carter Francis and Steve Martin*

Department of Materials Science & Engineering
Iowa State University of Science and Technology
Ames, IA

4.1 Abstract

With an increased demand in renewable energy sources, comes a need for storing energy in circumstances where such renewable energy sources are under-producing. All solid-state batteries are a promising solution to the fast growing and demanding field of energy storage. One challenge with manufacturing a cheap, safe and energy dense solid-state battery is finding the appropriate solid-state electrolyte material. Sulfide-based, glassy solid-state electrolytes are of particular interest due to the room temperature ionic conductivities of binary systems, $\sim 10^{-5}$ $S*cm^{-1}$. However, the phenomenon known has the mixed glass former effect (MGFE) has proven to optimized properties when two glass formers are mixed in varying ratios causing a non-linear, non-additive change in the physical properties such as the ionic conductivity. This phenomenon has been observed for other glass systems such as the sodium borophosphate, and the sodium thiophosphogermanates. This study aims to look at the sodium thioborosilicate system, $0.6Na_2S + 0.4[xBS_{3/2} + (1-x)SiS_2]$ which is the first detailed examination of this mixed glass former system. Infrared, Raman and nuclear magnetic spectroscopies were used to gain insight into the short-range order (SRO) of these glasses. Little networking of the SRO

* Corresponding author, swmartin@iastate.edu

units is seen due to the main structures being Si^1 and B^0 which contain one bridging sulfur, and no bridging sulfurs, respectively. Further addition of thioborate produces a multitude of SRO units (B^1, B^2, and B^4) in small fractions suggesting a competition of reactions are taking place. Upon investigation into the quantitative analysis of the NMR spectra and due to charge compensation, a small amount of free, unreacted sodium sulfide, less than 10 mol % of the total sodium sulfide in the system, is present and increases with increasing thioborate content.

4.2 Introduction

Renewable energy sources are becoming more prevalent today with as much as 36.6% energy generated by wind power in the state of Iowa in 2016.[1] While the renewable energy sources are high in demand, a more efficient, safer, and cost-effective means of energy storage is necessary to keep up with energy demands in today's society. Solid-state batteries are of great interest as prospective energy storage solutions. Their energy density can surpass that of traditional secondary, lithium batteries while providing a safer alternative by replacing a flammable, liquid, organic electrolyte with a non-flammable, solid-state electrolyte. Much research has been done in the realm of electrolyte materials ranging from polymer-gels, ceramics, and of particular interest, glasses.[2-5] Glasses provide the advantage of amorphous and isotropic characteristics that may be conducive for ionic conduction.

Much is known about oxide glasses from their glass transition temperatures, mechanical properties, the structure, etc. The ionic conductivity of oxide glasses has also been studied in lithium and sodium systems. Many alkali binary systems show ionic conductivities around 10^{-11} to 10^{-12} $(\Omega cm)^{-1}$.[6-8] Interestingly, the study of the phenomenon known as the mixed glass former effect (MGFE) has shown to, not only improve the ionic

conductivity, but other physical properties as well. This has been seen in systems such as the lithium thiosilicates, sodum borosilicates, sodium borophosphates, sodium thiophosphogermanates etc.[7,9-11] This phenomenon occurs when mixing two glass formers into a ternary glass while holding the modifier content constant. Consequently upon mixing, there is a non-linear and non-additive trend that results in an optimization of the physical property (i.e. ionic conductivity, density, Tg, etc).

Although oxide glasses have great stability, they exhibit poor ionic conductivities and therefore make poor electrolyte materials for use as solid-state electrolytes. In searching for a better ionic conductor, sulfide glasses prove to be more promising. The higher polarizability of sulfur reduces the activation energy associated with the doorway radius along with the coulombic activation energy.[12] This allows sodium ions to be freed up easier while allowing them to migrate through the structure of the glass easier as well. Binary systems have been studied, and show initial ionic conductivities of sulfide glasses to be around 10^{-6} $(\Omega cm)^{-1}$ for sodium ionic conductivity and 10^{-5} $(\Omega cm)^{-1}$ for lithium.[13,14] The potential for optimization of these ionic conductivities could be achieved through the study of the mixed glass former effect in sulfide glasses.

Some ternary sulfide systems have been studied including sodium borophosphates, sodium borosilicates, sodium thiophosphogermanates, etc. which exhibit a mixed glass former effect in certain properties.[6,7,15,16]

4.3 Background

4.3.1 Notation of SRO Units

A shorthand notation will be used in this paper to concisely describe the SRO structures examined in the sodium thioborosilicate system. The SRO structures and their corresponding notation can be seen in Fig. (1). For a boron unit with 3 bridging sulfurs the

notation will be B^3 where B indicates the central atom as given by the periodic table and 3 indicates the number of bridging sulfurs. Note that boron can be trigonally and tetrahedrally coordinated but this notation is not explicit in the coordination.

4.3.2 $yNa_2S + (1-y)B_2S_3$ Binary System

Cho et al. have studied the glass formability of the binary system $yNa_2S + (1-y)B_2S_3$ and showed that there are two glass forming regions. The lower modified regions ranges from $0 \leq y \leq 0.33$ and a higher modified region of $0.55 \leq y \leq 0.80$.[17]

The glass system studied here falls in the high-modified region. However, note that instead of y=0.6 in terms of $BS_{3/2}$, the modifier content translates to y=0.75 in terms of B_2S_3. At this composition the theoretical structure unit is a metathioborate (B^0) in which there are no bridging sulfurs (BS).[18,19] While there's essentially no networking in this glass, it is a decent glass former as demonstrated by the thermal stability range, the difference in crystallization temperature T_x and glass transition temperature T_g of ~70 C. While this seems rather low for oxide glasses, this is somewhat typical for the sulfide glasses.

Although oxide systems have the advantage of chemical stability, the sulfide systems initially prove to be much better ionic conductors. Typical room temperature, sodium ionic conductivities of oxide glasses are around 10^{-11} to 10^{-12} $(\Omega*cm)^{-1}$.[7,8,20] However, sulfide glass systems have sodium ionic conductivities of 10^{-6} $(\Omega*cm)^{-1}$. For this binary system, the room temperature, sodium ionic conductivity as reported by Patel is 8.3×10^{-6} $(\Omega*cm)^{-1}$.[13]

4.3.3 $yNa_2S + (1-y)SiS_2$ Binary System

Current studies suggest a wide glass forming range from y=0.0 to 0.7 for the sodium thiosilicates.[21,22] The modifier content of this system is in the higher range of glass formability with y=0.6. This will help potentially increase the ionic conductivity since it

incorporates more charge carriers. Structural studies of the sodium thiosilicates have indicated that the binary structure of the $0.6Na_2S + 0.4SiS_2$ composition is nominally the Si^1 unit. Although small fractions of ESi^2 and Si^0 do exist at this composition. This composition contains a majority of NBS with a small amount of BS. While one might expect that a NBS terminated by a sodium ion would have a lower conductivity, the ionic conductivity of this composition at room temperature is $4.17x10^{-5}$ $(\Omega*cm)^{-1}$. Even though this composition is comprised of a majority of NBS, the ionic conductivity is promising for an electrolyte material.

4.3.4 Mixed Glass Former System $0.6Na_2S + 0.4[xBS_{3/2} + (1-x)SiS_2]$

The sodium thioborates and sodium thiosilicates have exhibited superior ionic conductivities over that of the oxide binary systems, yet cannot compete with the ionic conductivities of electrolyte materials used today which possess room temperature ionic conductivities of $\sim10^{-3}$ $(\Omega*cm)^{-1}$. It has been seen in oxide mixed glass former effect systems that ionic conductivity has the potential to increase by two orders of magnitude. The mixed glass former effect occurs when mixing the ratio of glass formers (i.e. thioborate and thiosilicate) while keeping the modifier content constant and observing a non-linear and non-additive trend with respect to its physical properties. For instance, the sodium borophosphate glasses studied by Christensen et al. varies the ratio of boron oxide to phosphorus oxide while the sodium oxide content remains at 35 mol %.[8] In this system, the sodium phosphate binary has an ionic conductivity of 7.63×10^{-12} $(\Omega*cm)^{-1}$ while the sodium borate binary has an ionic conductivity of 2.93×10^{-10} $(\Omega*cm)^{-1}$. Upon the addition of boron oxide to phosphorus oxide the ionic conductivity begins to increase until it reaches a maxium of 2.34×10^{-9} $(\Omega*cm)^{-1}$.[8] This mixed glass former system exhibits a positive mixed glass former effect with respect to the ionic conductivity where the ionic

conductivity goes through a maximum. The mixed glass former system of the lithium thiosilicogermanates also exhibits a positive mixed glass former effect with respect to the ionic conductivity.[23] However, in the sodium thiophosphogermanate system, a negative mixed glass former effect was observed in the ionic conductivity.[15] To further understand the role of structure, and more specifically the role of the SRO structure in these mixed glass former systems, more systems need to be studied to strategically pinpoint the unique characteristics of this phenomenon.

4.4 Experiment

4.4.1 Preparation of Precursors

Sodium sulfide was dehydrated from sodium sulfide nonahydrate (Acros Oraganics, 98%) under vacuum at 250 C. Silicon sulfide was synthesized by combining stoichiometric amounts of silicon powder (Alfa Aesar, crystalline, 99.999%) and sulfur (Acros Organic, 99.999%) in an evacuated, sealed silica ampoule. The ampoule was allowed to slowly reach 900 C in a tube furnace and then held at temperature for 11 hours. Boron sulfide was synthesized in a similar matter but in a carbon coated silica ampoule as proposed by Bloyer *et. al*.[24] Stoichiometric amounts of boron (NOAH Technologies, crystalline, 99.5%) and sulfur. Again, the evacuated ampoule was placed into a tube furnace and slowly heated to 860 C where it was held at temperature for four hours. All reacted ampoules were transferred to a nitrogen glovebox where the reaction chambers were opened, milled, and further analysis done to ensure purity.

4.4.2 Preparation of Glass Samples

Samples were made from stoichiometric amounts of precursors described above. The powders were milled for 20 minutes in a steel millpot in a SpexMill. Once milled, samples were transferred to a carbon crucible and reacted in a nitrogen atmosphere in a

tube furnace for 5 minutes at 550 to 720 C depending on composition. All samples were subjected to no more than 2 % mass loss to ensure compositional accuracy. The sample melts were then quenched between two brass plates and characterized.

4.4.3 Raman Spectroscopy

Samples were packed in a sealed sample holder inside the nitrogen glovebox. Raman spectra were obtained for each glass using a Horiba LabRam Evolution High Resolution confocal Raman Microscope spectrometer equipped with a 532 nm laser. Spectra were obtained using 2 to 5 accumulations and ranging from 6 to 30 sec acquisition under a 10x objective lens. Only 25 to 50% power was used to prevent samples from crystallizing when exposed to the lazer.

4.4.4 Infrared Spectroscopy

Samples were prepared for infrared analysis in a nitrogen glovebox by diluting 2-3 wt % of sample in 200 mg of cesium iodide CsI and milled in a mortar and pestle. The mixture was then placed into a sample die and Specac press, and pressed under 2 tons of pressure. The infrared spectra were obtained using a Bruker IFS 66 v/s infrared spectrometer with an attach nitrogen antechamber. The samples were scanned from 4000 to 400 cm^{-1} over 32 scans with 4 cm^{-1} resolution.

4.4.5 ^{11}B MASS-NMR

The samples were milled and packed into a 4 mm zirconia rotor in a nitrogen glovebox. They were placed in a Bruker Avance II 600 MHz solid state NMR at room temperature. The samples were spun at 14 kHz to reduce chemical shift anisotropy and further resolve spinning sidebands from the central lines. A spin-echo experiment was done to reduce the additional signal from the probe. A pulse width of 2.5 microseconds and a delay time of 3 seconds was used for 512 scans. All spectra were indirectly referend using

the IUPAC convention by establishing a relative reference frequency using tetramethylsilane.[25] The spectra were analyzed using DMFit software.[26]

4.4.6 ^{29}Si MASS-NMR

The ^{29}Si NMR was obtained using Bruker Avance II 600 MHz solid state NMR at room temperature. Samples were packed in a 4 mm zirconia rotor inside a nitrogen glovebox. The samples were spun at 12kHz with a pulse width of 4.5 microseconds and a recycle delay time of 30 seconds. The number of scans acquired were 4096.

4.5 Results

4.5.1 Raman Spectroscopy

The Raman spectra of the sodium thioborosilicate glasses can be seen in Fig. (2). The pure binary sodium thiosilicate, x=0.0, shows two distinct features. At 370 cm^{-1} is assigned to the Si^1 structure and is most intense at x=0.0.[21] With the addition of boron sulfide, increasing x, this peak quickly decreases until x=0.6 where there is no evidence of this peak. The next most intense silicon peak at x=0.0 corresponds to the Si^0 unit at 405 cm^{-1}.[21] This peak becomes more intense with increase in x value reaching a max at x=0.4 and decreasing to zero at x=1.0 where no silicon exists. As x increases with more addition of boron sulfide, peaks emerge at 440 and 490cm^{-1}.[27] This unit corresponds to the B^2 unit and is seen between x=0.3 and x=1.0. These two, have relatively the same intensity,however, at x=0.9 and 1.0, the intensities of these peaks are not the same ratio with the peak at 440 cm^{-1} being larger than 490 cm^{-1} suggesting that a different structural feature may be growing in superimposed. The possible unit would be B^0 which is in agreement with what is seen with the infrared spectra that is reported later. Royle *et al.* have a similar orthothioborate peak present around 480 cm^{-1} suggesting some overlap between modes.

4.5.2 Infrared Spectroscopy

The infrared spectroscopy can be seen in figure 2. When x=0.0, the sodium thiosilicate binary, the main peaks are located at 435 cm^{-1} and 560 cm^{-1} corresponding to the ESi^2 and Si^1, respectively.[21,28] The ESi^2 unit follows a similar trend as seen in the Raman spectroscopy. It is most intense at x=0.0 and decreases with intensity has x-value increases until x=1.0 where no silicon is present. The Si^1 unit is most intense at x=0.0 and seems to decrease in intensity until x=0.3. Around x=0.4 line shape begins to change and the peak starts to shift to lower wavenumbers. Around 500 cm^{-1}, the Si^0 unit becomes more prevalent over the Si^1 until x=1.0 where not silicon is present. The infrared gives a better understanding of boron SRO starting to emerge. At low x-value is the B^0 SRO unit located at 800 cm^{-1}. This unit grows in intensity with increasing x-value and can be seen in the sodium thioborate binary, x=1.0. The next boron unit that appears is the B^2 unit located at 922 cm^{-1}.[18] This peak is seen around x=0.3 and begins to grow in intensity and then fade out until x=0.9. The pure sodium thioborate does not show evidence of B^2 in this region. At around x=0.4, a faint peak appears around 1015 cm^{-1} and grows in intensity until x=1.0 and is attributed to the B^1 unit.

4.5.3 ^{11}B MASS-NMR

Figure 4.4 shows the ^{11}B MASS-NMR spectra. The MASS-NMR revealed that there was a fair amount of oxide and oxy-sulfide units within these glasses. However, all oxide contamination from oxide and oxy-sulfide modes were calculated from peak areas to be less than 10 %. The first peak is attributed a four coordinated oxy-sulfide boron species BOS_3^- located at ~1 ppm. The trigonal oxide and oxy-sulfides BO_3, BO_2S, BOS_2 exist at 16, 31, and 46 ppm, respectively. These mixed oxy-sulfide trigonal units were fit with quadrupolar peaks and the fitting parameters are discussed next. The BO_3 has a C_q

value of 2.7 ± 0.1 MHz and an η of 0.20 ± 0.05. The BO_2S has a C_q value of 2.6 ± 0.1 MHz and an η of 0.4 ± 0.01 while the BOS_2 has a C_q of 2.5 ± 0.1 MHz and an η of 0.4 ± 0.01. The pure thioborate trigonal units lie between 58 to 65 ppm.[19,29] The first pure sulfide quadrupolar peak is located at 62 ppm and corresponds to the trigonal B^1 unit. Larink et al. did not distinguish this peak from a B^1 or B^2 unit; however, they assigned it to a mixture of the asymmetric trigonal sites.[30] This glass system deals with a higher modifier content and B^1 is solely designated to this peak due to the amount of sodium that would be expected to terminate the sulfurs. The Cq value of this peak is 2.4 ± 0.1 MHz and an η of 0.4 ± 0.01. Another peak that is overlapping with this peak is assigned to the trigonal B^0 unit at 66 ppm. This symmetric trigonal unit is shifted higher and is easier to distinguish from the asymmetric units.

4.5.4 ^{29}Si MASS-NMR

Figure 4.5 shows the ^{29}Si MASS-NMR spectra for the series. No spectrum is collected for x=1.0 since this is the pure sodium thioborate and no silicon exist. The spectra show a broad peak centered around 5.3 ppm for x=0.0 and gradually shifting downfield through the series to 6.5 ppm for x=0.9. Watson *et al.* contributes this peak to be either a Si^1 or an Si^0 unit.[21] These SRO units are difficult to resolve especially for broad spectrum obtained from amorphous materials. The chemical shifts are similar ranging from 6 to 8 ppm. The Si^1 unit is expected to be located at lower ppm shift due to shielding while the Si^0 is expected to be seen at higher chemical shift. A faint peak at -11.5 ppm is seen in the x=0.0 spectrum which is contributed to the edge sharing ESi^1 SRO unit. Progressing through the series with increasing boron content, this peak quickly diminishes with little NMR spectral evidence past x=0.2.

4.6 Discussion

A SRO model determined from the quantitative analysis of the ^{11}B and ^{29}Si MASS-NMR is shown below. From the SRO model, it can be seen that, beginning at x=0.0, the sodium thiosilicate binary, the fraction of Si^1 SRO units is not 1 as theoretically expected. However, the fraction of Si^1 is ~0.75. The existence of ESi^2 units ensures, for charge balance, the existence of equal numbers of Si^0 which is supported by the quantitative analysis of the ^{29}Si NMR and agrees with the literature. Moving towards the thioborate binary, there is an initial decrease of the fraction of Si^1 followed by an increase. From x=0.2 onward, the general trend is a continuous decrease until x=1.0 where no fraction of Si^1 exists. As mentioned, the existence of ESi^2 is present but in low abundance compared to the Si^1 SRO unit. The ESi^2 is only seen for the x=0.0 and 0.1. This does not agree with the vibrational spectroscopies. It may be possible that the NMR resolution is the issue since the signal-to-noise ratio of ^{29}Si NMR for samples similar to these is poor causing for the ESi^2 peak to essentially go unnoticed. The vibrational spectroscopies instead suggest that the ESi^2 unit persists throughout a majority of the series until about x=0.7 as seen in the infrared spectra. The Si^0 unit has a similar trend to the ESi^2 which corroborates the dissociation of Si^1 into ESi^2 and Si^0. However, the model does have small amounts of Si^0 throughout the entire series until x=1.0 unlike that of ESi^2. This is in fair agreement with the vibrational spectra which shows Si^1 most intensely at the sodium thiosilicate rich end but diminish with increasing thioborate concentration.

As the thioborate concentrate increases, the B^0 unit begins to emerge as the dominant SRO species. It grows in rapidly and continues to increase in nearly a linear fashion. Again, the fraction of B^0 at the pure sodium thioborate binary is not 1 as theoretically expected. However, a small fraction of B^4 units and other oxysulfides. The

fraction of B^4, at the sodium thioborate binary, is in fair agreement with past NMR experiments of sodium thioborate binary studies.[19,31] The B^1 units initially emerge at a similar rate to B^0. However, at $x \geq 0.3$, the rate begins to slow and becomes somewhat constant through the rest of the series to x=1. The B^4 SRO unit emerges slowly with a small fraction starting at x=0.1 and remains fairly constant throughout the entire series.

Upon further inspection of Fig. (5), the total fractions for compositions $x \geq 0.2$ do not add up to 1. In other sulfide systems, polysulfides have been observed in the Raman spectroscopy which would be indicated by a peak at ~470 cm^{-1}. [21,32] The lack of this structural peak in this systems suggests that sodium sulfide is most likely free Na_2S and not Na_2S_n polysulfide compounds where n is either 2 or 4. The polysulfide compounds suggest that sulfur is being taken up from the network creating a sulfur deficient network. Further analysis into the thermal properties does not show any signs of phase separation that is indicated by multiple glass transitions. Examination through x-ray diffraction showed no degree of crystallinity that may arise from unreacted sodium sulfide.

The amount of free sodium sulfide was calculated based on the quantitative NMR results and charge compensation. Fig. (6) shows the moles of free sodium sulfide for the different compositions in this sodium thioborosilicate series. The amount of free sodium sulfide is less than 10 mol % of the total sodium sulfide throughout the series and no free, unreacted sodium sulfide exists in the silicon-rich glasses. This small amount of free sodium sulfide may explain the lack of crystallinity undetected in the x-ray diffraction pattern. It is also seen that with the increase in the thioborate content is an increase in free sodium sulfide. While it is not immediately evident why the silicon-rich glasses favor full reaction with sodium sulfide over boron-rich glasses, creating more free sodium sulfide, a

possible explanation may lie in electronegativies. The electronegativity of silicon and boron is 1.90 and 2.04, respectively, while the electronegativity of sulfur is 2.58.[33] The largest electronegativity difference is silicon and sulfur with a difference of 0.68 while boron and sulfur have an electronegativity difference of 0.54. Silicon and sulfur exhibit a stronger, more ionic bond than that of boron and sulfur meaning silicon's affinity for sulfur is stronger than that of boron's. This may explain the general increase in free sodium sulfide with increasing thioborate concentration and more incorporation of sodium sulfide in the silicon-rich glasses.

Further investigation into binary sodium thioborate suggests that the reaction is entropy driven, giving rise to the many different SRO species that are present. The expected SRO unit would be the B^0, however, while there is a large fraction of B^0 this is not the sole SRO unit present. The many reactants visible in the different spectroscopic techniques are evidence of multiple competing reactions taking place to produce either B^0, B^1, B^4 and even mixed oxy-sulfide versions of these SRO units due to the small oxygen contamination. Boron's affinity for oxygen over sulfur, even in small amounts, may be increasing the amount of possible reaction pathways for these SRO units to form.

4.7 Conclusion

The SRO structures of the sodium thioborosilicate, $0.6Na_2S + 0.4[xBS_{3/2} + (1-x)SiS_2]$, system was examined through infrared, Raman, ^{11}B MASS-NMR and ^{29}Si MASS-NMR spectroscopies. It was seen that as the glass becomes boron rich the networking of the glass breaks down as seen in the SRO transition of primary Si^1 units to primary B^0. The quantitative NMR results and charge compensation suggest the existence of free, unreacted sodium sulfide which increased with increasing thioborate content. The sodium sulfide is present in very low concentrations that it is difficult to detect through

the means used here. The existence of many boron SRO units, however in small quantities, suggests that there are multiple competing reactions occurring to produce such units.

4.6 Acknowledgements

This research was supported by the National Science Foundation under DMR grants 1304977 and 0710564. The authors would like to take this time to thank the other members of the Iowa State Glass and Optical Materials research group along with Sarah Cady for her help with solid state NMR.

4.7 References

1 *Wind Energy in Iowa*, (2017).

2 Kumar, D. & Hashmi, S. A. Ionic liquid based sodium ion conducting gel polymer electrolytes. *Solid State Ionics* **181**, 416-423, doi:http://dx.doi.org/10.1016/j.ssi.2010.01.025 (2010).

3 Song, J. Y., Wang, Y. Y. & Wan, C. C. Review of gel-type polymer electrolytes for lithium-ion batteries. *Journal of Power Sources* **77**, 183-197, doi:http://dx.doi.org/10.1016/S0378-7753(98)00193-1 (1999).

4 Hayashi, A., Ohtomo, T., Mizuno, F., Tadanaga, K. & Tatsumisago, M. All-solid-state Li/S batteries with highly conductive glass–ceramic electrolytes. *Electrochemistry Communications* **5**, 701-705, doi:https://doi.org/10.1016/S1388-2481(03)00167-X (2003).

5 Youngblood, G. E., Miller, G. R. & Gordon, R. S. Relative Effects of Phase Conversion and Grain Size on Sodium Ion Conduction in Polycrystalline, Lithia-Stabilized β-Alumina. *Journal of the American Ceramic Society* **61**, 86-87, doi:10.1111/j.1151-2916.1978.tb09238.x (1978).

6 Christensen, R., Byer, J., Olson, G. & Martin, S. W. The glass transition temperature of mixed glass former 0.35Na2O+0.65[xB2O3+(1−x)P2O5] glasses. *Journal of Non-Crystalline Solids* **358**, 826-831, doi:http://dx.doi.org/10.1016/j.jnoncrysol.2011.12.068 (2012).

7 Christensen, R., Olson, G., Martin, S. W. & Kieffer, J. *Na+ Ion conduction in and the Structures and Properties of 0.33Na2O+0.66[xB2O3+(1-x)2SiO2] Mixed Glass Former Glasses*.

8 Christensen, R., Olson, G. & Martin, S. W. Ionic Conductivity of Mixed Glass Former 0.35Na2O + 0.65[xB2O3 + (1 – x)P2O5] Glasses. *The Journal of Physical Chemistry B* **117**, 16577-16586, doi:10.1021/jp409497z (2013).

9 Christensen, R., Olson, G. & Martin, S. W. Structural Studies of Mixed Glass Former 0.35Na2O + 0.65[xB2O3 + (1 – x)P2O5] Glasses by Raman and 11B and 31P Magic Angle Spinning Nuclear Magnetic Resonance Spectroscopies. *The Journal of Physical Chemistry B* **117**, 2169-2179, doi:10.1021/jp308494a (2013).

10 Bischoff, C. *The Mixed Glass Former Effect in $0.5Na_2S+0.5[xGeS_2+(1-x)PS_{5/2}]$ Glasses* Doctor of Philosophy thesis, Iowa State University, (2013).

11 Deshpande, V. K., Pradel, A. & Ribes, M. The mixed glass former effect in the Li2S : SiS2 : GeS2 system. *Materials Research Bulletin* **23**, 379-384, doi:http://dx.doi.org/10.1016/0025-5408(88)90012-8 (1988).

12 Martin, S. in *Handbook of Solid State Batteries Materials and Energy* (ed Leonard C. Feldman) Ch. 14, 433-501 (World Scientific, 2016).

13 Patel, H. *Impedance Spectroscopy and NMR Studies of Fast Ion Conducting Chalcogenide Glasses* Ph.D. thesis, Iowa State University, (1993).

14 Hayashi, A., Minami, K. & Tatsumisago, M. High lithium ion conduction of sulfide glass-based solid electrolytes and their application to all-solid-state batteries. *Journal of Non-Crystalline Solids* **355**, 1919-1923, doi:https://doi.org/10.1016/j.jnoncrysol.2008.12.020 (2009).

15 Martin, S. W., Bischoff, C. & Schuller, K. Composition Dependence of the Na+ Ion Conductivity in 0.5Na2S + 0.5[xGeS2 + (1 – x)PS5/2] Mixed Glass Former Glasses: A Structural Interpretation of a Negative Mixed Glass Former Effect. *The Journal of Physical Chemistry B* **119**, 15738-15751, doi:10.1021/acs.jpcb.5b07383 (2015).

16 Bischoff, C., Schuller, K., Dunlap, N. & Martin, S. W. IR, Raman, and NMR Studies of the Short-Range Structures of 0.5Na2S + 0.5[xGeS2 + (1–x)PS5/2] Mixed Glass-Former Glasses. *The Journal of Physical Chemistry B* **118**, 1943-1953, doi:10.1021/jp4111053 (2014).

17 Cho, J. *Preparation and Characterization of B2S3-Based Chalcogenide Glasses* Doctor of Philosophy thesis, Iowa State University, (1995).

18 Bloyer, D. R., Cho, J. & Martin, S. W. Infrared Spectroscopy of Wide Composition Range xNa2S + (1 –x)B2S3 Glasses. *Journal of the American Ceramic Society* **76**, 2753-2759 (1993).

19 Hwang, S. J. *et al.* Structural Study of xNa2S + (1 − x)B2S3 Glasses and Polycrystals by Multiple-Quantum MAS NMR of 11B and 23Na. *Journal of the American Chemical Society* **120**, 7337-7346, doi:10.1021/ja9800481 (1998).

20 Martin, S. W. Ionic Conduction in Phosphate Glasses. *Journal of the American Ceramic Society* **74**, 1767-1784 (1991).

21 Watson, D. E. & Martin, S. W. Short range order characterization of the Na2S+SiS2 glass system using Raman, infrared and 29Si magic angle spinning nuclear magnetic resonance spectroscopies. *Journal of Non-Crystalline Solids* **471**, 39-50, doi:https://doi.org/10.1016/j.jnoncrysol.2017.04.032 (2017).

22 Pradel, A., Taillades, G., Ribes, M. & Eckert, H. 29Si NMR structural studies of ionically conductive silicon chalcogenide glasses and model compounds. *Journal of Non-Crystalline Solids* **188**, 75-86, doi:https://doi.org/10.1016/0022-3093(94)00662-8 (1995).

23 Pradel, A. *et al.* Mixed Glass Former Effect in the System 0.3Li2S−0.7[(1−x)SiS2−xGeS2]: A Structural Explanation. *Chemistry of Materials* **10**, 2162-2166, doi:10.1021/cm980701j (1998).

24 Martin, S. & Bloyer, D. Preparation of High-Purity Vitreous B_2S_3. *Journal of the American Ceramic Society* **73**, 3481-3485 (1990).

25 Harris, R. K., Becker, E. D., Cabral de Menezes, S. M., Goddfellow, R. & Granger, P. NMR Nomenclature. Nuclear spin properties and conventions for chemical shifts (IUPAC Recommendations 2001). *Pure and Applied Chemistry* **73**, 1795-1818 (2001).

26 Massiot, D. *et al.* Modelling one- and two-dimensional solid-state NMR spectra. *Magnetic Resonance in Chemistry* **40**, 70-76, doi:10.1002/mrc.984 (2002).

27 Royle, M., Cho, J. & Martin, S. W. Raman spectroscopy studies of xNa2S+(1−x)B2S3 glasses and polycrystals. *Journal of Non-Crystalline Solids* **279**, 97-109, doi:http://dx.doi.org/10.1016/S0022-3093(00)00344-6 (2001).

28 Cho, J. & Martin, S. in *Role of Ceramics in Advanced Electrochemical Systems* Vol. 65 (ed American Ceramic Society) (1995).

29 Hwang, S. J. *et al.* Quantitative study of the short range order in B2O3 and B2S3 by MAS and two-dimensional triple-quantum MAS 11B NMR. *Solid State Nuclear Magnetic Resonance* **8**, 109-121, doi:https://doi.org/10.1016/S0926-2040(96)01280-5 (1997).

30 Larink, D., Eckert, H. & Martin, S. W. Structure and Ionic Conductivity in the Mixed-Network Former Chalcogenide Glass System [Na2S]2/3[(B2S3)x(P2S5)1–x]1/3. *The Journal of Physical Chemistry C* **116**, 22698-22710, doi:10.1021/jp3068365 (2012).

31 Sills, J. A., Martin, S. W. & Torgeson, D. R. 11B NMR studies of the short range order in wide composition range xNa2S+(1-x)B2S3 glasses. *Jornal of Non-Crystalline Solids* **168**, 86-96 (1994).

32 El Jaroudi, O., Picquenard, E., Gobeltz, N., Demortier, A. & Corset, J. Raman Spectroscopy Study of the Reaction between Sodium Sulfide or Disulfide and Sulfur: Identity of the Species Formed in Solid and Liquid Phases. *Inorganic Chemistry* **38**, 2917-2923, doi:10.1021/ic9900096 (1999).

33 Allred, A. L. & Rochow, E. G. Electronegativities of carbon, silicon, germanium, tin and lead. *Journal of Inorganic and Nuclear Chemistry* **5**, 269-288, doi:https://doi.org/10.1016/0022-1902(58)80004-4 (1958).

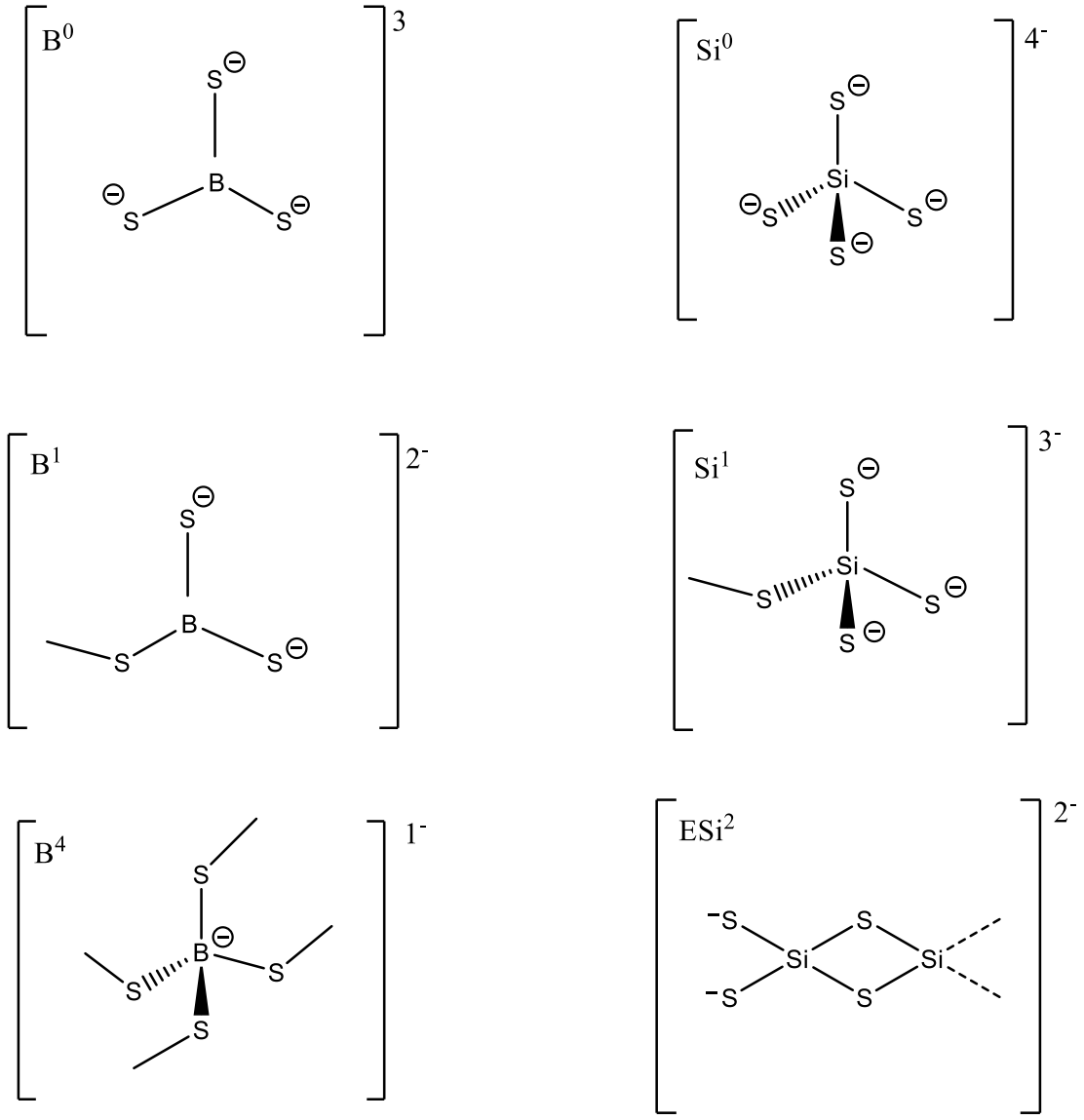

Figure 4.1. The SRO structures and their corresponding notion.

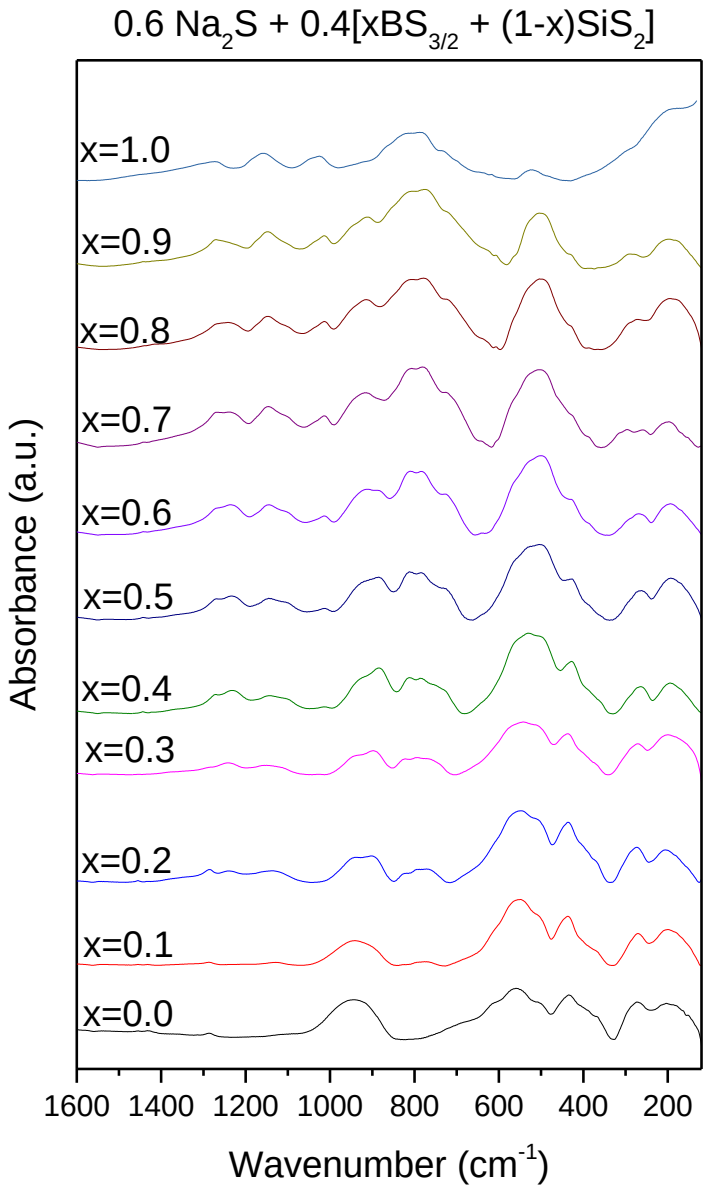

Figure 4.2. The mid- and far-infrared spectra of the sodium thioborosilicates.

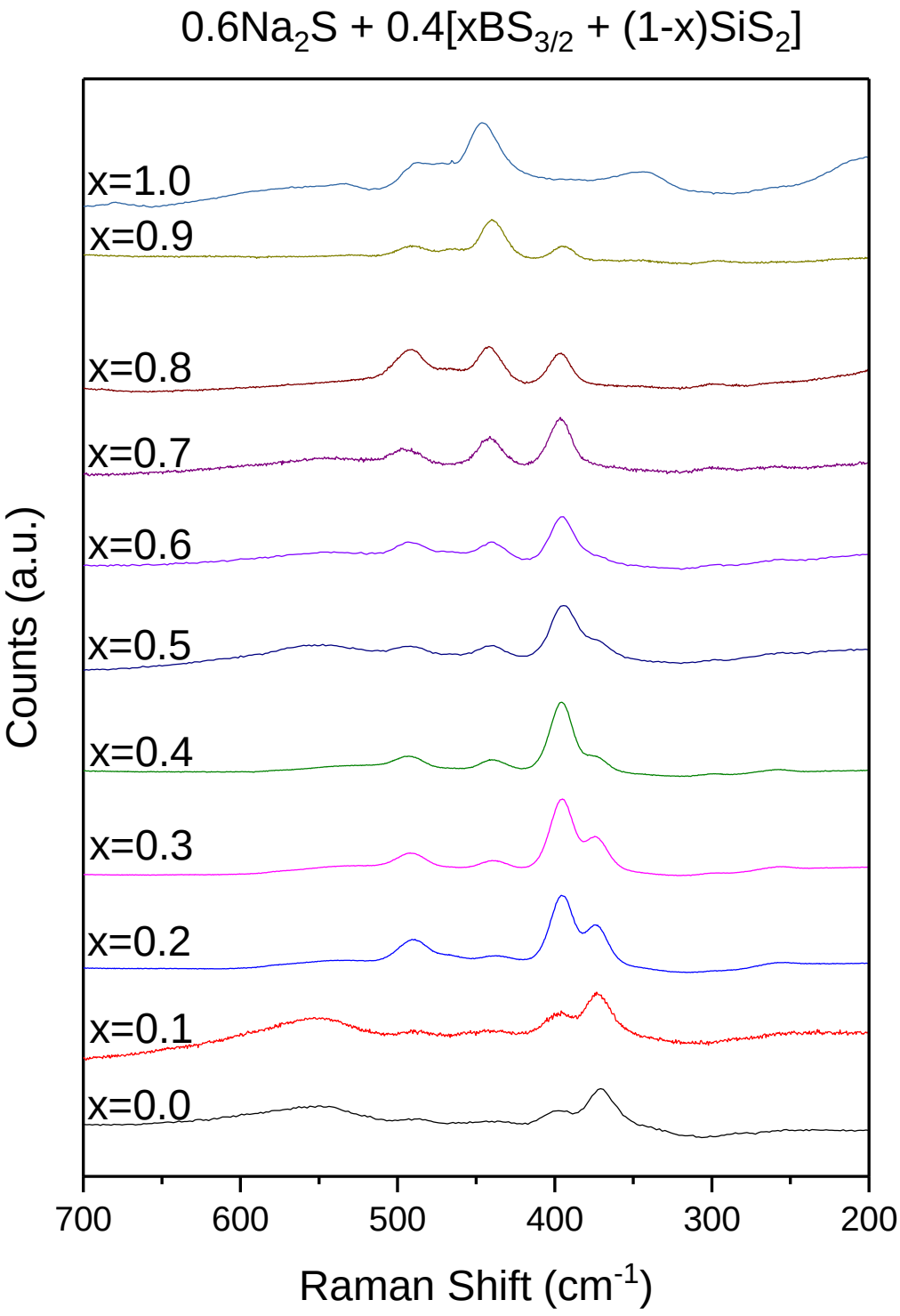

Figure 4.3. The Raman spectra of the sodium thioborosilicates.

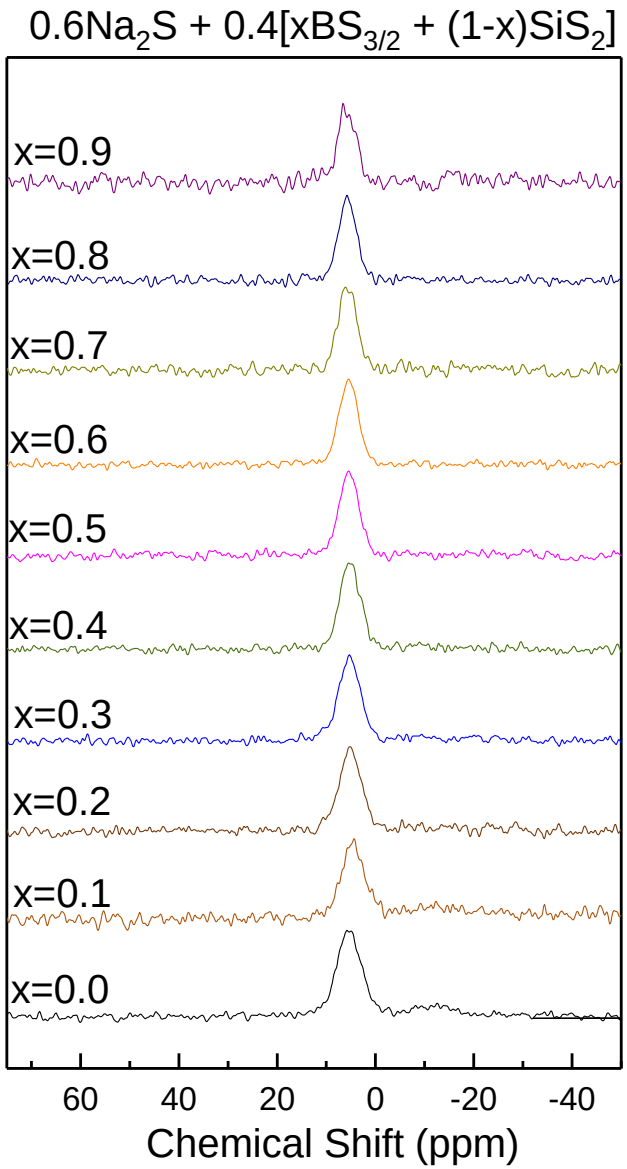

Figure 4.4. The ^{29}Si MASS-NMR of the sodium thioborosilicates.

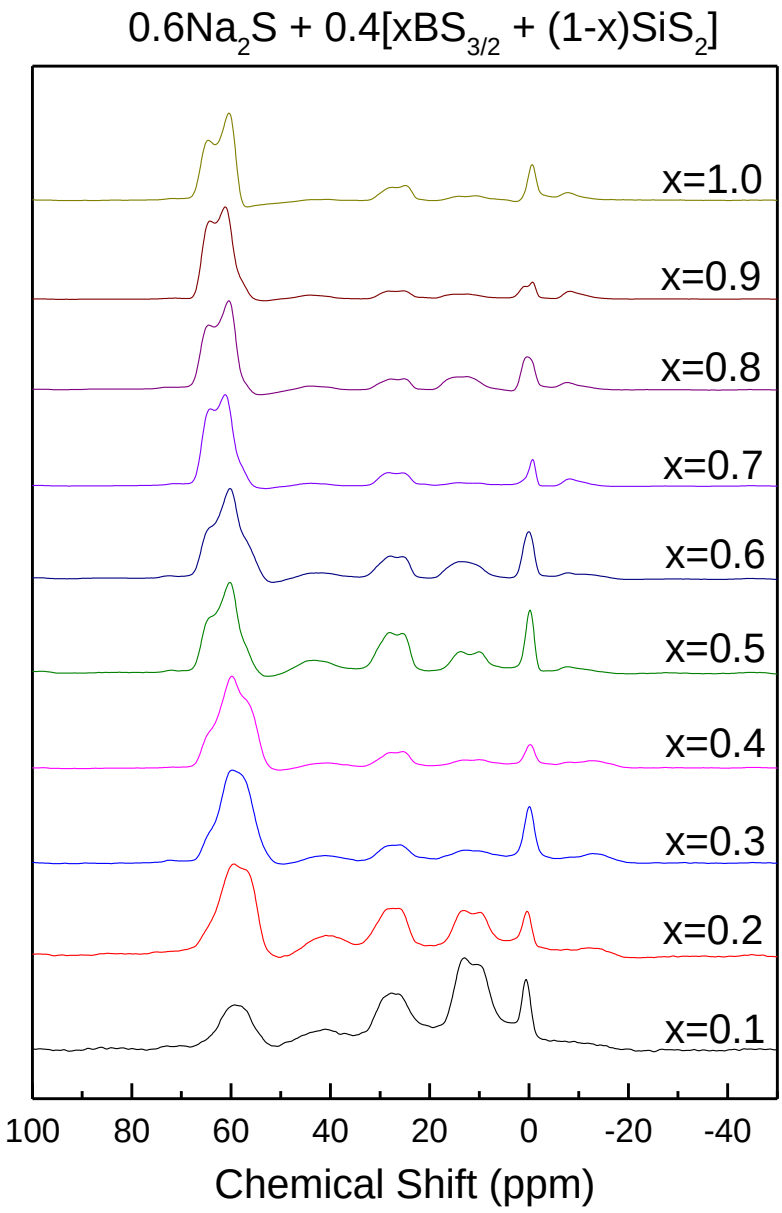

Figure 4.5. The 11B MASS-NMR of the sodium thioborosilicates.

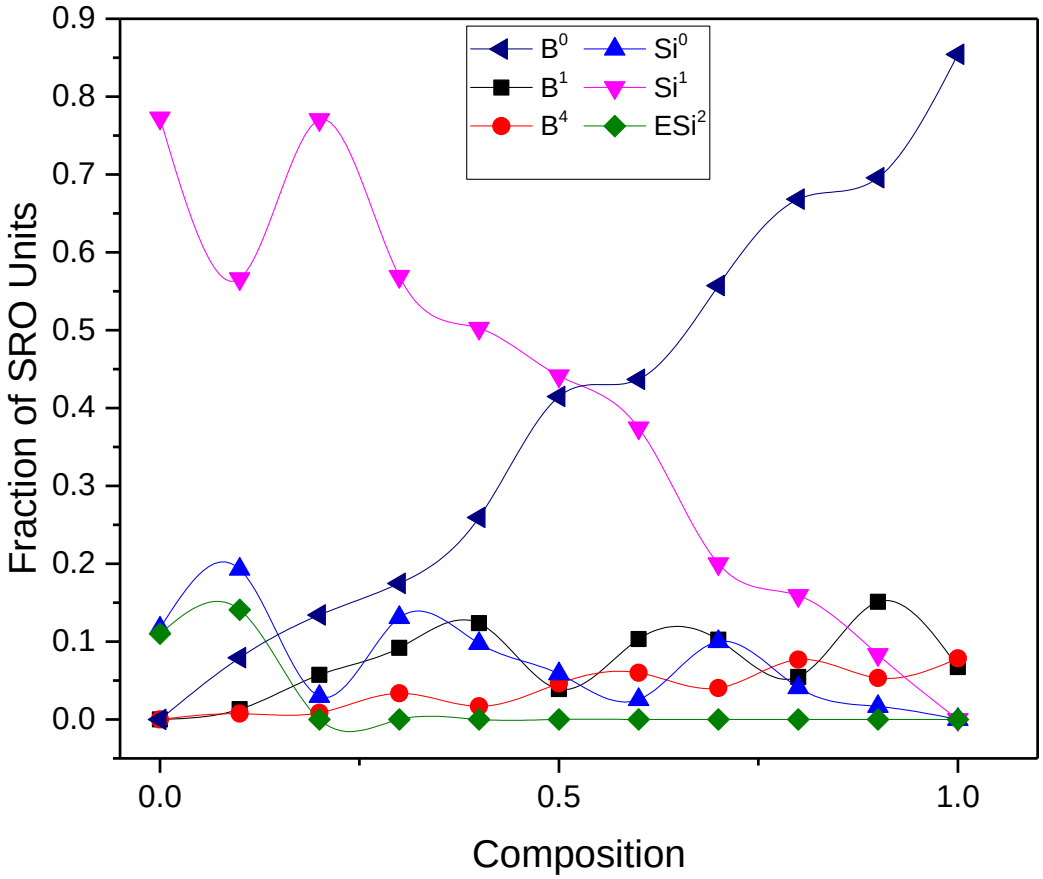

Figure 4.6. The SRO model of the sodium thioborosilicates

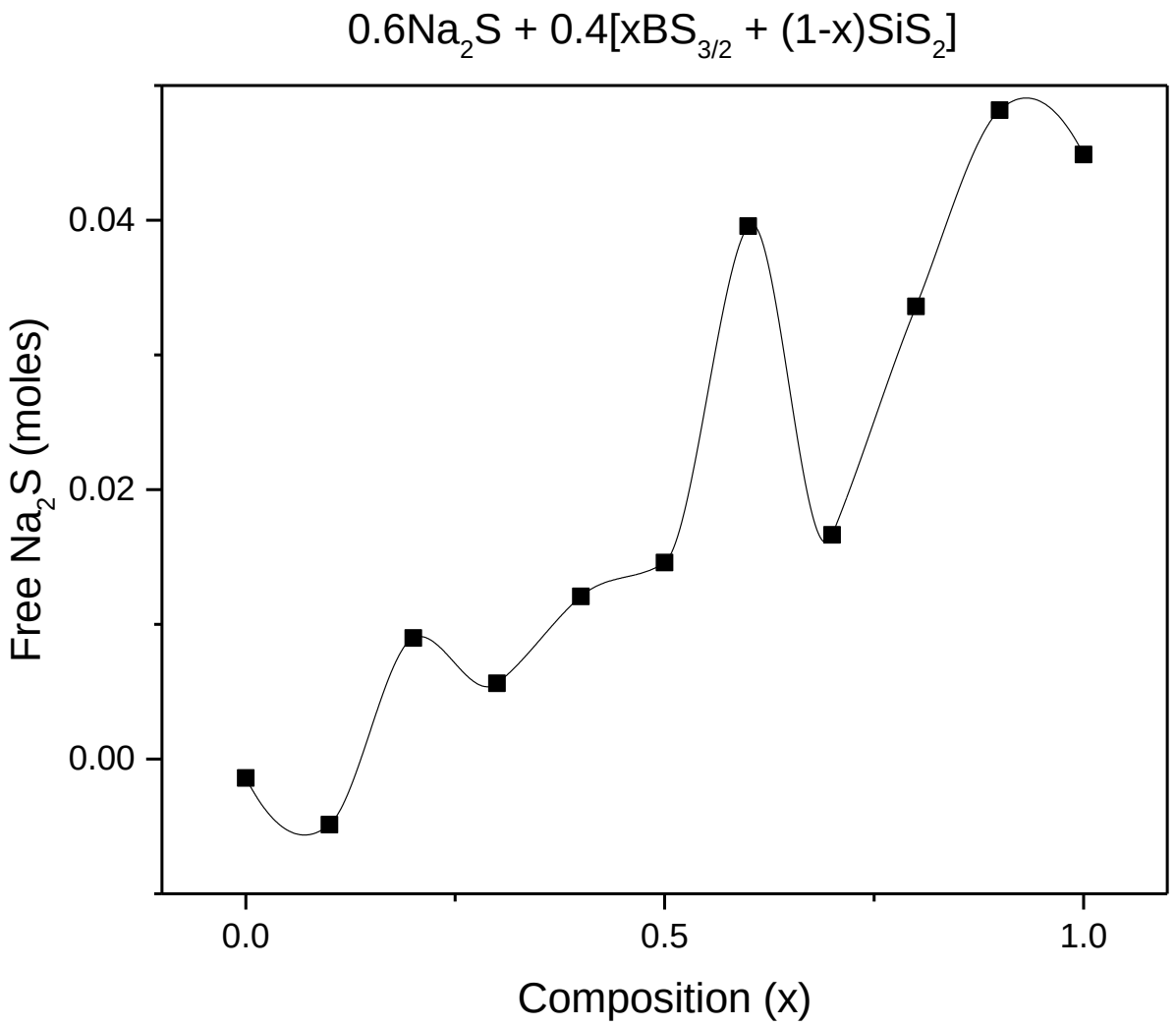

Figure 4.7. The mol% of free sodium sulfide for each composition of the sodium thioborosilicates.

CHAPTER 5. IONIC CONDUCTIVITIES OF THE SODIUM THIOBOROSILICATE MIXED GLASS FORMER SYSTEM $0.6Na_2S + 0.4[xBS_{3/2} + (1-x)SiS_2]$

A paper to be submitted the Journal of Non-Crystalline Solids

Brittany Curtis, Carter Francis and Steve Martin*

Department of Materials Science & Engineering
Iowa State University of Science and Technology
Ames, IA

5.1 Abstract

Solid-state electrolytes are becoming of increasing interest during the development of all solid-state batteries. Sulfide-based, glassy solid-state electrolytes are an attractive alternative over the liquid, organic electrolytes. The amorphous structure of these materials may prove to be superior ionic conductors over materials that produce grain boundaries. This study examined the mixed glass former effect with respect to the ionic conductivity of a sodium thioborosilicate system, $0.6Na_2S + 0.4[xBS_{3/2} + (1-x)SiS_2]$. The ionic conductivities were determined using electrochemical impedance spectroscopy. It was seen that there was a general negative mixed glass former effect in the ionic conductivities. However, with respect to the activation energy of ionic conduction, the mixed glass former effect exhibited a positive trend in the silicon-rich samples, and a negative trend in the boron-rich samples. The negative MGFE of the ionic conductivities in these glasses may be attributed to the decreasing molar volume that was calculated from experimental density measurements. Free sodium sulfide may be playing a role as well since the amount of free, unreacted sodium sulfide increases with the

* Corresponding author, swmartin@iastate.edu

increasing thioborate concentration. Further analysis into the activation energy, specifically the Christensen Martin Anderson Stuart model of ionic conduction suggests that the strain energy is minimal and that the binding energy portion of the total activation energy is the largest contributing factor.

5.2 Introduction

All solid-state batteries are of increasing interest to meet demands as new alternative energy sources are being developed. Currently, lithium-ion batteries are the more popular and well-known secondary battery. However, while these batteries have widespread use lending to their popularity and versatility, there have been many safety concerns arising from battery failure of these types of batteries.[1,2] In many cases, it is caused by dendritic formation leading to thermal runaway, which in turn causes the flammable inorganic electrolyte to ignite.[3-5] Due to these potentially catastrophic events, the focus has turned to the development of an all solid-state battery (ASSB) as a safer, and a more energy dense alternative to lithium-ion batteries. While lithium-ion batteries are more widely used, the low abundance of lithium tends to drive up the costs meaning that lithium metal batteries could potentially be rather expensive to manufacture. Sodium metal batteries could prove to be an inexpensive substitute in the battery market. There are some major differences between the two alkali metals. As already referenced is the natural abundance. Lithium metal is about 20 ppm in the Earth's crust whereas sodium is much higher with 23,600 ppm in the Earth's crust.[6,7] Sodium is also heavier than lithium meaning that it ultimately would not be a viable alternative for portable devices. Sodium is a little over 3 times heavier than that of lithium. Consequently, the larger size of sodium may impede its ability, as a solid-state electrolyte, to conduct as well as lithium making it difficult to reach the target ionic conductivity of 10^{-3} S/cm.[8]

More research into the field of solid-state electrolytes may be able to produce the competitive ionic conductivities needed. Many materials have been studied including polymer gel, ceramic, glass ceramic, and, of particular interest to this study, pure glassy materials.[4,9-13] While oxide glasses are known to be very poor ionic conductors (10^{-12} to 10^{-10} S/cm), their sulfide analogs show much improvement by roughly 6 orders of magnitude larger ionic conductivities (10^{-6} to 10^{-5} S/cm).[14-17] While the binary sulfide glasses still have insufficient ionic conductivities for their use in all solid-state batteries, it has been seen that these properties have been optimized through the mixed glass former effect which is explained in more detail in the background section of this paper. This paper aims to study the ionic conductivity of the glass system sodium thioborosilicate, $0.6Na_2S + 0.4[xBS_{3/2} + (1-x)SiS_2]$ as it relates to the mixed glass former effect and better understand the structural roles affecting the ionic conductivity.

5.3 Background

5.3.1 Mixed Glass Former Effect

As previously mentioned, this paper will explore the phenomenon of the mixed glass former effect with particular interest giving to the ionic conductivity. Our research group and others have done many studies of the mixed glass former effect on various systems.[15,17-20] The mixed glass former effect is a phenomenon which observes a non-linear and non-additive trend in physical properties upon mixing two glass formers in varying ratio from one binary system to the next through a ternary system of both glass formers. The glass formers of interest in this study are boron sulfide ($BS_{3/2}$) and silicon sulfide (SiS_2) while the modifier, sodium sulfide (Na_2S) is held constant. A positive mixed glass former effect is a positive deviation from linearity with a maximum in the physical property as is the case for the ionic conductivity of the sodium borophosphates.[15]

A negative mixed glass former effect can also occur as indicated by the ionic conductivity in the mixed glass former system of the sodium thiogermanophosphates.[18] This is similar to the positive mixed glass former effect, however, instead of a positive deviation there is a negative deviation from linearity with a minimum in the physical property.

5.4 Experimental Procedures

5.4.1 Preparation of Precursors

In order to prepare the glasses, the base materials needed to be synthesized as well. Sodium sulfide is available commercially, however, to increase the purity of sodium sulfide sodium sulfide nonahydrate (Acros Oraganics, 98%) was dehydrated under vacuum at 250 C. Silicon sulfide and boron sulfide are not available commercially at the purities needed to ensure good glass formation. Therefore, silicon sulfide was synthesized by combining stoichiometric amounts of silicon powder (Alfa Aesar, crystalline, 99.999%) and sulfur (Acros Organic, 99.999%) in an evacuated, sealed silica ampoule inside a nitrogen glovebox. The ampoule was then removed and loaded into a mullite, tube furnace and allowed to slowly reach 900 C in a tube furnace and then held at temperature for 11 hours. Boron sulfide was synthesized in a similar matter but in a carbon coated silica ampoule as proposed by Bloyer et. al.[21] Stoichiometric amounts of boron (NOAH Technologies, crystalline, 99.5%) and sulfur. Again, the evacuated ampoule was placed into a tube furnace and slowly heated to 860 C where it was held at temperature for four hours. All reacted ampoules were transferred to a nitrogen glovebox where the reaction chambers were opened, milled, and further analysis done to ensure purity.

5.4.2 Preparation of Glass Samples

Samples were made from stoichiometric amounts of precursors described above. The powders were milled for 20 minutes in a steel millpot in a SpexMill. Once milled, samples were transferred to a carbon crucible and reacted in a nitrogen atmosphere in a tube furnace for 5 minutes at 550 to 720 C depending on composition. All samples were subjected to no more than 2 % mass loss to ensure compositional accuracy. The sample melts were then quenched between two brass plates and characterized.

5.4.3 Impedance Spectroscopy

The ionic conductivities were obtained using a Novocontrol Broadband Dielectric Spectrometer using an Alpha A series analyzer. Annealed, glass disk samples that were ~15 mm in diameter and 1 to 2 mm in thickness were painted with conductive silver paint. They were loaded into a puck-like, sealed sample holder with a known capacitance. The sample was loaded into the sample cell of the instrument, ran from room temperature to 50 degrees below the glass transition temperature, and scanned from 10^{7} to 10^{-1} Hz. The data was fit using WinFit software. An example fitting of a complex impedance plot can be seen in Fig. 5.1.

5.5 Results

The direct current (DC) ionic conductivities were determined at different temperatures ranging from room temperature to 50 C below the glass transition which varied based on the composition. The DC ionic conductivities were determined using the equation below:

$$\sigma_{D.C.} = \frac{1}{R} \cdot \frac{t}{A}$$

where $\sigma_{D.C.}$ is the DC conductivity, R is the resistance, t is the thickness of the sample,

and A is the area of the sample. The resistance of the sample is found through an alternating current experiment where the real and imaginary parts of the impedance were plotted to construct a Nyquist plot. This plot was then fit with an equivalent RC circuit model where the magnitude of the impedance is described by the expression below:

$$|Z| = \frac{R}{1+(\omega RC)^2} - j\left(\frac{\omega R^2 C}{1+(\omega RC)^2}\right) \quad (2)$$

where ω is the angular frequency, C is the constant phase element, j is the imaginary component $\sqrt{-1}$. The first part of the expression describes the real part of the impedance and the second portion describes the imaginary part of the impedance. When the angular frequency is essentially zero, indicative of direct current, then the impedance goes to R and this value is used in eq. (1) to calculated the DC ionic conductivity at the various temperatures. Fig. 5.2 shows the Arrhenius plot of the conductivities. As the thioborate concentration increases (increasing x-value), the ionic conductivities decrease. To get a better idea of the mixed glass former effect with respect to the ionic conductivity, the ionic conductivities at 30, 90, and 130 C were plotted against the composition x-value (Fig. 5.3). From this compositional plot, we can see there is a negative deviation from linearity from x=0.1 to x=0.3 where after there is a positive deviation with a local maximum iat x=0.4.

To determine the activation energy of ionic conduction, the Arrhenius equation for conductivity was used and is shown in eq. (3).

$$\sigma_{D.C.} = \frac{\sigma_0}{T} exp\left[-\frac{\Delta E_{Act}}{RT}\right] \quad (3)$$

The pre-exponential factor is indicated by σ_0, T is the temperature, R is Boltzmann's constant, and ΔE_{Act} is the activation energy for ionic conductivity. The activation energies were determined by rearranging the above equation into eq. (4).

$$ln(\sigma_{D.C.} * T) = \frac{\Delta E_{act}}{RT} + ln(\sigma_o) \quad (4)$$

The activation energies were determined from the generated Arrhenius plots and can be seen in Fig. 5.4 for each composition. The Arrhenius plot exhibits a positive deviation from linearity in the silicon-rich portion while around x=0.5 where is begins to exhibit a negative deviation from linearity. The activation energy of the boron-rich samples is relatively unchanged until the pure sodium thioborate sample where a large increase in the activation energy is seen.

5.6 Discussion

As briefly, mention in the results section, the ionic conductivity shows a negative deviation from linearity, which is indicative of a negative mixed glass former effect. The ionic conductivity of the sodium thiobosilicate is $4.17x10^{-5}$ $(\Omega*cm)^{-1}$ while the sodium thioborate has a lower ionic conductivity of $2.94x10^{-6}$ $(\Omega*cm)^{-1}$. As seen in the Arrhenius plot, the ionic conductivity decreases with increasing boron content. The decreasing ionic conductivity may be due to a few different reasons including molar volume, the amount of free sodium sulfide, and the interactions of sulfur with silicon and boron on an atomic level.

Fig. 5.5 shows the calculated molar volume for each composition. As seen, the molar volume decreases with increasing x-value. The smaller the molar volume, the less amount of space for sodium atoms to migrate through the glass structure. In this case the sodium thioborosilicate has a smaller molar volume which may indicate a higher activation energy barrier for sodium to conduct. A more in-depth discussion of the molar volume and densities of these glasses can be seen in the paper by Curtis *et al.*[22]

As previously published, Curtis *et al.*[23] also study the structure of these glasses. It was seen the small amounts of free, unreacted sodium sulfide exists in small quantities (less than 10 mol% at the most). While only a small amount, this can be a contributing factor to the diminishing ionic conductivity with increased thioborate content. The ionic conductivity can be expressed by the equation below:

$$\sigma = \mathrm{nZe}\mu \tag{5}$$

where n is the number of mobile ions per unit volume, Z is the charge of the mobile ion, and e is the electric charge, and μ is the mobility of the ions. The number of mobile ions per unit volume decreases when more free, unreacted sodium sulfide is generated. Since n decreases with increasing free sodium sulfide, it can easily be seen that the ionic conductivity decreases as well.

Little is understood about why the boron-rich glasses are not accepting as much sodium sulfide into the structure as the silicon-rich ones. One explanation may lie in the strength of the bonds. Investigating the electronegativity differences, the silicon sulfur bond has the largest difference proving to be more ionic and stronger than that of the boron sulfur bond. The stronger interaction that silicon has on a terminating sulfur means a weakening of the interaction between sodium and the corresponding sodium. This not only explains why the silicon may uptake more sodium sulfide since it has a stronger attraction to sulfur but why the ionic conductivity is higher in the sodium thiosilicate binary.

5.6.1 Christensen Martin Anderson Stuart Model

The Anderson-Stuart model for ionic conduction is one of the most well accepted models for this type of application. It consists of two main portions to the overall activation energy of ionic conduction: the strain energy and the binding energy.[24] Both

portions describe the activation energy for ionic conduction. Table 5.2 shows the fitting parameters used for both the strain energy and the binding energy. The strain energy can be defined by:

$$E_S = \pi G \frac{\lambda}{2}(r - r_d)^2 \quad (6)$$

where E_s is the strain energy, G is the shear modulus r_d is the doorway radius and r_{Na} is the radius of the sodium ion. Little is reported on the shear modulus of these sulfide glasses but the glass transition temperature can give insight into the general trend of the shear modulus.[25,26] The glass transition temperatures for each composition are shown in Fig. 5.7. Overall, the glass transition temperature decreases from the sodium thiosilicates to the sodium thioborates in a nearly linear fashion. Therefore, the shear modulus portion of the activation energy will have a similar trend due to the direct relationship between the strain energy and the shear modulus. As seen, the Tg indicates a decrease in strain energy. However, upon comparison to the experimental activation energy, it is seen that the sodium thiosilicate has a lower activation energy than that of the sodium thioborate. Therefore, the strain energy is barely effecting the overall trend of the activation energy. This may inform that the binding energy has more influence on the total activation energy than the strain energy. In Fig. 5.8, shows the calculated strain energy using an approximation of the shear modulus of a similar sodium sulfide glass system studied by Bischoff *et al* based on the trend in the glass transition temperature .[27] The composition dependence of the strain energy is fairly constant and has a small contribution to the overall activation energy.

The binding energy was determined using the equation below:

$$E_b = \frac{M_{Na} Z_{Na} Z_S e^2}{4\pi\varepsilon_0\varepsilon_\infty}\left(\frac{1}{r_{Na} + r_S} - \frac{1}{r_{Na} + r_S + \lambda/2}\right) \quad (7)$$

where E_b is the binding energy, Z_{Na} is the valence of the sodium (1), Z_S is the valence on sulfur (2), e is the electric charge, ε_0 is the permittivity of free space, ε_∞ is the high frequency permittivity of each sample, r_{Na} is the radius of sodium, r_s is the radius of sulfur, and λ is the jump distance. The binding energy was calculated for each composition and the results can be seen in Fig 5.9. It should be noted that the binding energy matches the trend of the experimental activation energy well. This is due to how the Madelung's constant (Md) was determined. It is difficult to determine Madelung's constant for these glasses due to the lack of long range order and periodicity. Therefore, Md was back calculated by setting the binding energy and the strain energy equal to the experimental activation energy and solving for Md. The values for the Madelung's constants are shown in Table 5.2. This calculation is also secondary check to how reliable is the Christensen Martin Anderson Stuart model. While there is much variation in the values from composition to composition, they are within reason to other glass systems.[18] From the binding energy calculation, it is seen that the Coulombic binding energy has a larger effect on the overall activation energy.

5.7 Conclusion

The D.C. ionic conductivity of the sodium thioborosilcate glass system, $0.6Na_2S + 0.4[xBS_{3/2} + (1-x)SiS_2]$, was determined by electrochemical impedance spectroscopy. It was seen that there is a negative mixed glass former effect with respect to the ionic conductivity with the ionic conductivity being much less in the sodium thioborate binary than the sodium thiosilicate. It was proposed that this may be due to increase amounts of free, unreacted sodium sulfide and a decrease in molar volume. The activation energy of ionic conduction was modeled with the Christensen Martin Anderson Stuart model and found fair agreement between experimental and modeled behavior.

5.7 Acknowledgements

This research was supported by the National Science Foundation under DMR grants 1304977 and 0710564. The authors would like to take this time to thank the other members of the Iowa State Glass and Optical Materials research group.

5.8 References

1 Lisbona, D. & Snee, T. A review of hazards associated with primary lithium and lithium-ion batteries. *Process Safety and Environmental Protection* **89**, 434-442, doi:https://doi.org/10.1016/j.psep.2011.06.022 (2011).

2 Wen, J., Yu, Y. & Chen, C. A Review on Lithium-Ion Batteries Safety Issues: Existing Problems and Possible Solutions. *Materials Express* **2**, 197-212, doi:10.1166/mex.2012.1075 (2012).

3 Wang, Q. *et al.* Thermal runaway caused fire and explosion of lithium ion battery. *Journal of Power Sources* **208**, 210-224, doi:https://doi.org/10.1016/j.jpowsour.2012.02.038 (2012).

4 Rosso, M. *et al.* Dendrite short-circuit and fuse effect on Li/polymer/Li cells. *Electrochimica Acta* **51**, 5334-5340, doi:https://doi.org/10.1016/j.electacta.2006.02.004 (2006).

5 Monroe, C. & Newman, J. Dendrite Growth in Lithium/Polymer Systems: A Propagation Model for Liquid Electrolytes under Galvanostatic Conditions. *Journal of The Electrochemical Society* **150**, A1377-A1384 (2003).

6 Ene-Parent, J. & Zikovsky, L. Neutron activation analysis of laundry dryer lint. *Journal of Radioanalytical and Nuclear Chemistry* **247**, 197-198, doi:10.1023/A:1006712408990 (2014).

7 Carmichael, R. S. *Practical Handbook of Physical Properties of Rocks and Minerals*. (CRC Press Inc., 1989).

8 Slater, M. D., Kim, D., Lee, E. & Johnson, C. S. Sodium-Ion Batteries. *Advanced Functional Materials* **23**, 947-958, doi:10.1002/adfm.201200691 (2013).

9 Song, J. Y., Wang, Y. Y. & Wan, C. C. Review of gel-type polymer electrolytes for lithium-ion batteries. *Journal of Power Sources* **77**, 183-197, doi:http://dx.doi.org/10.1016/S0378-7753(98)00193-1 (1999).

10 Kumar, D. & Hashmi, S. A. Ionic liquid based sodium ion conducting gel polymer electrolytes. *Solid State Ionics* **181**, 416-423, doi:http://dx.doi.org/10.1016/j.ssi.2010.01.025 (2010).

11 Kumar, D. & Hashmi, S. A. Ion transport and ion–filler-polymer interaction in poly(methyl methacrylate)-based, sodium ion conducting, gel polymer electrolytes dispersed with silica nanoparticles. *Journal of Power Sources* **195**, 5101-5108, doi:http://dx.doi.org/10.1016/j.jpowsour.2010.02.026 (2010).

12 Hayashi, A., Ohtomo, T., Mizuno, F., Tadanaga, K. & Tatsumisago, M. All-solid-state Li/S batteries with highly conductive glass–ceramic electrolytes. *Electrochemistry Communications* **5**, 701-705, doi:https://doi.org/10.1016/S1388-2481(03)00167-X (2003).

13 Youngblood, G. E., Miller, G. R. & Gordon, R. S. Relative Effects of Phase Conversion and Grain Size on Sodium Ion Conduction in Polycrystalline, Lithia-Stabilized β-Alumina. *Journal of the American Ceramic Society* **61**, 86-87, doi:10.1111/j.1151-2916.1978.tb09238.x (1978).

14 Christensen, R., Olson, G., Martin, S. W. & Kieffer, J. *Na+ Ion conduction in and the Structures and Properties of 0.33Na2O+0.66[xB2O3+(1-x)2SiO2] Mixed Glass Former Glasses*.

15 Christensen, R., Olson, G. & Martin, S. W. Ionic Conductivity of Mixed Glass Former 0.35Na2O + 0.65[xB2O3 + (1 – x)P2O5] Glasses. *The Journal of Physical Chemistry B* **117**, 16577-16586, doi:10.1021/jp409497z (2013).

16 Cho, J. *Preparation and Characterization of B2S3-Based Chalcogenide Glasses* Doctor of Philosophy thesis, Iowa State University, (1995).

17 Larink, D., Eckert, H. & Martin, S. W. Structure and Ionic Conductivity in the Mixed-Network Former Chalcogenide Glass System [Na2S]2/3[(B2S3)x(P2S5)1–x]1/3. *The Journal of Physical Chemistry C* **116**, 22698-22710, doi:10.1021/jp3068365 (2012).

18 Martin, S. W., Bischoff, C. & Schuller, K. Composition Dependence of the Na+ Ion Conductivity in 0.5Na2S + 0.5[xGeS2 + (1 – x)PS5/2] Mixed Glass Former Glasses: A Structural Interpretation of a Negative Mixed Glass Former Effect. *The Journal of Physical Chemistry B* **119**, 15738-15751, doi:10.1021/acs.jpcb.5b07383 (2015).

19 Bischoff, C. *The Mixed Glass Former Effect in $0.5Na_2S+0.5[xGeS_2+(1-x)PS_{5/2}]$ Glasses* Doctor of Philosophy thesis, Iowa State University, (2013).

20 Deshpande, V. K., Pradel, A. & Ribes, M. The mixed glass former effect in the Li2S : SiS2 : GeS2 system. *Materials Research Bulletin* **23**, 379-384, doi:http://dx.doi.org/10.1016/0025-5408(88)90012-8 (1988).

21 Martin, S. & Bloyer, D. Preparation of High-Purity Vitreous B_2S_3. *Journal of the American Ceramic Society* **73**, 3481-3485 (1990).

22 Curtis, B., Francis, C. & Martin, S. W. *Glass Transition Temperatures and Densities of the Sodium Thioborosilicate Mixed Glass Former System* $0.6Na2_S + 0.4[xBS_{3/2} + (1-x)SiS2]$ (2018).

23 Curtis, B., Francis, C. & Martin, S. W. *Structural Investigation of the Sodium Thioborosilicate Mixed Glass Former System* $0.6Na_2S + 0.4[xBS_{3/2} + (1-x)SiS_2]$ (2018).

24 ANDERSON, O. L. & STUART, D. A. Calculation of Activation Energy of Ionic Conductivity in Silica Glasses by Classical Methods. *Journal of the American Ceramic Society* **37**, 573-580 (1954).

25 Dyre, J. C. Colloquium: The glass transition and elastic models of glass-forming liquids. *Reviews of Modern Physics* **78**, 953-972 (2006).

26 Goldstein, M. Viscous Liquids and the Glass Transition: A Potential Energy Barrier Picture. *The Journal of Chemical Physics* **51**, 3728-3739, doi:10.1063/1.1672587 (1969).

27 Bischoff, C., Schuller, K. & Martin, S. W. Short Range Structural Models of the Glass Transition Temperatures and Densities of 0.5Na2S + 0.5[xGeS2 + (1 – x)PS5/2] Mixed Glass Former Glasses. *The Journal of Physical Chemistry B* **118**, 3710-3719, doi:10.1021/jp411942t (2014).

Table 5.1. The mol% of free sodium sulfide of the available sodium sulfide determined through ^{11}B NMR, ^{29}Si NMR and charge compensation.

Composition	**Percent of Free Na_2S**
0	0
0.1	0
0.2	1.5
0.3	0.9
0.4	2.0
0.5	2.4
0.6	6.6
0.7	2.8
0.8	5.6
0.9	8.0
1	7.5

Table 5.2. Values for the corresponding parameters used in determining strain and Coulombic binding energies of the Christensen Martin Anderson Stuart Model.

Composition (x)	G (Pa)	r_{Na} (m)	r_D (m)	ε_{hf} (pF)	Md	λ cation (m)
0	1.67E+10	9.70E-11	6.50E-11	10.37	1.38	3.89E-10
0.1	1.65E+10	9.70E-11	6.50E-11	12.20	1.99	3.88E-10
0.2	1.60E+10	9.70E-11	6.50E-11	10.16	1.36	3.87E-10
0.3	1.56E+10	9.70E-11	6.50E-11	9.18	1.61	3.85E-10
0.4	1.52E+10	9.70E-11	6.50E-11	8.82	1.72	3.81E-10
0.5	1.48E+10	9.70E-11	6.50E-11	8.65	1.62	3.81E-10
0.6	1.43E+10	9.70E-11	6.50E-11	9.24	1.59	3.79E-10
0.7	1.39E+10	9.70E-11	6.50E-11	11.03	1.38	3.78E-10
0.8	1.36E+10	9.70E-11	6.50E-11	9.82	1.49	3.77E-10
1	1.31E+10	9.70E-11	6.50E-11	11.72	1.59	3.74E-10

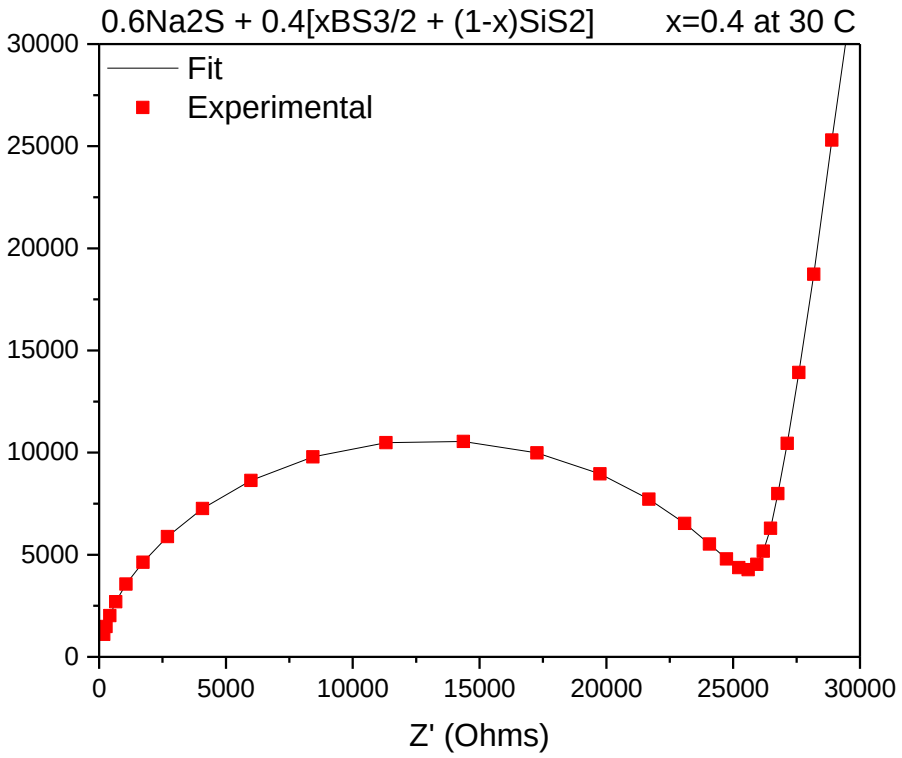

Figure 5.1. Example fitting of a complex impedance plots for sample x=0.4 at 30 C.

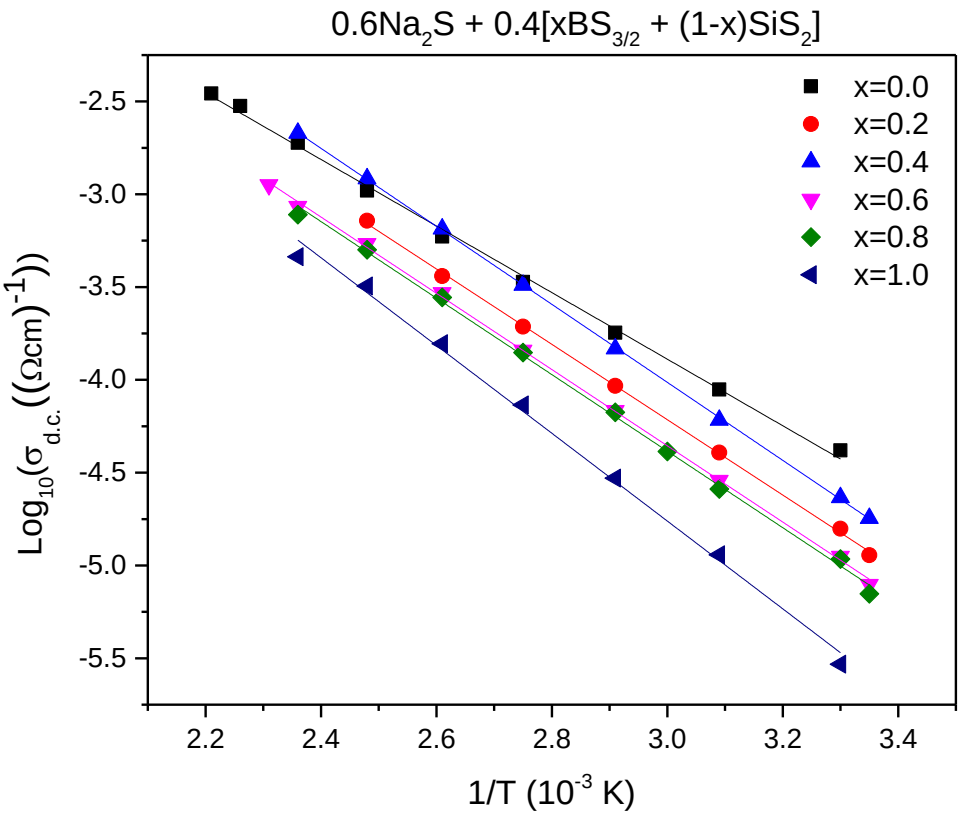

Figure 5.2. The Arrhenius plots of the D.C. conductivity for the sodium thioborosilicate system. Only every other sample is shown for ease of visibility.

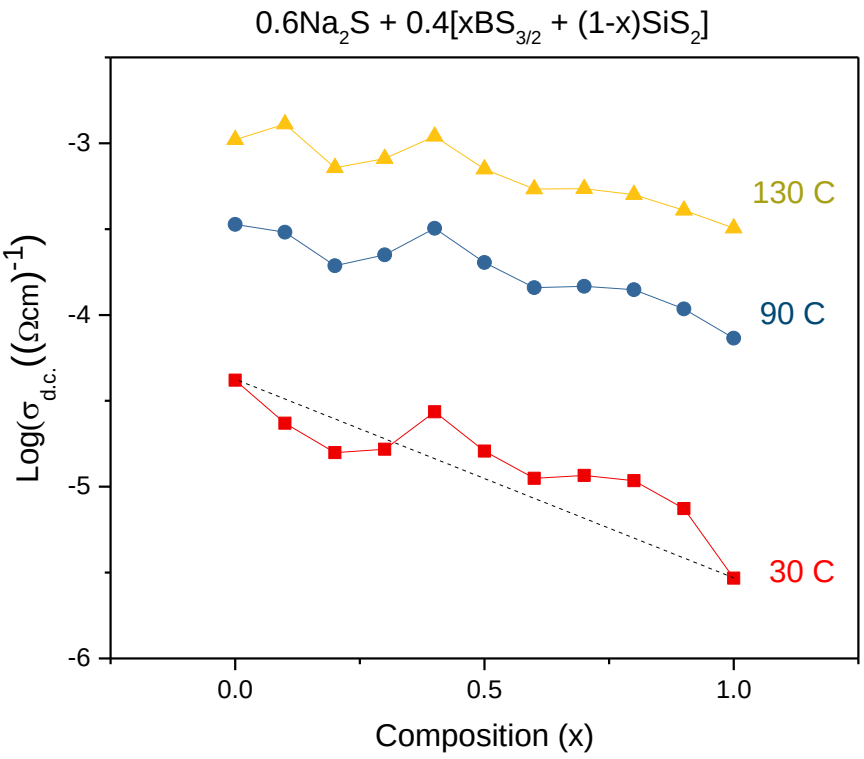

Figure 5.3. The D.C. ionic conductivity at for each composition in the sodium thioborosilicate system reported at 30, 90 and 130 C.

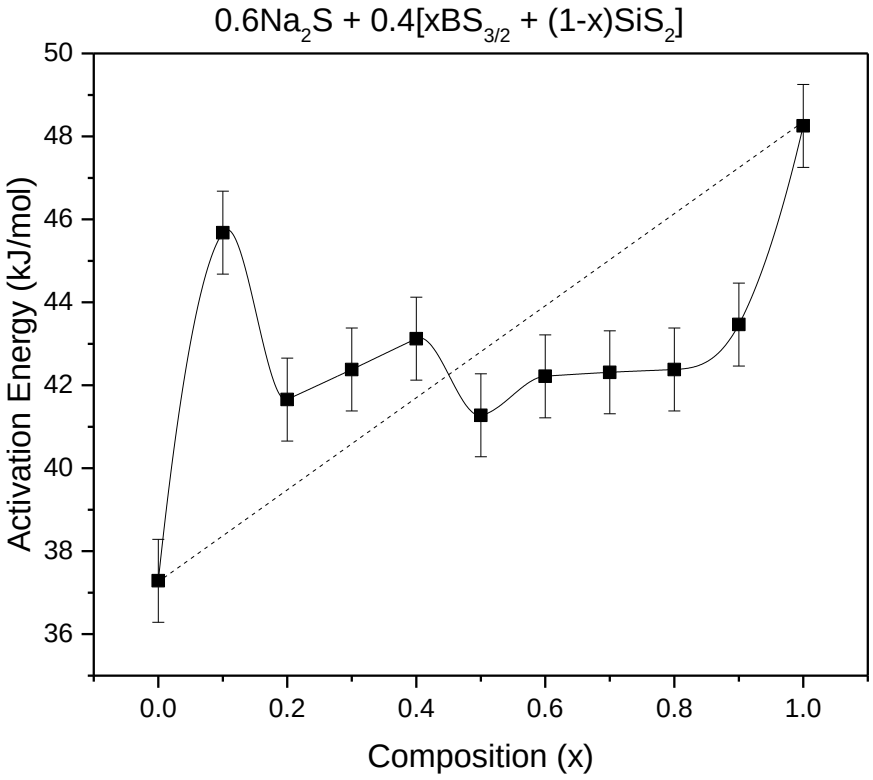

Figure 5.4. The experimental activation energy determined from the slope of the Arrhenius plot for each composition.

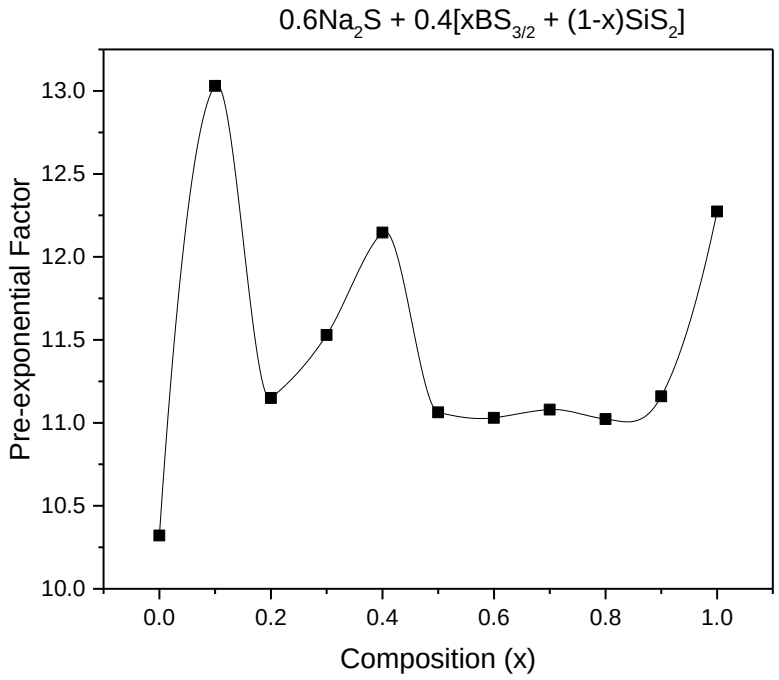

Figure 5.5. The pre-exponential factor for each composition of glass in the sodium thioborosilicate system.

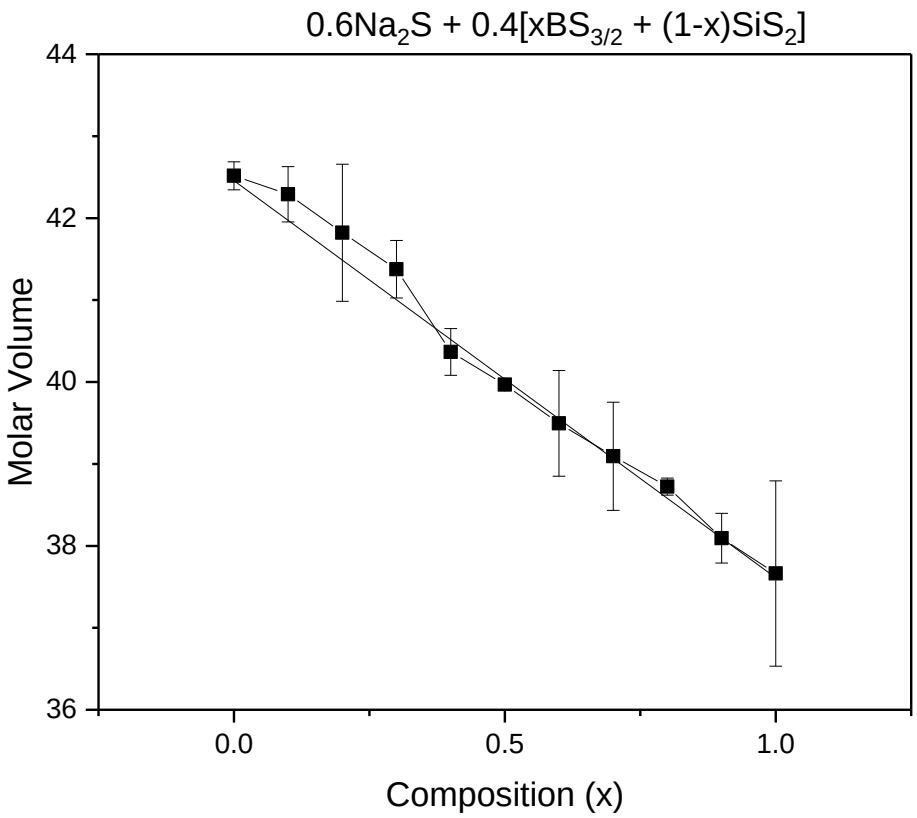

Figure 5.6. The experimental molar volume determined for each glass composition in the system.

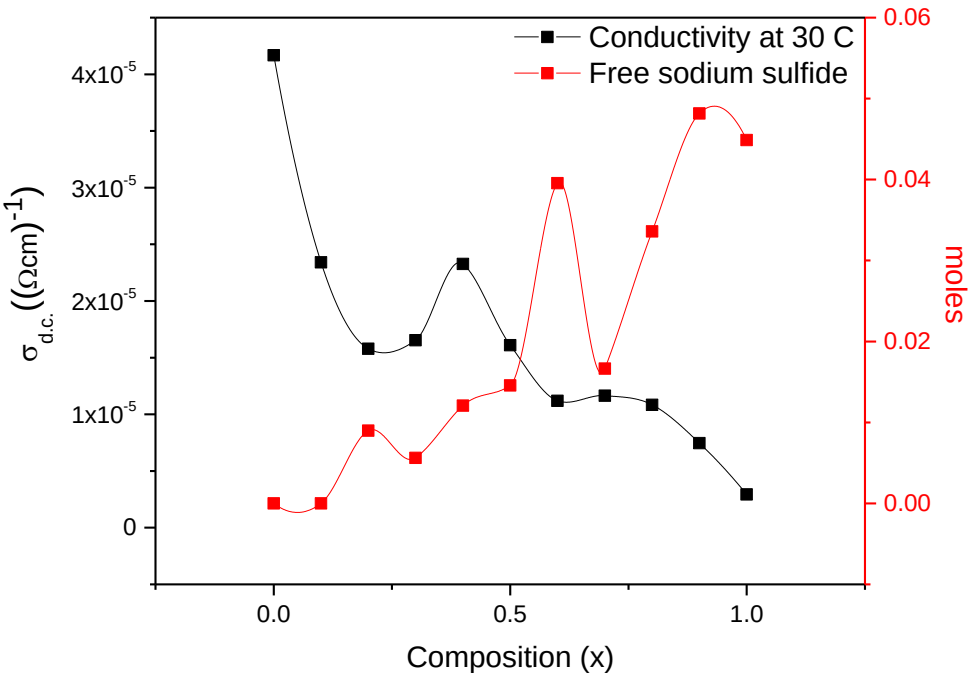

Figure 5.7. The comparison of the ionic conductivity and the free, unreacted sodium sulfide for each composition.

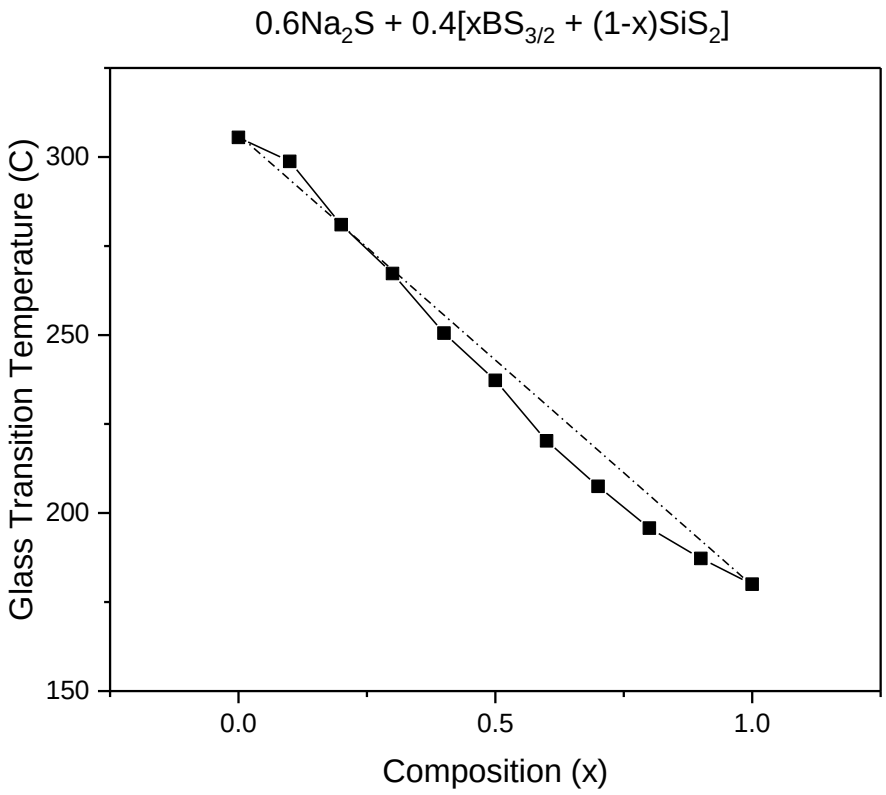

Figure 5.8. The glass transition temperature plotted against composition.

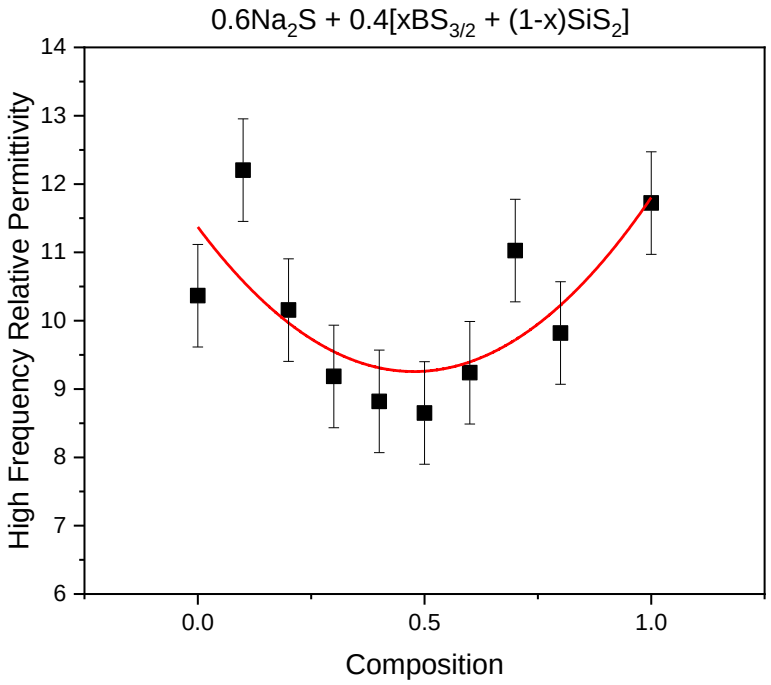

Figure 5.9. High frequency relative permittivity determined at -80 C for the sodium thioborosilicate glasses.

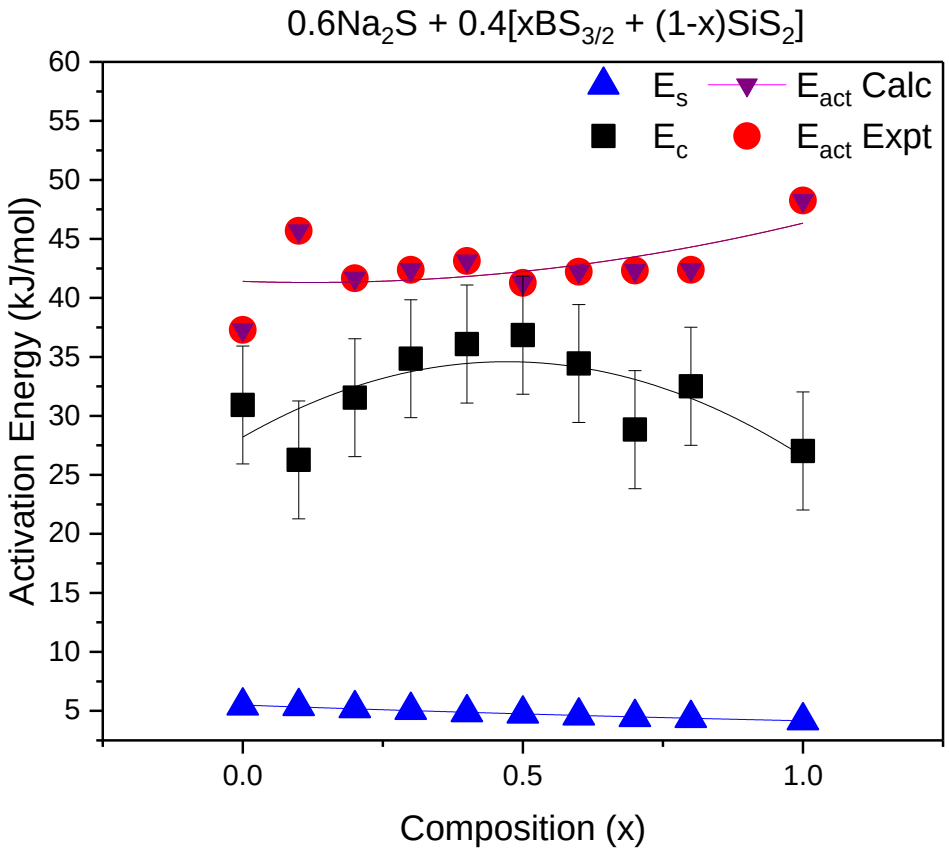

Figure 5.10. The calculated strain, binding and activation energy along with the experimentally determined activation energy for the sodium thioborosilicates.

CHAPTER 6. GLASS TRANSITION TEMPERATURES AND DENSITY OF THE SODIUM THIOBOROSILICATE MIXED GLASS FORMER SYSTEM $0.6Na_2S + 0.4[xBS_{3/2} + (1-x)SiS_2]$

A paper to be submitted the Journal of Non-Crystalline Solids

Brittany Curtis, Carter Francis and Steve Martin*

Department of Materials Science & Engineering
Iowa State University of Science and Technology
Ames, IA

6.1 Abstract

Solid-state batteries are proving to be a good alternative to lithium-ion batteries which have been known to have safety concerns. By replacing the liquid, organic electrolytes with a glassy, solid-state electrolyte, these safety concerns could possibly be prevented. An interesting phenomenon occurs in ternary glasses where there is a non-additive, non-linear trend in the physical properties upon mixing two glass formers in varying ratios. This is known as the mixed glass former effect (MGFE). The MGFE was examined in the sodium thioborosilicate system, $0.6Na_2S + 0.4[xBS_{3/2} + (1-x)SiS_2]$, in both the glass transition temperature (Tg) and density. The glass transition temperature was found to overall decrease from sodium thiosilicate to sodium thioborate with a slight negative deviation from linearity of the ternary systems. The density also decreased but showed a more significant negative deviation in the silicon-rich samples then returned to linear behavior. The molar volume had an inverse relationship to the density where there was a positive deviation in the silicon-rich samples.

* Corresponding author, swmartin@iastate.edu

6.2 Introduction

All solid-state batteries are becoming of increasing interest as a safer alternative to lithium-ion batteries. Replacing the organic, liquid electrolyte with a solid electrolyte may prevent dendritic formation that is known to occur in lithium-ion batteries.[1] The lack of dendritic formation will prevent short-circuiting which can lead to thermal runaway causing the organic electrolyte to ignite.[2-5] Many solid-state alternatives are being explored such as polymer, polymer gels, ceramic, glasses and glass ceramics.[6-8] Glasses are of particular interest due to their amorphous behavior. The grain boundary lacking structure prevents a pathway for dendritic growth that is facilitated in crystalline materials.

Currently, the most widely used secondary battery is the lithium-ion battery. Apart from the safety concerns of these batteries, they are also quite costly due to the rarity of lithium. Sodium has a similar chemistry to lithium and may prove to be a cheaper replacement. Sodium is over a thousand times more abundant in the Earth's crust than lithium.[9,10] However, sodium is larger than lithium making it less attractive for portable devices. These sodium metal batteries would be great for grid-scale energy storage devices such as storage for wind turbines.

While oxide glasses are chemically durable and strong, their ionic conductivities are not high enough to be used as an electrolyte material for a solid-state battery. Sulfide-based glasses have proven to have increased ionic conductivities of 5 to 6 orders of magnitude over the oxides. However, the ionic conductivities of the binary sodium sulfide glasses are not competitive with the conductivities necessary for solid-state batteries. Nevertheless, upon mixing two glass formers in varying ratios, from one binary to the next through a ternary system, it has been seen that a non-linear, non-additive trend

in physical properties is seen. This phenomenon is known as the mixed glass former effect (MGFE) and has been studied for multiple glass systems of both oxide and sulfide based glasses.[11-14]

6.2.1 Notation of SRO Units

A shorthand notation will be used in this paper to concisely describe the SRO structures examined in the sodium thioborosilicate system. For a boron unit with 3 bridging sulfurs the notation will be B^3 where B indicates the central atom as given by the periodic table and 3 indicates the number of bridging sulfurs. Note that boron can be trigonally and tetrahedrally coordinated but this notation is not explicit in the coordination.

6.3 Experimental

6.3.1 Sodium Sulfide

Sodium sulfide was prepared by dehydrating sodium sulfide nonahydrate (Acros Organics, 98%) at 250 C for 50 hours under vacuum. Once dehydrated, the sample was sealed under vacuum and transferred to the nitrogen glovebox.

6.3.2 Silicon Sulfide

Silion sulfide was prepared from stoichiometric amounts of elemental powders. Silicon (Alfa Aesar, crystalline, 99.999%) and sulfur (Acros Organic, 99.999%) were massed out inside a nitrogen glovebox and packed into a silica ampoule. The ampoule was sealed with a hose and hose-clamp, removed from the glovebox and flame-sealed under vacuum. It was then loaded into a mullite tube furnace, slowly ramped to 900 C and held for 11 hours and then allowed to freely cool to room temperature. The reacted ampoule was then introduced into the glovebox where the contents was removed and milled into a powder. Further characterization of the silicon sulfide was done to ensure purity.

6.3.3 Boron Sulfide

Boron sulfide was synthesized using a similar method described by Bloyer *et al*.[15] Boron (NOAH Technologies, crystalline, 99.5%) and sulfur were combined in stoichiometric amounts and packed into a carbon-coated ampoule. It was sealed with a hose and hose-clamp, removed from the glovebox and flame-sealed under vacuum. Once sealed, it was loaded into a furnace, slowly ramped to 850 C and held for 4 to 5 hours. It was then slowly cooled to room temperature and placed into the glovebox. It was then removed from the ampoule, milled to a powder in a SpexMill and characterized to ensure purity.

6.3.4 Preparation of Glass Samples

All samples were prepared in a nitrogen glovebox and made from stoichiometric amounts of the precursors. These samples were milled for 20 minutes using a Spex mill to pre-react the powders and reduce excess vaporization when melting. The samples were then melting in a mullite tube furnace attached to the glovebox for 5 min at 550 to 720 C depending on composition. A mass loss was obtained once the first melt has cooled in the vitreous carbon crucible to ensure the mass lost did not exceed 2 wt %. Once this is obtained, the sample is melted a second time and annealed at 30 to 50 degrees below the Tg for 40 min then allowed to cool to room temperature at 2 C per min.

6.3.5 Glass Transition Temperatures

Glass transition temperatures ($T_{g)}$ for glassy samples were determined through differential scanning calorimetry (DSC). A Perkin Elmer Diamond DSC with water/alcohol external chiller was used to measure the samples. Sample sizes varied from 5-10 mg and all samples were hermetically sealed into aluminum pans inside of a nitrogen glove box. Additionally, a purge gas of nitrogen at a flow rate of 20 ml/min was

used to further control the environment. A survey scan was conducted first to determine estimates of glass transition and crystallization temperatures. A secondary sample then was run in range of 50 to30 degrees above T_g. These samples were cycled three times reduce stress build up and establish a known thermal history. As such the samples were heated and cooled at 20 degrees Celsius per minute. From these tests the glass transition temperatures reported are based on the average of the T_gs from the heating of the second and third cycles. All T_g's, after cycling, were reproducible in the range of ±2 degrees when the same sample was run multiple times. The onset of the transition temperature was determined using the Perkin Elmer software and is based on drawing tangent lines to the baseline before the transition occurs and during the transition. A sample of the determination of onset can be seen in Fig. 6.1

6.3.6 Density

Samples tested for density were prepared from bulk annealed samples and measured by the Archimedes method using mineral oil (density of 0.838 g/cc) as the immersive fluid. Masses of 0.5 to 2 grams were used. Care was taken to remove any surface bubbles to prevent inconsistencies in measurements. All measurements occurred in a nitrogen glove box with contamination levels of oxygen and water < 5ppm.

All measurements were preformed using a Metler Toldeo balance (model: XS105 Duel Range) with a complimentary density apparatus. The balance was calibrated with a calibration weight and found to agree within ± 0.0001 g. The atmospheric mass was obtained in the nitrogen atmosphere and the submerged mass was determined from the sample in mineral oil. Multiple measurements were preformed to determine average value and experimental error.

6.4 Results

6.4.1 Glass Transition Temperature

The reported glass transition temperatures can be seen in Fig. 6.2. With increasing boron content, a large, fairly linear decrease in transition temperature can be seen. The highest values associated with the pure sodium thiosilicate (T_g = 305 C) and the lowest associated with the pure sodium thioborate glass (T_g= 180 C). Cho reported the glass transition temperature of this sodium sulfide boron sulfide to be 157 C which is about 20 C.[16] According to Cho, the glasses were melted at temps about 200 C higher than the procedure listed here. This could account for the small discrepancies in the glass transition temperature of the sodium thioborate. Upon adding more boron, a slight positive deviation from linearity occurs in the high silicate region and the glass transition temperatures then proceeds to drop quickly. In the region of x=0.3 to x=1.0 (the pure thioborate sample) a slight negative deviation from linearity can be further observed. Although seemingly small, because of the large change in glass transition temperatures between the end members it should be noted that the deviation is around 10 degrees Celsius at the x=0.7 borate end.

6.4.2 Density and Molar Volume

The densities of the sample can be seen in Fig. 6.3. They show a downward sloping trend as silicon is replaced by boron in the glass. There are minor deviations from linearity. There may be slight negative deviation in linearity in the silicon-rich glasses. Additionally, the x=0.4 glass appears to show a large deviation from the other points measured. Even over multiple batches and samples, the x=0.4 glass appears to have an uncharacteristically high density. At the higher borate end a minimum can be seen at the x=0.8 compositional value. The error also increases in the high borate end.

The calculated molar volumes follows from the densities reported above and can be seen in Fig. 6.4. The molar volume was calculated through dividing the molar mass of one mole of glass by the density of the glass.

$$V_m = \frac{M_m}{\rho} \quad (1)$$

The density is given by ρ and M_m is the molar mass of a formula unit. As such the molar volume reported describes the average volume occupied by each atom. A downward trend is seen, with an anomalous point at x=0.4. Similarly, there is a peak around x=0.8 and x=0.9 on the high borate end, however the x=1.0 seems to follow closely the linear downward trend.

6.5 Discussion

6.5.1 Glass Transition Temperature

The glass transition temperatures of the sodium thioborosilicate system are experiencing very slight deviations from linearity suggesting that the mixing of glass formers has little influence on creating a mixed glass former effect with respect to the Tg. A small negative deviation from linearity as x-value increases can be seen, however, it is faint. The overall trend decreases from sodium thiosilicate to sodium thioborate. Upon further investigation of the bonding, Fig. 6.5, shows the number of bridging sulfurs (BS) and the non-bridging sulfurs (NBS). As shown, the bridging sulfurs decreases in a similar fashion to the glass transition temperature, this suggests that as the networking of these glass decreases, the glass is inherently less thermally stable lending to the observed trend in T_g.

6.5.2 Density and Molar Volume

The mixed glass former effect with respect to the density has a slight region of negative deviation in the silicon rich end followed by a positive deviation tending towards the boron-rich glasses. The overall decrease in density from x=0.0 to x=1.0 is due to the replacement of silicon with boron. Silicon is more massive than boron but this must also suggest that little volume change is occurring when interchanging species. Therefore, the decrease in mass from silicon to boron must be accounting for a larger effect to the density than volume changes occur. The molar volume may offer more insight into this phenomenon. The sodium thiosilicate has a molar volume of 42.5 cm^3/mol and a molar mass of 83.7 g/mol. For the sodium thioborate, the molar volume was calculated to be 37.66 cm^3/mol and has a molar mass of 70.4 g/mol. From sodium thiosilicate to sodium thioborate the molar volume decreases slightly while there's a larger decrease in the molar mass of 13.3 g/mol. This supports that the molar mass of the interchanging species has a larger effect on the density while having little effect on the molar volume.

6.7 Conclusion

The glass transition temperatures and densities along with the corresponding molar volumes have been reported for the sodium thioborosilicate sytem, $0.6Na_2S + 0.4[xBS_{3/2} + (1-x)SiS_2]$. The glass transition temperatures were obtained through DSC while the density was found using the Archimedes method for determining density. It was seen that the Tg of the series was fairly linear with a decrease from the sodium thiosilicate ot the sodium thioborate. The density and molar volume show similar linear trends with some small deviations in the silicon-rich glasses.

6.8 Acknowledgements

This research was supported by the National Science Foundation under DMR grants 1304977 and 0710564. The authors would like to take this time to thank the other members of the Iowa State Glass and Optical Materials research group.

6.8 References

1 Monroe, C. & Newman, J. Dendrite Growth in Lithium/Polymer Systems: A Propagation Model for Liquid Electrolytes under Galvanostatic Conditions. *Journal of The Electrochemical Society* **150**, A1377-A1384 (2003).

2 Rosso, M. *et al*. Dendrite short-circuit and fuse effect on Li/polymer/Li cells. *Electrochimica Acta* **51**, 5334-5340, doi:https://doi.org/10.1016/j.electacta.2006.02.004 (2006).

3 Lisbona, D. & Snee, T. A review of hazards associated with primary lithium and lithium-ion batteries. *Process Safety and Environmental Protection* **89**, 434-442, doi:https://doi.org/10.1016/j.psep.2011.06.022 (2011).

4 Wang, Q. *et al.* Thermal runaway caused fire and explosion of lithium ion battery. *Journal of Power Sources* **208**, 210-224, doi:https://doi.org/10.1016/j.jpowsour.2012.02.038 (2012).

5 Wen, J., Yu, Y. & Chen, C. A Review on Lithium-Ion Batteries Safety Issues: Existing Problems and Possible Solutions. *Materials Express* **2**, 197-212, doi:10.1166/mex.2012.1075 (2012).

6 Hayashi, A., Ohtomo, T., Mizuno, F., Tadanaga, K. & Tatsumisago, M. All-solid-state Li/S batteries with highly conductive glass–ceramic electrolytes. *Electrochemistry Communications* **5**, 701-705, doi:https://doi.org/10.1016/S1388-2481(03)00167-X (2003).

7 Martin, S. in *Handbook of Solid State Batteries Materials and Energy* (ed Leonard C. Feldman) Ch. 14, 433-501 (World Scientific, 2016).

8 Song, J. Y., Wang, Y. Y. & Wan, C. C. Review of gel-type polymer electrolytes for lithium-ion batteries. *Journal of Power Sources* **77**, 183-197, doi:http://dx.doi.org/10.1016/S0378-7753(98)00193-1 (1999).

9 Carmichael, R. S. *Practical Handbook of Physical Properties of Rocks and Minerals*. (CRC Press Inc., 1989).

10 Ene-Parent, J. & Zikovsky, L. Neutron activation analysis of laundry dryer lint. *Journal of Radioanalytical and Nuclear Chemistry* **247**, 197-198, doi:10.1023/A:1006712408990 (2014).

11 Christensen, R., Olson, G. & Martin, S. W. Ionic Conductivity of Mixed Glass Former 0.35Na2O + 0.65[xB2O3 + (1 – x)P2O5] Glasses. *The Journal of Physical Chemistry B* **117**, 16577-16586, doi:10.1021/jp409497z (2013).

12 Martin, S. W., Bischoff, C. & Schuller, K. Composition Dependence of the Na+ Ion Conductivity in 0.5Na2S + 0.5[xGeS2 + (1 – x)PS5/2] Mixed Glass Former Glasses: A Structural Interpretation of a Negative Mixed Glass Former Effect. *The Journal of Physical Chemistry B* **119**, 15738-15751, doi:10.1021/acs.jpcb.5b07383 (2015).

13 Deshpande, V. K., Pradel, A. & Ribes, M. The mixed glass former effect in the Li2S : SiS2 : GeS2 system. *Materials Research Bulletin* **23**, 379-384, doi:http://dx.doi.org/10.1016/0025-5408(88)90012-8 (1988).

14 Pradel, A. *et al.* Mixed Glass Former Effect in the System 0.3Li2S−0.7[(1−x)SiS2−xGeS2]: A Structural Explanation. *Chemistry of Materials* **10**, 2162-2166, doi:10.1021/cm980701j (1998).

15 Martin, S. & Bloyer, D. Preparation of High-Purity Vitreous B_2S_3. *Journal of the American Ceramic Society* **73**, 3481-3485 (1990).

16 Cho, J. *Preparation and Characterization of B2S3-Based Chalcogenide Glasses* Doctor of Philosophy thesis, Iowa State University, (1995).

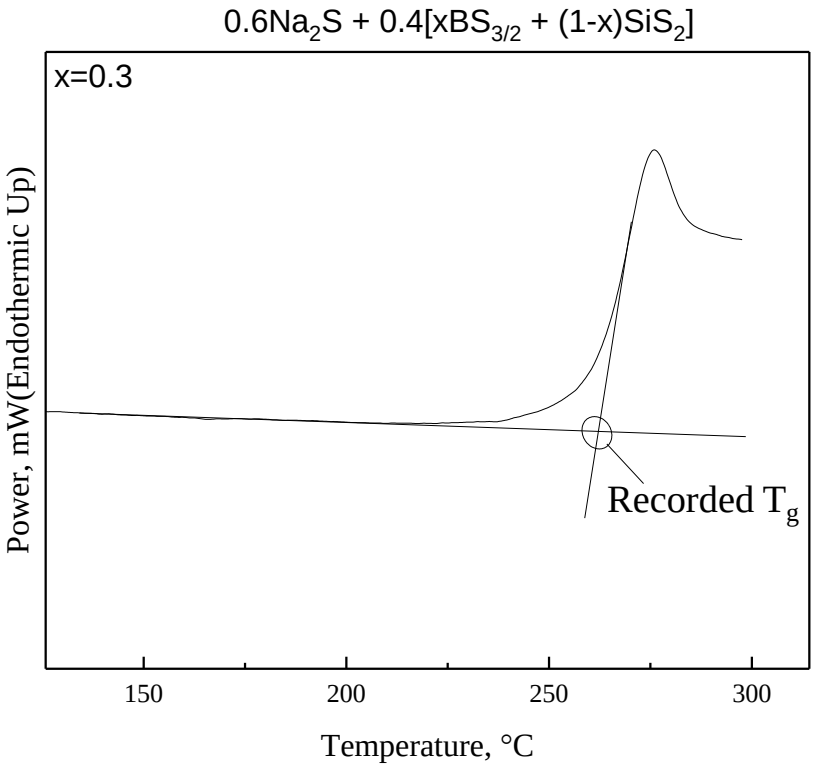

Figure 6.1. Example of the calculated onset from the DSC scan of a sodium thioborosilicate glass sample (x=0.3).

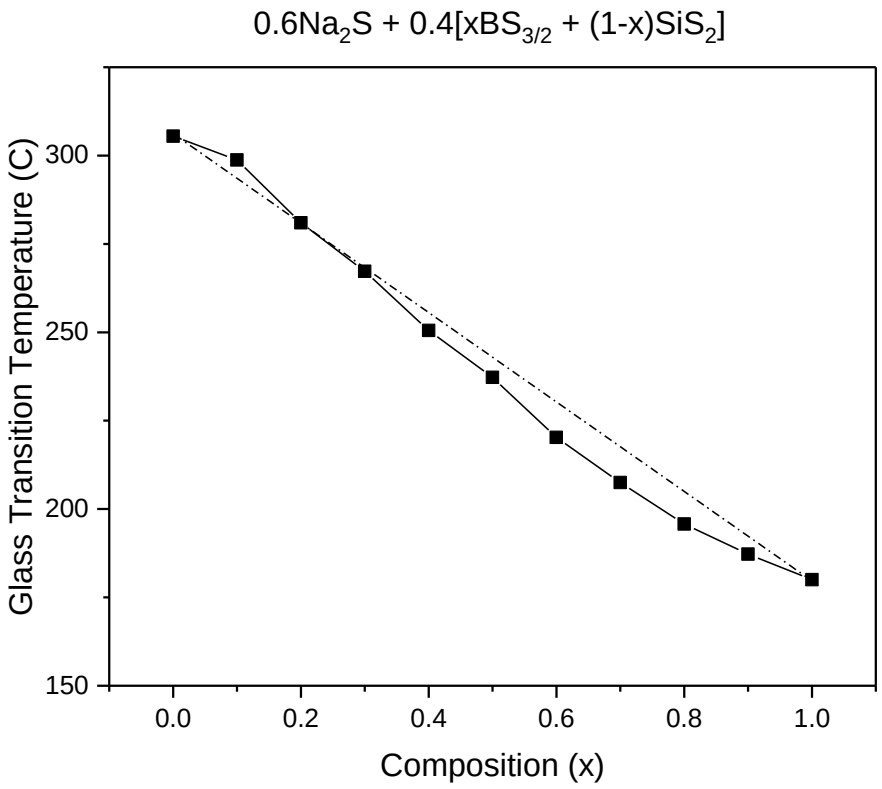

Figure 6.2. The glass transition temperatures for each composition in the series $0.6Na_2S + 0.4[xBS_{3/2} + (1-x)SiS_2]$.

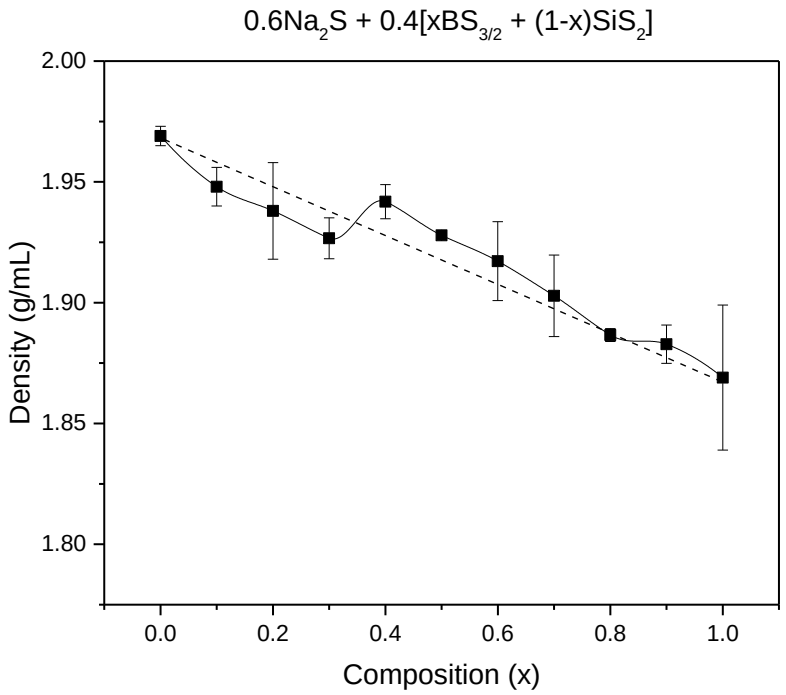

Figure 6.3. Experimentally obtained densities reported for each composition of the sodium thioborosilicate series obtained using the Archimedes method.

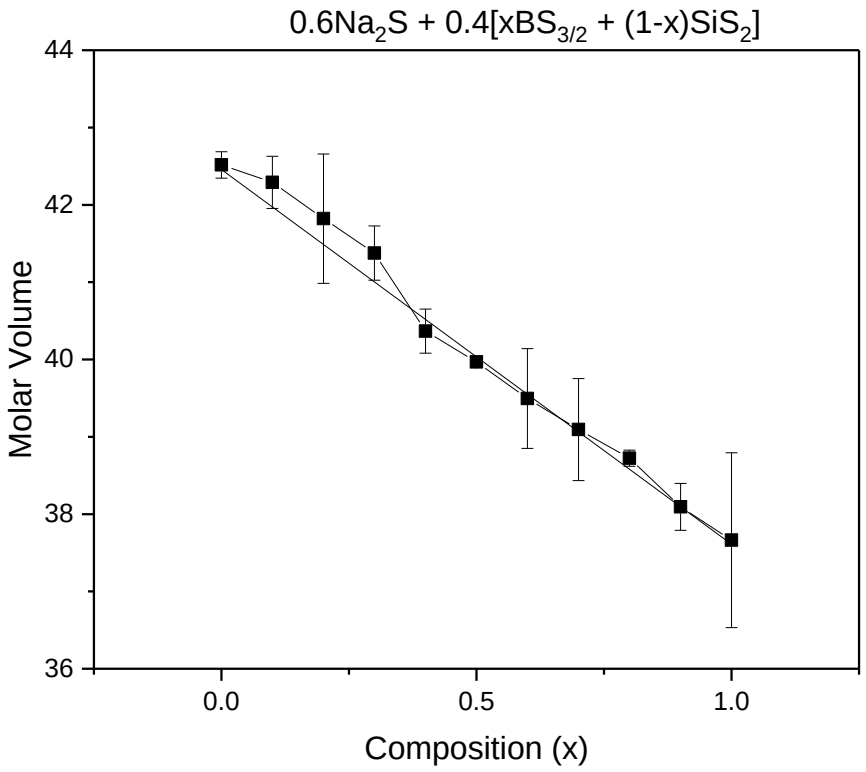

Figure 6.4. Molar volumes calculated from experimental densities for each composition.

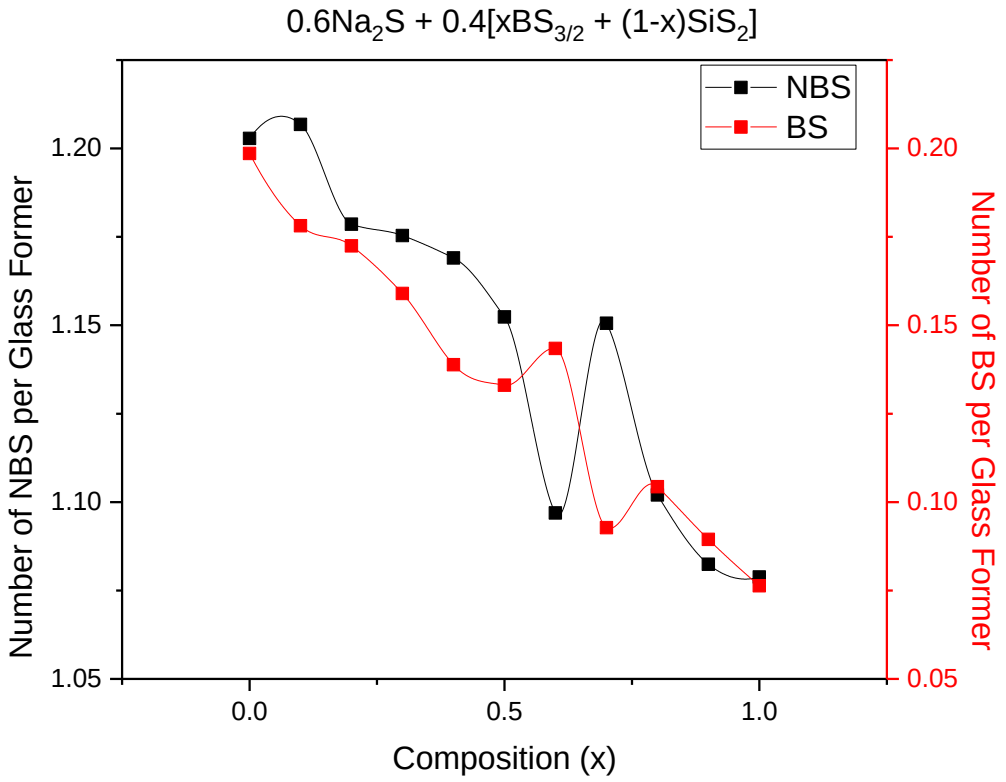

Figure 6.5. The number of non-bridging sulfurs (NBS) and bridging sulfurs (BS) calculated for each composition of the sodium thioborosilicate system.

CHAPTER 7. CONCLUSIONS

7.1 General Conclusions

The mixed glass former effect of many sodium based glass systems were investigated for their use as solid-state electrolytes for all solid-state batteries. The sodium borogermanates structure was examined to fully understand the role of boron in the system. However, upon initial studies of the sulfide-analogous systems, uniform glass that did not phase separate were difficult to obtain. Among the glasses that did form homogenous glasses, their working range made it difficult to produce annealed disks needed for ionic conductivity measurements. The most successful sulfide-based system was the sodium thioborosilicates, which made uniform glasses with large working ranges. In turn, these glasses formed annealed glass disks rather well.

The structural investigation into the sodium thioborosilicate system, $0.6Na_2S + 0.4[xBS_{3/2} + (1-x)SiS_2]$, was done by infrared, Raman and NMR spectroscopies and showed that the with the addition of boron into the system, the silicon Si^1 dimers become depolymerized while producing B^0 units as the dominant structural species. From quantitative results of the ^{11}B and ^{29}Si MASS-NMR along with charge compensation, the existence of free, unreacted sodium sulfide emerged with the increasing boron content.

The ionic conductivities of this system were examined by electrochemical impedance spectroscopy. A negative mixed glass former effect was observed in the ionic conductivity while a positive mixed glass former effect is observed in the activation energy in the silicon-rich side while transferring to a negative mixed glass former effect in the boron-rich end. The Christensen Martin Anderson Stuart Model was used to model

the activation energy of these glasses. It was found that the model agreed well with the experimentally determined activation energies.

The glass transitions and densities of these glasses were determined through DSC and the Archimedes method for density, respectively. The glass transition temperature had a downward sloping trend that was fairly linear with small, negative deviations from linearity. The density obtained had an initial negative mixed glass former effect in the silicon-rich samples that returned to a linear trend in the boron-rich samples. The molar volume, consequently, had an inverse relationship of the density where a positive deviation from linearity occurred in the silicon-rich samples and returning to a linear trend in the boron-rich samples.

7.2 Acknowledgements

I'd first like to thank my advisor Dr. Steve W. Martin for his guidance on this project. Many thanks goes to my committee members: Dr. Nicola Bowler, Dr. Gordon Miller, Dr. Aaron Rossini, and Dr. Xiaoli Tan.

I would also like to thank my fellow GOM group members and especially Carter Francis who has made this process more enjoyable. I wish you the best in your graduate studies at University of Wisconsin-Madison.

Thank you to Dr. Sarah Cady, Dr. Aaron Rossini, and Dr. Randall Youngman for your guidance of NMR both instrumentation and analysis.

I owe a lot of gratitude to my fellow graduate students who have become great friends over the years. Thank you to Stephanie Choquette, Hannah Bearinger, Connor Daily, Tim Cullinan, Matthew Rolchigo, John Graham, Ryan Gebhardt, Perry Antonelli, and Kurt Bearinger. You all truly made these year worthwhile and exciting.

Special thanks to my great friend, Annie Wilkinson, with whom I've had the

pleasure to endure this ride since our undergraduate studies. Thank you for your encouragement and your strong belief that I am as deserving as those who have come before us.

Many thanks and love to my father, Dwight Curtis, who stuck with me through the hard times when things got difficult. And thank you to my mother, Judy Baker, and sister Stephanie.

This research was supported by the National Science Foundation under DMR grants 1304977 and 0710564.